UNIVERSITY OF CAPE TOWN
IYUNIVESITHI YASEKAPA • UNIVERSITEIT VAN KAAPSTAD

A numerical investigation of the dynamic behaviour of continuous, multi-span railway bridges

by
Chad Ludwig

Supervised by
Professor Pilate Moyo

Co-supervised by
Dr. Fulvio Busatta

Dissertation submitted in fulfilment of the requirements for the degree of Master of Science in Engineering

University of Cape Town

Department of Civil Engineering

February, 2018

"L'apprendimento non esaurisce mai la mente"

"Learning never exhausts the mind"
– Leonardo da Vinci

Plagiarism Declaration

I, Chad Ludwig, declare that this thesis titled, *'A numerical investigation of the dynamic behaviour of continuous, multi-span railway bridges'*, and the work presented in it are my own. I declare that:

- This work was done wholly while enrolled at this University.
- I understand the meaning of plagiarism and acknowledge that it is wrong.
- This work has been composed solely by myself and that it has not been submitted, in whole or in part, in any previous application for a degree.
- Where the work of others is consulted, the author(s) is attributed by reference or acknowledgement.

Signed by candidate

Chad Ludwig

Date: September 13, 2018

Abstract

The dynamic behaviour of railway bridges has been investigated for over a century [Ichikawa et al., 2000]. With the introduction of high speed trains in recent history, a host of complex problems regarding resonance have been observed and studied. These studies, which include Bjorklund [2004]; Gabaldón et al. [2009]; Goicolea et al. [2002]; Rigueiro et al. [2010]; Kumaran et al. [2003]; Kwark et al. [2004] and Xia and Zhang [2005], have focused on resonance in relatively short-spanned simply supported railway bridges. New design methods were incorporated in design codes such as *Eurocode* (EN 1991-2) [2003] to address these problems in practice. In the past, railway bridges were designed for static effects, while dynamic effects were accounted for by the application of an amplification factor. It has become increasingly necessary to perform a full dynamic analysis, especially with regard to high speed trains. In the case of continuous, multi-span railway bridges carrying heavy haul trains, such an analysis is not explicitly specified. Design codes, even as recent as the modern *Eurocode* (EN 1991-2) [2003], do not address scenarios where axle loads are higher than 30 tonnes/axle, or trains become very long.

Previous work on the dynamic behaviour of continuous bridges is limited. The dynamic properties of continuous beams was studied as early as Lin [1962], and more recently by Saeedi and Bhat [2011]. The response of continuous beams or bridges subjected to moving forces or masses was studied by Cheung et al. [1999], Johansson et al. [2013] and Ichikawa et al. [2000]. These investigations were limited to analytical methods to determine the dynamic properties (natural frequencies and mode shapes) and response of beams or bridges.

In this research, the response of multi-span, continuous bridges trafficked by heavy haul trains travelling at low to moderate speeds was investigated. The study comprises an investigation of bridges with spans ranging from one to ten, and span lengths of 40 m, 45 m and 50 m modelled using the Finite Element Method in SOFiSTiK. Loading is based on heavy haul trains, which were modelled using the moving forces load model. Natural frequencies and mode shapes were obtained, and displacements and accelerations were calculated for train speeds varying from 20 km/h to 100 km/h. A case-study of the Olifants River Viaduct (ORV), the longest continuous railway bridge in South Africa, is also carried out.

From the study it is evident that as the number of bridge spans increase, the envelope of natural frequencies in the concentrated zone increase but the frequencies become very closely spaced, indicating that the modes might be difficult to determine

experimentally. Displacement and accelerations were generally higher in the first and last span of the multi-span models. A difference in maximum displacements was only noticeable when comparing models with the number of spans ranging from $1 - 4$, thereafter maximum displacements were not affected by the number of spans in the model. Accelerations increased as the speed increased. At low speeds, the number of spans did not significantly influence the peak deck acceleration, however, at higher speeds models with the greater number of spans generally had lower maximum accelerations.

Acknowledgements

It would not have been possible to write this thesis without the continued support and motivation I received. I would like to express my appreciation to the following:

First, and foremost, my supervisor, Professor Pilate Moyo. Professor Moyo was my undergraduate supervisor when I wrote my final year research project in 2011. I was encouraged my his contagious passion and deep interest in the field of structural dynamics. I am grateful for all the support and guidance he has provided me with, and for the vast amount knowledge he willingly shared with me.

My co-supervisor, Dr. Fulvio Busatta, for his continued professional advice, time and support throughout this research.

The University of Cape Town and the Concrete Materials and Structural Integrity Research Unit (CoMSIRU) for providing funding, facilities and an environment conducive to producing high quality research. The staff and students, whom I am honoured to call my colleagues, provided continued support and made this experience one to remember.

Transnet for allowing CoMSIRU to conduct their research on the Olifants River Viaduct.

The National Research Foundation (NRF) and Aurecon South Africa for providing funding for this thesis.

Finally, my family and friends for their continued love and support. I would not have been able to do this without you.

Contents

List of Figures

List of Tables

List of symbols and abbreviations

A ..... Cross-sectional area

E ..... Elastic modulus

f_0 ..... Fundamental frequency of a dynamical system

I ..... Moment of inertia

L ..... Length

λ ..... Critical wavelength between axles

ϕ ..... Mode shape

ω ..... Circular frequency

ρ ..... Mass density

t ..... Time

v ..... Velocity

ζ ..... Damping factor

DAF ..... Dynamic amplification factor

FEM ..... Finite Element Method

HH ..... Heavy haul

m, c, k ..... Small letters refer to single degree of freedom systems

$\mathbf{M}, \mathbf{C}, \mathbf{K}$ ..... Bold, capitals refer to matrices of multi-degree of freedom systems

ORV ..... Olifants River Viaduct

Further symbols and abbreviations are explained as they appear in the thesis.

Chapter 1

Introduction

1.1 Background

Advancements in railway engineering, structural engineering & materials, experimental testing methods and the use of computer programs have resulted in a considerable amount of research in railway bridge dynamics since the mid-nineteenth century. In fact, the problem of moving loads or masses acting on beam-type structures such as bridges has been investigated for over a century, with the behaviour and response being the main focus [Ichikawa et al., 2000]. The method of these investigations include analytical studies, experimental work and numerical modelling. Frýba [1996] has made a considerable contribution to dynamics of railway bridges by exploring theoretical modelling and some experimental work in the field. The dynamic characteristics of railway bridges is discussed, and the parameters which influence the dynamic response of railway bridges are well described in his work [Frýba, 1996].

According to Wang et al. [1993], girders are the most prevalent type of bridge today, especially for rail traffic. They are relatively easy to design in comparison to other bridges, especially with the advancement of computer aided engineering and design software. Designing railway bridges for dynamic effects due to moving loads from train traffic has been considered since the early stages of railways [Goicolea et al., 2002]. A bridge will either experience an increase or decrease in static stresses, displacements and accelerations when it experiences loading from a moving train. In the recent past the increase was designed for through the application of a dynamic amplification factor (DAF), which represents the ratio of the increase with respect to the static response for a single moving load [Goicolea et al., 2002]. For a single moving load the dynamic factor was always found to be sufficient, however, in the case of multiple moving loads (i.e., axles of a train) the factor does not consider the problem of resonance, an anomaly which occurs when the frequency of the train's

axle coincides with the natural frequency of the bridge.

Henceforth, modern design codes such as *Eurocode* (EN 1991-2) [2003] have included, as a requirement in some cases, a detailed dynamic analysis be conducted. This entails time integration of dynamic equations for a model of the railway bridge while being subjected to a series of moving loads which are representative of each axle of a train [Goicolea et al., 2002]. The model may also be analysed by reducing the number of degrees of freedom from a modal analysis, which substantially reduces the number of equations to integrate. The method used to solve the analysis may be analytical (only for simple systems) or using a Finite Element Method (FEM) based program. The basis for whether the DAF or a dynamic analysis should be used in the design of a new railway bridge as defined by *Eurocode* (EN 1991-2) [2003] is shown in Figure 1.1.

Construction methods for girders have also been optimised, and as a result there exists approaches such as the balanced cantilever and incrementally launching to build these types of bridges with numerous spans on the largest scales. The balanced cantilever method involves a pier segment being constructed first, followed by the typical girder segments, one by one or simultaneously from either side of the pier, and the bridge is normally joined at mid-span of each span [Chen and Duan, 1999]. For the incrementally launched method the piers are also constructed first. The girder is then constructed in segments on a series of rollers or sliding bearings in a casting yard located at one of the abutments. Once a segment is cast it is launched and positioned on the permanent bearings using a series of jacks, and the next segment is cast.

Sub-categorically, girders may be normally reinforced or prestressed, and may be defined by different cross-sections such as slabs, beams or box-girders. According to Chen and Duan [1999], prestressed concrete (PSC) box-girder bridges cast in-situ are normally suited for spans ranging from 30 m to 180 m (currently the longest on record is 330 m on the Shibanpo Yangtze River Bridge, China). To find a structurally efficient, economical and aesthetically pleasing solution, PSC box girders are normally constructed in a number of spans and joints are often eliminated to make spans continuous. Careful consideration needs to be made regarding thermal movements, shrinkage & creep, prestress losses and maintenance. These are, however, not the only challenges and are often not the most critical. Complex problems, such as vibrations and fatigue, have come to the forefront of railway bridge engineering, especially since the introduction of high speed rail.

Dynamic problems associated to railway bridges are generally found in two of the four

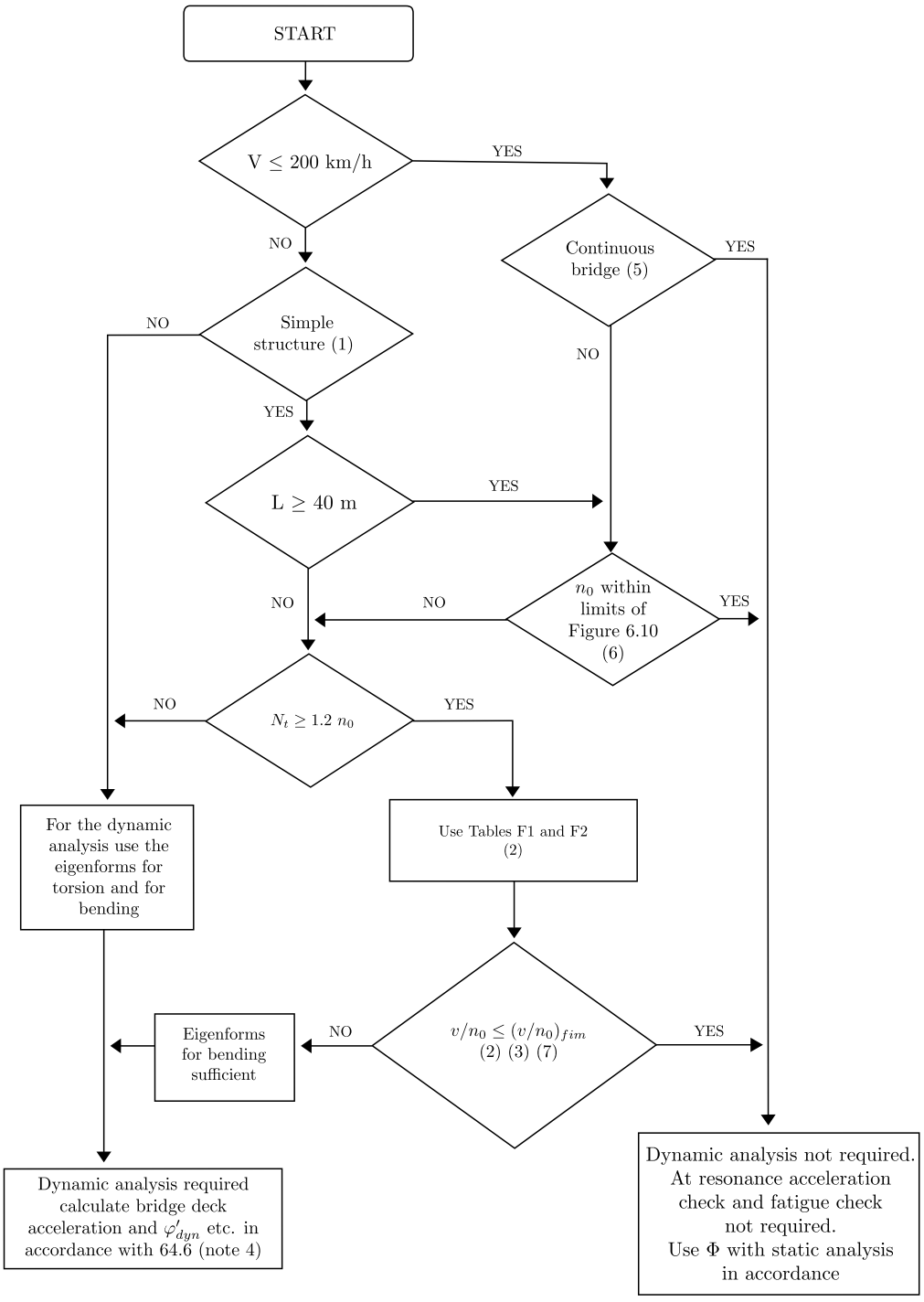

Figure 1.1: Flow chart for railway bridge design approach according to *Eurocode* (EN 1991-2) [2003].

categories in Figure 1.2. The first is associated to high speed (HS) rail (top left of Figure 1.2). According to *Eurocode* (EN 1991-2) [2003], dynamic effects might affect the bridge serviceability if the operating speed of trains exceeds 200 km/h. Generally, the dynamic response of bridges increases with increasing train speed. With the rapid evolution of high speed trains in Europe and Asia the problem is ubiquitous and has led to extensive research into the field of railway bridge dynamics. Secondly, heavy haul (HH) trains (bottom right of Figure 1.2) which travel at low to moderate speeds (50 - 70 km/h) but characterised by heavy axle loads of between 250 kN and 400 kN and having especially long sequences of wagons with identical wheelbases might induce an amplification in bridge response which may lead to large forces. This is of special interest because long trains are not normally covered in codes of practice. If vibrations are excessive the consequences might lead to increased track maintenance costs and might magnify the effect of track and/or wheel irregularities.

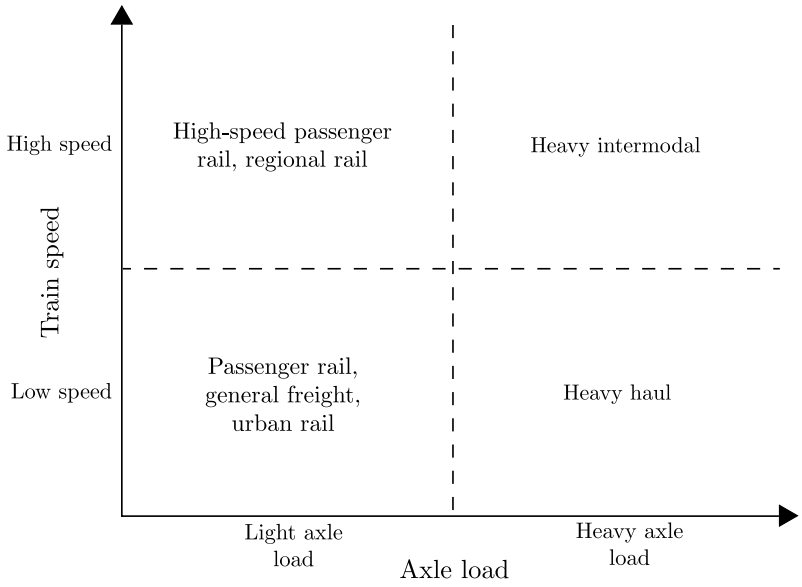

Figure 1.2: Rail categories defined by speed and axle load [Van Der Meulen and Möller, 2012].

High speed trains have not been introduced in South Africa yet. While there is a significant network of passenger railways, they are low speed and in most cases bridges on these networks do not requrie dynamic analysis. The heavy haul railway network, on the otherhand, is subjected to dynamic effects which must be considered. South Africa is rich in natural resources such as coal and iron ore, and heavy haul rail is one of the primary transportation mediums for these commodities. The Department of Mineral Resources [2015] reported that exports of iron ore more than tripled from 1993 (19 Mt) to 2014 (62 Mt). The demand for iron ore drove the price from R 50

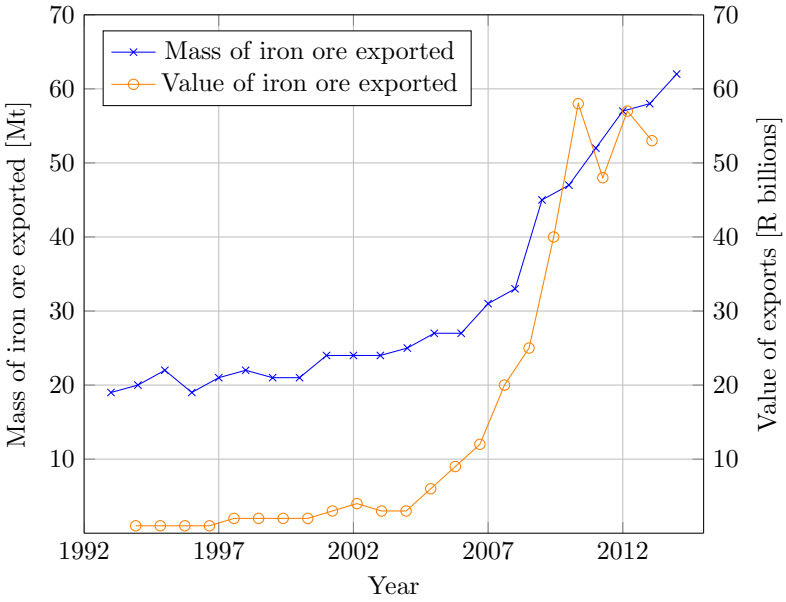

Figure 1.3: Iron ore export volumes and rand value of exports from 1993 to 2014 [Department of Mineral Resources, 2015].

/t to R 855 /t over the same period, and was at its highest in 2011 when the price breached the R 1100 /t mark. The staggering growth of ore export and it's value over that period is clearly shown in Figure 1.3. These statistics are somewhat backed by Kuys [2009] whom forecasted that iron ore exports would more than double from 2006/7 (34 mtpa) to 2014/15 (78 mtpa) where mtpa stands for million tonnes per annum.

This thesis is aimed at investigating the dynamic behaviour continuous, multi-span railway bridges subjected to forces from long heavy haul trains using FEM. A case study of the Olifants River Viaduct (ORV) will also be conducted. The ORV is a 23-span continuous, PSC box-girder railway bridge that is located in the Western Cape of South Africa. The bridge, which was constructed in the early 1970s using the incrementally launched method, is a critical part of infrastructure, being located on the railway line which connects mining areas in the Northern Cape to the shipping port of Saldanha where predominantly iron ore is exported.

Since the bridge's opening in the 1970s the mining areas around Sishen have expanded. This, along with the increasing demand and competition from foreign markets have led Transnet Freight Rail (TFR), the owners and operators of the line, to progressively increase the capacity of the line [Busatta and Moyo, 2015]. An operational plan was sanctioned by TFR whereby railway traffic was increased by [Busatta and Moyo, 2015; Kuys, 2009]:

i. Increasing the axle loads of the wagons.

ii. Increasing the length of the train by adding additional wagons.

iii. Increasing the operating speed of trains.

iv. Adding new crossing loops on the line.

Numerical modelling consists of a number of different mathematical methods and techniques (the Finite Element Method, Finite Difference, etc.) which can be suited to solving structural dynamics problems. It is advantageous and ideal for this particular investigation, based on the following:

i. It provides quantities which are not directly measurable or difficult to accurately measure on a real structure, such as stresses and displacements.

ii. It provides structural response quantities at a greater number of degrees of freedom than in an experimental test where cabling, sensors and data acquisition channels pose limitations in the number of instrumented positions.

iii. The structural response under different operational conditions, such as changing train mass and speed, can be simulated and investigated.

The Finite Element Method, used for this study, is a well known numerical method for solving engineering and physics problems which can be defined by partial differentiable equations [Fish and Belytschko, 2007]. Commercial software packages such as Abaqus, Adina and ANSYS implement FEM to solve user-defined problems. In this study, SOFiSTiK has been chosen as the most appropriate package due to its capability to model moving loads [Sofistik AG, 2015].

The engineering motivation behind this investigation is discussed in section 1.2, followed by the research aims, objectives and limitations. The research methodology is summarised in section 1.4 and the remaining structure of the dissertation is presented in section 1.5.

1.2 Engineering motivation

Currently, the longest heavy haul production train in the world operates on the Sishen-Saldanha ore export line in South Africa. The Olifants River Viaduct (ORV),

a 1035 m long PSC box-girder bridge, is located on this particular railway line. The single-track bridge consists of two 495 m continuous girders, separated by a simply supported drop span of 45 m and is supported with RC piers at spans of 45 m. The ORV experiences forces very unique to most railway bridges, with the longest heavy haul train in the world reaching up to 4.1 km in length and wagons weighing in the order of 30 tonnes/axle (approximately 300 kN/axle) and travelling at low to moderate speeds (maximum permitted speed on the ORV is 50 km/h). The large mass of the HH train is likely to induce a high vehicle-bridge mass ratio, and when coupled during train passage may significantly reduce the natural frequencies of the bridge. A reduction in frequencies will result in a reduction of the critical speed at which potential vibration problems could occur. The repetitive action of axles, which exceed a count of 1500 in the 4.1 km long train, might also exacerbate fatigue.

The majority of research on the dynamic behaviour of railway bridges has focussed on high speed passenger rail with relatively light axle loads, where most of the concerns surround passenger comfort, passenger safety and train safety. Furthermore, most of these investigations, as will be shown in the literature review, have been conducted on relatively short bridges, often with a single span. With numerical methods such as FEM and the availability of commercial software packages such as SOFiSTiK, as well as the increase of computing power, large dynamic problems can be investigated. However, for an increasing number of spans in continuous, multi-span railway bridges the dynamic properties become highly complex, and there is difficulty in, firstly, modelling moving loads and the computational time required to solve linear systems under moving loads, and secondly, that large structures lead to a large number of degrees of freedom. This is a drawback which is to be addressed by this thesis.

The underlying motivating factor for this research is that the dynamic behaviour of continuous PSC bridges which experience loads such as described above has not been well investigated and documented. This thesis, therefore, will focus on obtaining the dynamic properties and response of large scale, continuous, multi-span railway bridges trafficked by long trains with high axle loads and large train-bridge mass ratios, travelling at low to moderate speeds using FEM.

The key research questions which will be addressed are:

i. Can the critical spans, in terms of dynamic response, in multi-span railway bridges subjected to HH trains be identified, and if so which spans are critical?

ii. How does the train speed, mass and the number of bridge spans affect the dynamic amplification of continuous railway bridges?

iii. What deductions can be made in terms of peak deck acceleration in terms of the following parameters: train speed, train mass and number of continuous spans?

1.3 Research aims, objectives & limitations

The objective of this research is to improve the understanding of the dynamic behaviour of continuous, multi-span railway bridges, under long HH train loading. This will be done by investigating the dynamic response of different configurations of continuous, multi-span railway bridges. With that, we will be able to determine what effect bridge configuration (number of continuous spans and span length) and train speed have on the dynamic response of a bridge. In terms of bridge type and loading, the Olifants River Viaduct, described in section 1.2, will be used as a case for this study. The bridge is chosen because it is the longest continuous railway bridge in South Africa and several field measurements of the dynamic properties of the bridge have been carried out. The train loading will be based on the moving forces idealisation, and two different loading conditions be will be studied; the moving forces load model without considering the mass of the train, and the moving forces load model with the inclusion of the train mass by mass lumping at the nodes of the girder. The outcomes will not only improve the understanding of continuous, multi-span girders, but also better inform assessment and monitoring by the inclusion of the ORV as a case-study.

The investigation will be conducted numerically using Finite Element (FE) modelling and analysis, the advantages of which were discussed in section 1.1. Results from the numerical FE study will be compared to an analytical study and experimental measurements in a case-study. By combining this work with the case-study we shall be able conclude on how to better inform dynamic monitoring and assessment of large-scale, continuous, multi-span railway bridges. The commercial software package, SOFiSTiK, will be used to implement different configurations of continuous, multi-span girders and the loading from a HH train to conduct the analysis. SOFiSTiK has been validated for the Finite Element Method and is an appropriate tool for dynamic analysis [Sofistik AG, 2015].

The aims are summarised as follows:

i. Critically review the technical literature regarding the dynamics of railway bridges, with particular reference to defining the characteristics of the dynamic

problems in railway bridges, modelling train loading, and the investigation of the dynamic response of some existing railway bridges.

ii. Developing a numerical model of a simply supported bridge, based on the geometries of the ORV, using the Finite Element Method as implemented in the computer software package, SOFiSTiK.

iii. Determine the modal properties (natural frequencies and mode shapes) of the bridge configurations by conducting a Finite Element modal analysis.

iv. Model heavy haul train loads based on the current trains which traffic the ORV.

v. Conduct dynamic analyses of the bridge under different train crossings to determine and compare displacement and acceleration time histories at points of interest. This will be done under different conditions to determine the effect of certain variables in the model. The variables under consideration will be the number of continuous spans, span lengths and travel speed of the train. The span-depth ratio of the girder will remain constant.

vi. Model the ORV, and extract the dynamic properties as well as response to differing train speeds, and compare it to the available analytical investigation and experimental measurements.

vii. Provide recommendations on improvements to the model or methods and techniques used in the model.

This research is limited to the above and FEM will not specifically consider any of the following:

i. Wind.

ii. Prestressing effects (stiffness & prestress losses).

iii. Creep and shrinkage.

iv. Thermal effects.

v. Rail and wheel irregularities.

vi. Derailment actions.

vii. Soil-structure interaction.

viii. The height of the piers.

1.4 Research methodology

This investigation has been divided into a five stage process with the ultimate goal of conducting a quantitative comparison of different loading scenarios and bridge assemblies. The research methodology purely describes the numerical process of determining the dynamic response of a bridge through a dynamic analysis. The different stages are listed below before being described further below.

i. Selection of parameters and variables.

ii. Creating the FE model.

iii. Conducting modal analysis and extracting the numerical modal properties.

iv. Modelling the train loading.

v. Conducting a dynamic analysis and extracting outputs.

At the first stage the parameters of the numerical model will be chosen and set. These include materials and their properties, cross-sections and geometry of the bridge, boundary conditions, and the type of finite elements. The variables that will be tested (the train speed, length of bridge spans and the number of bridge spans) will also be selected.

The parameters which were defined above will be used as the inputs to the numerical model which is constructed at the second stage. The numerical model will hold properties of mass, stiffness and damping of the bridge. This part of the research aims to compare how different aspects of the bridge and loading might affect the dynamic response of a multi-span structure.

At the next stage a numerical modal analysis will be conducted to determine the dynamic properties: natural frequencies and mode shapes.

Train loading can then be modelled before conducing a dynamic analysis of the bridge to simulate the response to different train speeds. The outputs of interest which will be studied are the acceleration and displacement time-histories of the bridge deck at points of interest.

A case-study, which aims to model the ORV will also be presented. Here, a more precise model will be produced so that the dynamic properties and certain responses can calculated for comparison with (i) some selected measurements taken from

ambient vibration testing (AVT) and monitoring of the structure, and (ii) the same outputs from an analytical study (with results of (i) and (ii) provided by other authors).

1.5 Outline of the dissertation

Chapter 1 provided an introduction to the dissertation. A background is developed before the motivation behind this dissertation is presented. The aims and limitations are discussed, as well as a brief and succinct methodology.

Chapter 2 contains a critical review of the literature to provide the necessary technical background required to undertake this study. Dynamic problems in railway bridges, design aspects and studies on the dynamic response of railway bridges are covered.

Chapter 3 provides the methodology of this work, discusses the selection of parameters and presents the properties used in the Finite Element model.

Chapter 4 provides a discussion of the results and a comparison between the numerical results of the different scenarios. The bridge response is analysed for the two different load models and results in terms of modal properties, acceleration and displacement are presented.

Chapter 5 presents the ORV as a case-study. Measurements which have been taken through the experimental testing and monitoring of the ORV, and results from an analytical study will be compared to the results from the numerical model.

Chapter 6 presents the closing remarks of the study and makes recommendations for future research.

Chapter 2

Railway bridge dynamics: a literature review

2.1 Introduction

The dynamics of railway bridges is a broad and complex topic. This study will focus on continuous girder type railway bridges for heavy haul operations. The investigation will consider the response of various bridge configurations to moving trains. The subject of continuous bridges has been investigated as early as Lin [1962] who looked at the natural frequencies and mode shapes of continuous beams. There has subsequently been a significant amount of research dedicated to issues such as the speed and type of trains, the geometrical and material properties of the bridge and the influence of other factors such as rail irregularities and train-track-structure interaction. This, amongst other issues, has been well summarised by Frýba [1996].

This review covers, firstly, some of the characteristics of dynamic problems in railway bridges. The inherent factors affecting the dynamic characteristics of railway bridges are defined. This will show that heavy haulage railway vehicles may cause dynamic problems which should be carefully considered during design and/or assessment of railway bridges. Secondly, vehicle load models which have been used in past research is discussed. Finally, the dynamic properties and response to moving loads of continuous beam-type structures are reviewed. Here, a lack of research in the response of continuous, multi-span railway bridges subjected to long trains travelling at low to moderate speeds becomes evident.

2.2 Characteristics of dynamic problems in railway bridges

The study of railway bridge dynamics is a broad and complex field. Among other factors, this is due to the many different types of bridge structural systems, the science of materials and the nature of rail loads. Dynamic problems, in general, are more complicated than static problems because of their time-varying nature. By definition, both loading and response vary with time, and therefore a dynamic problem does not have a single solution; instead a succession of solutions corresponding to all times of interest must be established to create a response time history [Clough and Penzien, 2003]. The second, and more fundamental difference between static and dynamic problems, is the influence of inertial and damping forces on the equilibrium condition of a system.

The dynamics of railway bridges involves the response of the bridge to the passage of locomotives and wagons and is dependent on a number of parameters. The factors include [Frýba, 1996]:

i. The mass, rigidity and damping of the structure.

ii. The span length of the bridge.

iii. The structural and material properties of the rail and sleepers.

iv. The presence or absence of ballast, and hence the dynamic characteristics of the ballast.

v. The speed of the train in passage.

vi. The length of the vehicle.

These factors can be categorised into two groups as follows: (1) those associated with the bridge and track (i. to iv.) and (2) those associated with the train (v. to vi.). The load transfer mechanism from the train, through the ballasted track and into a bridge is complex. This complexity lies mostly in the train loading and it's interaction with the rail, and the characteristics of the ballast (or track system). The interaction of the loading with the rail is dependent on the dynamic characteristics of the train, which is often difficult to quantify, and the interaction forces at the wheel-rail interface. There are also uncertainties in the way the dynamic properties of the ballast are defined and modelled.

Dynamic problems are of special interest in high speed and heavy haul railway bridges. In the case of high speed rail, when trains operate at speeds greater than 200 km/h (according to *Eurocode* (EN 1991-2) [2003]), the amplitude of the dynamic response might tend to resonant levels. Resonance is defined as a phenomenon whereby the frequency of an applied load equals the undamped natural frequency [Clough and Penzien, 2003]. This anomaly might result in higher response of displacements and accelerations and in the case of ballasted railway bridges, the possible risks which may consequent include a reduction in passenger comfort, destabilisation of the ballast and derailment due to displacements & accelerations exceeding the serviceability limit state. If the bridge has been constructed using reinforced or prestressed concrete, cracks may form if the moment and shear forces induced are significant enough.

Investigations, such as those conducted by Goicolea et al. [2002], Kwark et al. [2004] and Xia and Zhang [2005], exemplifies the issue of resonant phenomena on bridges with high speed trains. The Tajo Viaduct in Spain, which was studied by Goicolea et al. [2002], consists of simply supported spans 38 m long. The fundamental frequency of the bridge is $f_0 = 3.31$ Hz, hence for a speed of 219 km/h the excitation wavelength is $\lambda = 18.4$ m which closely coincides with the regular spacing of 18.7 m between bogies and resonance was observed. In the particular case of resonance of bridges on high speed lines the consequence of highest concern is passenger discomfort and derailment due to higher amplitude accelerations. Generally, at high speeds and due to relatively short trains, there is little impact on the structural performance.

Trains on heavy haul railway bridges operate at speeds less than 100 km/h where resonance is not normally an issue, however, other problems may be apparent. Heavy haul trains are normally significantly longer than high speed trains, and axle loads are significantly high. Derailment and destabilisation of the ballast remains a risk, but the repetitive action of high axle loads is more likely to result in fatigue and a reduction of the service life of the bridge. The nature of the heavy haul locomotives and wagons, as well as the complex response of continuous railway bridges nonetheless make it difficult to model or predict this. As will be shown in this literature review, most studies tend to focus on railway bridges on high speed lines, there is only limited available research on continuous, multi-span railway bridges with heavy haul trains. Presumably, this is due to the fact that heavy haul rail is limited to only a few countries internationally and studies which have been done are stored as internal reports of companies.

Martino [2011] studied the dynamic response of the Banafjal bridge, a steel-concrete composite bridge with a single span of 42 m. The type of rail traffic considered was

the Swedish Arrow freight train with axle loads of 25 tonnes/axle. In Martino's [2011] numerical investigation, resonant phenomena was observed at speeds as low as 60 km/h for all load models investigated. The approximate spacing between axles coincided with the wavelength of the first natural frequency of the bridge when the train speed equalled 60 km/h. This study demonstrates that resonance may occur at speeds much less than 200 km/h, and that more investigations are required to develop a better understanding of the effects and possible consequences.

The dynamic effects of railway vehicles on bridges, as summarised by Frýba [1996], is presented in Figure 2.1. The broad spectrum of implications clearly show the advanced and complex nature of railway bridge dynamics. To add to these effects there are also those which are not considered in this dissertation, such as the track system, temperature effects and the soil-structure interaction. It is impossible to analyse a bridge while accounting for all of these factors because, firstly, there are too many unknowns that are difficult to quantify and, secondly, the computational effort required to produce such an analysis will be significant.

The above mentioned research on bridges on high speed and freight railway bridges is a succinct summary of the current status quo. The speed of trains investigated were generally high, and the structures are either relatively short spanned or light weight. The dynamic problems defined herewith, along with their possible consequences, are generally dealt with quite well in modern design codes such as *Eurocode* (EN 1991-2) [2003]. However, the following two particular issues arise: (1) There is little evidence

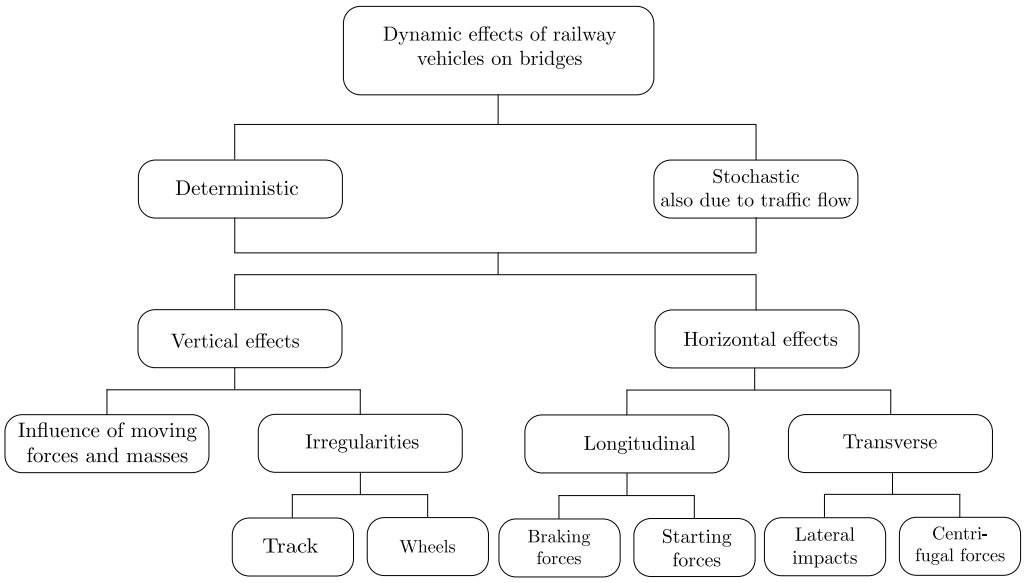

Figure 2.1: Dynamic effects of railway vehicles on bridges [Frýba, 1996].

of structural monitoring and assessment to produce information pertaining to the actual dynamic behaviour of large-scale, multi-span, continuous railway bridges, and (2) that the case of loads produced by heavy haul locomotives and wagons of very long trains has not been investigated extensively. Considering that the main objective of this thesis is to conduct a parametric investigation of the dynamic properties and response of continuous multi-span railway bridges subjected to long consists of locomotives and wagons of heavy haul trains, two further areas of interest will be reviewed further in the following section, one being vehicle load models; the second being the dynamic behaviour of continuous beams and bridges.

2.3 Vehicle load models of train traffic

There are a number of idealisations of trains, ranging from the moving concentrated forces to the train-interaction model which are reviewed in this section. The advantages and disadvantages of each of these models are discussed in reasonable detail below. Whereas load models which are defined in codes such as *Eurocode* (EN 1991-2) [2003] are only applicable to the design of new railway bridges, those reviewed herein are made in context of assessing the response of existing railway bridges, and where possible, examples of the application of the models are presented. Comment will also be made with regards to applying the load models as long sequences of locomotives and wagons for heavy haul trains.

2.3.1 Moving concentrated load

The simplest approach for modelling a moving train is to assume axle loads to be a series of moving point loads. An illustration of the model is shown in Figure 2.2. This model, which has been used extensively in the investigation of railway bridges, is based on the direct time integration of the dynamic equations of the structure.

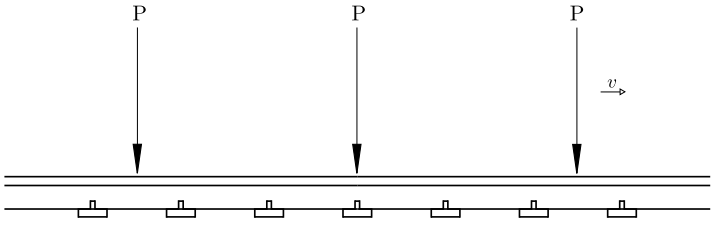

Figure 2.2: An idealisation of the moving forces load model [Rigueiro et al., 2010].

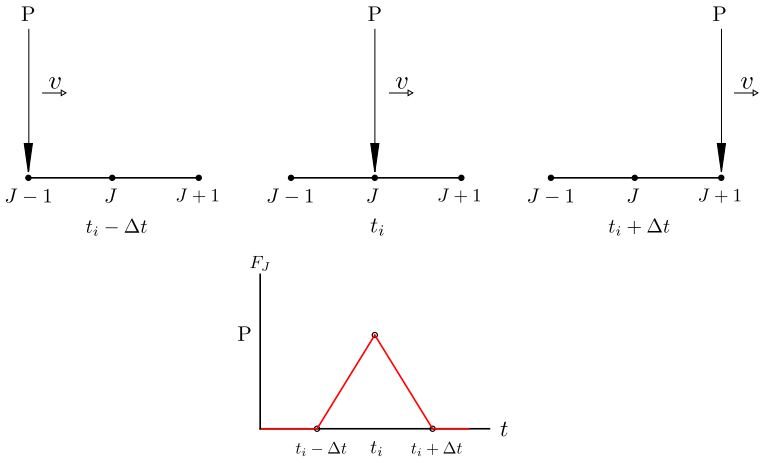

Figure 2.3: Nodal force time history for a single axle load of P travelling at velocity v [Gabaldón et al., 2009].

The notion of the moving forces model is discussed in Frýba [1996], Chopra [2012] and Clough and Penzien [2003]. With this load model the inertial effects are considerably less than the effect of their weight, thus the inertial forces can be ignored. According to Frýba [1996], this is generally acceptable for medium and large bridges, with spans greater than 30 m. In FEM, the moving forces model is easily implemented by defining the axle load of a train as load histories at each node [Gabaldón et al., 2009]. If an axle of load P is located on node j at time t_i, then a nodal load of P_j is assigned to that node. This is illustrated for a single axle in Figure 2.3.

Rigueiro et al. [2010] presented a numerical investigation of the dynamic response of three existing medium-span railway viaducts (Viaduct 1, 8 and 12) whereby the influence of the ballasted track and different load modelling methodologies are taken into account. The viaducts were simply-supported, single-span, twin slabs varying between 11.44 m to 23.50 m in span length. Each of the twin slabs carried a direction of traffic. The slabs were prestressed and had a variable depth with an average mass per unit length of approximately 205 kN/m (21 tonnes/m). The ballast had an average depth of 0.60 m, depending on the thickness of the slab. Rigueiro et al. [2010] emphasised that the line of supports for two of the viaducts were not collinear when considering both decks, and the last viaduct was skewed relative to the longitudinal axis.

A comparison was made between the moving forces load model and the vehicle-interaction model (reviewed later) in a case-study on the viaducts. The moving forces model investigated by Rigueiro et al. [2010] was based on a train model where each bogie has two axles represented by two forces in the moving forces model. The

moving forces model in the case-studies comprised of two different locomotive types and two train types, namely: Locomotive 1116, Locomotive 1047, Train ICE and Train EC. The numerical simulation was based on the characteristics of real trains for which measurements of the response were available, this is summarised in Table 2.1 [Rigueiro et al., 2010].

Table 2.1: Characteristics of real trains investigated by Rigueiro et al. [2010].

Viaduct	Train	$F_{locomotive}$ (kN)	$F_{carriages}$ (kN)	Speed (km/h)
1	Locomotive 1116	210.93	-	130
	Train ICE (7 vehicles)	204.05	127.53	140
8	Locomotive 1047	215.00	-	85
	Train EC (10 vehicles)	210.93	127.53 [a] 135.62 [b]	159
12	Locomotive 1116	210.93	-	150

[a] 1st carriage.

[b] remaining carriages.

The computed and measured natural frequencies were generally within 10 % which is acceptable. The viaducts dynamic response to the moving forces models was simulated using coefficients of viscous damping obtained from measurements. Three different ballasted track models were also investigated, but Rigueiro et al. [2010] concluded that none of the different track models influenced the acceleration response of the viaducts in the lower frequency range up to about 15 to 20 Hz. Figures 2.4 to 2.6 each provide a comparison between the numerical and measured accelerations of the three viaducts. The train models were based on the real trains specified and were converted into the moving forces load model.

Rigueiro et al. [2010] provides an elaborate study of the response of railway bridge viaducts using different train and track models. The FE model was validated with mode shapes and natural frequencies from experimental measurements which resulted in very good agreement of simulated and measured bridge response. The results also show that there is an insignificant difference in the use of the moving forces model versus the interaction model, even up to a speed of 150 km/h.

Martino [2011] investigated the dynamic response of a railway bridge using three load models based on the Steel Arrow freight train. The bridge, named Banafjäl, is a single-span, 42 m long and 7.7 m wide composite bridge. The deck is reinforced concrete and transfers the load from the rail to two simply supported steel beams. The horizontal curvature of the bridge has a radius of 4000 m.

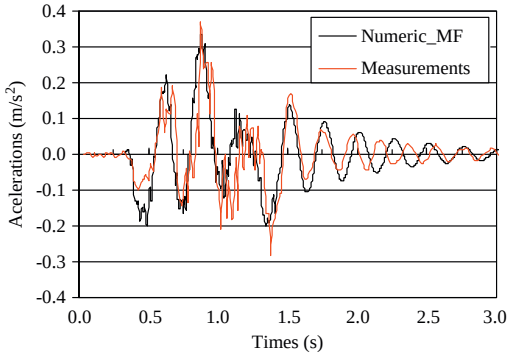

Figure 2.4: This comparison between the measured and simulated response acceleration for viaduct 1 and locomotive 1116 shows a good correlation between the numerical and measured accelerations. There are two notable discrepencies, firstly at approximately 0.5 s the numerical model overestimates the acceleration by a factor of approximately 2. Secondly, once the train has passed (after approximately 1.5 s) the accelerations are dampened and for a period between 2.0 s and 2.5 s the numerical acceleration is out of phase with the measured acceleration [Rigueiro et al., 2010].

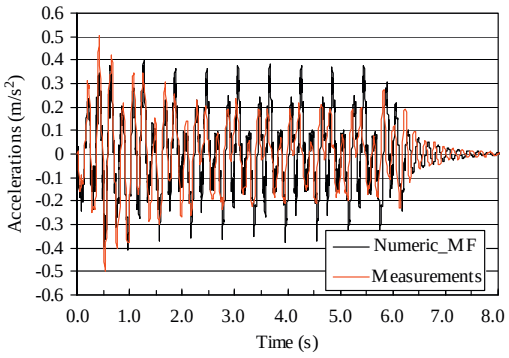

Figure 2.5: This comparison between the measured and simulated response acceleration for viaduct 8 and Train EC is not as clear as in 2.4 above. The amplitudes of the numerical model closely match the measurements up to 2.0 s. Between 2.0 s and 6.0 s the numerical model overestimates the acceleration peaks. After the train has passed the model is able to accurately predict the dampening of the bridge [Rigueiro et al., 2010].

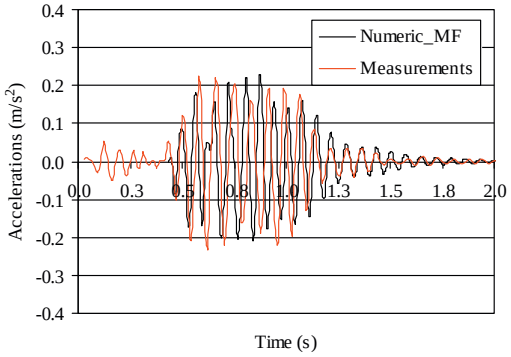

Figure 2.6: The comparison between the measured and simulated response acceleration for viaduct 12 and locomotive 1116 is generally good. The numerical model is not able to identify the small accelerations before the train passes over the point of interest, but during and after train passage the amplitudes are closely matched [Rigueiro et al., 2010].

The train specified is composed of two locomotives and twenty-six coaches. The three load models were based on:

- Moving concentrated forces,
- Multi-degree of freedom train-wagon systems (As discussed further below and shown in Figure 2.11), and
- Single degree of freedom sprug-masses (As discussed further below and shown in Figure 2.10).

The latter two load models will be discussed in more detail in the following section of this review. Martino [2011], who investigated the response between speeds of 50 km/m and 200 km/h, found that the dynamic amplification of each load model is highest at the critical speed of 120 km/h. Resonant vibrations were also clearly detected at 60 km/h for the moving forces model and sprung-mass model as can be seen in Figure 2.7. Furthermore, the comparison between the different load models found that the concentrated forces model provided an upper bound of the response acceleration at mid-span of the bride, compared to the train-wagon system which provided a lower bound. Generally, at non-resonant speeds all three models are in good agreement.

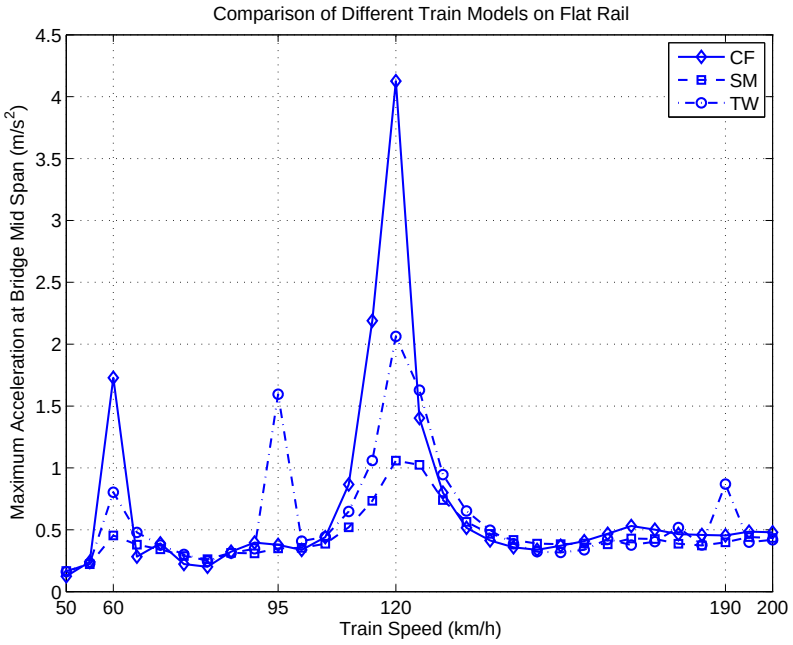

Figure 2.7: Comparison of the concentrated forces, train-wagon and sprung-mass load model for speeds between 50 km/h to 200 km/h, for $\Delta v = 5$ km/h and where CF stands for concentrated forces, SM for sprung-mass, and TW for train-wagon [Martino, 2011].

The resonant phenomena which were identified at speeds of 60 km/h and 120 km/h were due to the excitement of the bridges first eigenmode of 2.37 Hz [Martino, 2011]. The critical wavelengths for these two speeds was calculated to be 7 m and 14 m respectively. It is interesting to note that the train-wagon model has identified two other peaks at 95 km/h and 190 km/h. These speeds do not excite any of the bridges symmetric eigenmodes, but Martino [2011] noticed that the main frequencies that compose the signal when the train-wagon load model is used is $f_1 = 1.87$ Hz, $f_2 = 2.37$ Hz and $f_3 = 3.73$ Hz. At the critical speed of 95 km/h the critical lengths of the first and third mode is approximately 14 m and 7 m respectively, identical to the critical wavelengths at 60 km/h and 120 km/h for the first eigenmode. Martino [2011] believes that this could be due to the inertial effect of the wagons which stimulates the second mode of the model. Unfortunately, no field measurements were available for the investigation, however, results seem to be within reason.

In summary of the moving forces load models, it can be concluded that the model provides results which are in good agreement with both measured data and other provided numerical models at non-resonant speeds. The simplicity of the model is an advantage during numerical investigations due to faster computational time. Further, the only parameter required for the model is the axle load of the train being modelled. Unfortunately, the inertial effect of the vehicle is not considered but the mass of the vehicle can be added to the mass of the bridge for the analysis. If resonance is of importance in a particular investigation alternative models which consider vehicle-rail interaction should be considered. This type of model is discussed in the following section.

2.3.2 Moving concentrated load with masses

If the inertial forces of the vehicle are significant the mass of the vehicle can be fixed at midspan of the bridge, or in some cases in the first third of the span [Frýba, 1996]. This simplification also stands when the action of a whole train is investigated and the mass is evenly distributed along the bridge, even speeding up the analysis [Frýba, 1996].

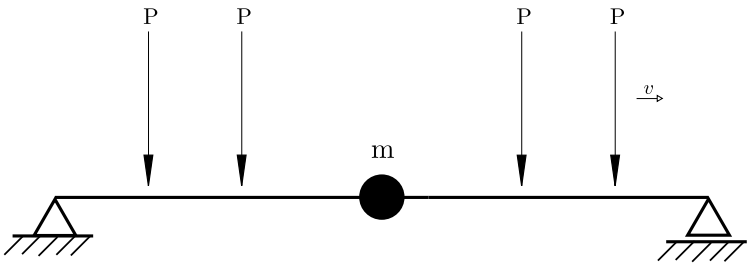

Figure 2.8: Moving concentrated forces model with train mass lumped at midspan.

According to *Eurocode* (EN 1991-2) [2003], the added mass of the train may be ignored in most cases. Neglecting the mass when the weight of the train is considerable, as is such the case for heavy haul trains, may have a significant impact on the dynamic response and it is likely that the deck acceleration and the critical train speed at which resonance occurs will be estimated incorrectly. Whereas both these cases may still result in acceptable values for the limit state designs, there will be inaccuracies if they were applied for assessment purposes.

Research on dynamics of heavy haul railway bridges hasn't been as extensively explored as high speed rail, and there has been no indication that this technique has been applied when the literature was analysed for this review. It may also be important to investigate the difference in performance of two models which do and do not account for the added mass of the train.

2.3.3 Moving masses

An axle load of a train can also be adequately be represented as a concentrated mass, as shown in Figure 2.9. This allows the weight and the inertia force to be accounted for [Frýba, 1996].

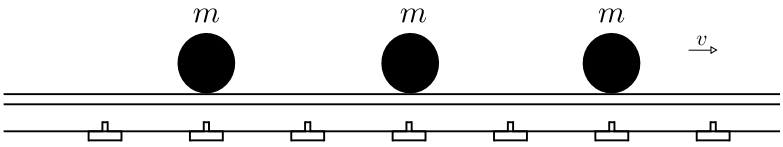

Figure 2.9: Moving concentrated mass model.

Mao and Lu [2011] studied the critical speed and resonance behaviour of railway bridges subjected to moving trains. In the study, numerical investigations using

FEM were carried out to examine the variation in the critical speed with the amount of moving mass. Mao and Lu [2011] reinforces the notion that when the train mass is significant with regards to the bridge mass (i.e., the vehicle – bridge mass ratio is high), the bridge fundamental frequency will be altered and the train mass should therefore be considered in the model. However, this may be more challenging than it appears. As put forward by Mao and Lu [2011], if the variation of the effective combined mass in the system is significant, in fact, the frequency of the system cannot be treated as a constant and there will be no clearly defined resonance speeds. Mao and Lu [2011] then recommends that an effective frequency of the of the bridge-moving mass system be determined.

The only other challenge arising from the moving mass load model is the capability of commercial FE software packages to model it by treating it as a mass and not converting it to a force. Nonetheless, the model has been used in investigations such as Ichikawa et al. [2000] and Saeedi and Bhat [2011] which are alluded to later in the review.

2.3.4 Vehicle interaction load models

Vehicle interaction models aim to simulate the inertial effect of a passing train. The models are constructed by idealising a vehicle as a moving sprung mass connected to an unsprung mass in contact with the rail. These models can be as complex as a full train-wagon system or just as individual axles. Dynamical properties are assigned to the model such that the vehicle has a mass associated with it, as well as a stiffness and damping component. These types of interaction models requires a complex system of nonlinear partial differentiation equations to be solved in order to calculate the contact force between the train and rails.

Rigueiro et al. [2010] investigated the dynamic response of medium-span railway viaducts while accounting for the ballast and using both the moving forces model and the train-structure interaction model. The interaction model used simulated the vehicle with a two degree of freedom, spring mass system consisting of the vehicle mass, m_v, supported by a linear spring and damper connected in parallel to the wheel mass, m_w [Rigueiro et al., 2010]. The stiffness and damping, denoted by k_v and c_v respectively, corresponds to the suspension of the vehicle. The model is illustrated in Figure 2.10.

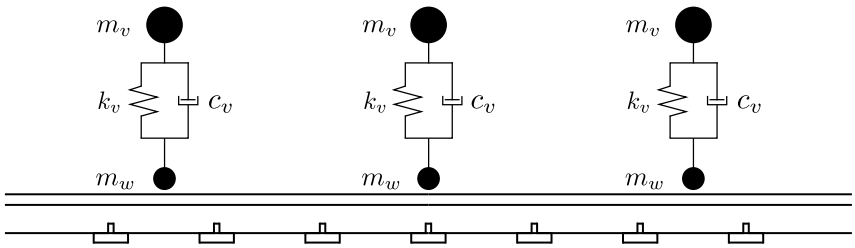

Figure 2.10: Interactive rail vehicle model [Gabaldón et al., 2009; Rigueiro et al., 2010].

The interaction model is comprehensive, but it comes with challenges. Firstly, the parameters such as spring stiffness and damping of the train suspension are difficult to estimate, unless the information is readily availble from the train manufacturer. Secondly, contact algorithms can be used to capture the interaction, however, the accurate computation of the dynamic contact between elastic bodies become complex due to rapid variations of acceleration, velocity and stress fields [Rigueiro et al., 2010]. Solving dynamic problems using the Newmark scheme with the Trapezoidal rule is stable for linear analysis, Rigueiro et al. [2010] noted, but the solution to dynamic contact problems is unstable. Rigueiro et al. [2010] stabilised the solution by introducing numerical dissipation into the time-step analysis to control oscillations from gap constraints at contact points.

The analysis of the acceleration time history clearly showed two distinctive regions. The first region corresponded to the forced vibration of the viaduct during loading, and the second corresponded to the free vibration after the train had passed. Rigueiro et al. [2010] found that the computed frequencies were lower than the measurement. This is likely due to the fact that the mass of the vehicle in the numerical simulation is taken into account by adding mass to the viaducts. After the train's passage the added mass remained in the model. This resulted in the the first natural frequency being underestimated by approximately 7 %. Rigueiro et al. [2010] concluded that the two different load models were only distinguishable in the time domain only for maximum accelerations. When the response was analysed in the frequency domain, for frequencies up to approximately 10 Hz, the different models did not influence the frequency content.

There are instances of a further extension to the sprung-mass model whereby the inertial effect of the train is also accounted for. The model can be thought of as a complete and rigorous vehicle model. Whereas the sprung-mass model the interaction between different axles of the same car is removed, this does not apply for the train-wagon model. The car body is modelled as a rigid mass having second moments of

area about the horizontal axes in both the transverse and longitudinal directions. The same applies to each of the bogies. Each wheel has a mass and the primary suspension between the bogie and wheel set is idealised as a spring-damper system. The same applies to the secondary suspension between the car body and the bogie.

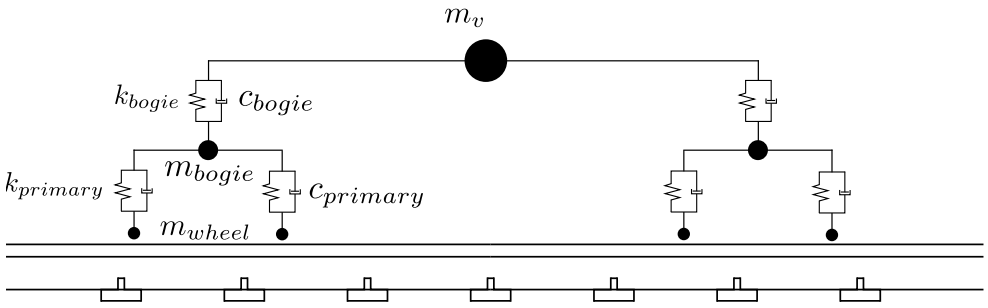

Figure 2.11: Complete train-wagon interaction model used by Martino [2011].

Generally, slight variations of the model appears in literature, depending on the complexity of the researcher's requirements and the available parameters. In a three-dimensional finite element analysis of high speed train-bridge interactions, Song et al. [2003] used a 38 DOF train model based on a TGV-type high speed articulated train. In comparison, Kumaran et al. [2003] used a 17 DOF train model in their dynamic study of rail sleepers in a track-structure system. Detailed models with a high number of DOFs such as these are computationally expensive and require detailed parameters of the train in order to calculate the appropriate properties when idealising it in an FE model.

In an investigation into the dynamic behaviour of a two-span continuous concrete bridge under moving high speed trains Kwark et al. [2004] also adopted such a rigorous train model. The Yeon-Jae bridge investigated is situated approximately 120 km south of Seoul, South Korea. It is a continuous, prestressed concrete, simple box-girder with two equal spans of 40 m each. The dynamic characteristics of the bridge are given in Table 2.2. The Korean high speed train which operates on the bridge is a unique train; successive passenger coaches are separated by a bogie such that each train does not behave independently.

Table 2.2: Dynamic properties of the Yeon-Jae bridge studied by Kwark et al. [2004].

Fundamental natural frequency	Analysis	4.30 Hz
	Test	4.35 Hz
Critical speed	Analysis	289.5 km/h
	Test	292.8 km/h
Effective beating interval		18.7 m
Damping ratio		2.4 %

Kwark et al. [2004] conducted a numerical analysis for speeds from 50 km/h to 300 km/h, increasing the speed in steps of 25 - 50 km/h. A comparison of maximum vertical displacement between a concentrated moving forces model and the interaction model was carried out. Kwark et al. [2004] found that the numerical response of the bridge was in good agreement with the actual response of the bridge. The interaction model used in the study may produce conservative results, but Kwark et al. [2004] recommended using a model that considers the interaction be used when dynamic behaviour is being investigated.

Results from Kwark et al. [2004] show that low displacements (less than 1.5 mm) of the bridge deck were obtained even up to resonant speeds of 300 km/h. Only the fundamental frequency was used to validate the model, and no correlation of mode shapes were shown. When comparing the two load models, Kwark et al. [2004] shows that they are in good agreement with one another, however, the interaction model unexpectedly estimates a greater dynamic amplification factor compared to the moving forces model. This contradicts what most other authors have reported.

Martino [2011] also investigated a train-wagon model in his numerical study. In the study, Martino [2011] modelled the Steel Arrow train as a interaction vehicle. The train which transports iron ore between mines and steel mills in the north of Sweden usually consists of two power cars and twenty-six coaches. The axle load of the power car is approximately 19.5 tonnes and the coaches carry approximately 25 tonnes per an axle. The comparison between load models generally showed that the train-wagon model provided the lower bound dynamic response of the bridge. The models are in very good agreement at non-resonant speeds and each model is is able to identify resonant peaks in the bridge. The only anomaly which needed further investigation was the two peaks identified by the train-wagon model at speeds of 95 km/h and 190 km/h.

In summary of the load models reviewed, the studies show the use of the moving concentrated load models provide satisfactory performance but they do not capture the train-track interaction. The concentrated moving forces models were in good agreement with measured data and with the the vehicle interaction models at non-resonant speeds. At resonance, the concentrated forces model overestimates the dynamic amplification of the structure. It was advised that the sprung-mass or train-wagon interaction models be used where ever possible. However, a limiting factor of the interaction models is that more information is required to construct an accurate model. If this information is not available or accurate, results may be unreliable and the concentrated forces model should rather be applied. The investigations reviewed involved trains with relatively low axle loads, and therefore low train-bridge mass ratios. In the case of very heavy trains with axle loads which leads to high train-bridge mass ratios, it is clear that the dynamic properties of the bridge will be altered during train passage. It is therefore necessary to account for the additional mass by, for example, equally distributing it and lumping it at the nodes of the FE model of the bridge.

2.4 Dynamic performance of continuous girder bridges

The dynamic properties and response of a continuous beam is complex. Surprisingly, according to Saeedi and Bhat [2011], the dynamic behaviour of continuous, multi-span beams has not been studied extensively. That being said in the general sense, there has been even less investigations into the dynamic behaviour of multi-span railway bridges. Most of the investigations, such as Cheung et al. [1999], Ichikawa et al. [2000] and Johansson et al. [2013], which have been conducted choose not to use FEM for their studies for reasons such as the amount of input and computational power required. These authors have favoured the use of analytical approaches to find an exact solution to the problem of moving forces and masses on continuous beams in a simpler and faster manner so that it can be used in the early stages of the design process, and with little effort. In this section, the dynamic behaviour and response of continuous beam-type structures are reviewed.

2.4.1 Dynamic behaviour

According to Frýba [1996], the most important dynamic characteristics of railway bridges are their natural frequencies. Frýba [1996] shows that the calculation of natural frequencies for continuous beams is similar to that of single span beams. The calculation is solved span-wise, resulting in a concentration of natural frequencies. These concentrated zones (or clusters) contain a number of natural frequencies equal to the number of spans in the beam, at a close spacing, assuming a constant beam cross-section.

The determination of natural frequencies and mode shapes for a continuous beam was studied as early Lin [1962], who investigated free vibrations of a continuous beam on uniformly spaced elastic supports. In the study elastic supports were assumed to provide constraints in the vertical direction, and rotationally. By example, Lin [1962] used a 6 span continuous beam to compute (numerically) the eigenvalues for different spring stiffness for the supports.

The first noteworthy outcome from Lin's [1962] investigation is regarding the spatial periodicities in mode shapes. Lin [1962] showed that the mode shape for a beam with number of spans N, with elastic interior supports and hinged exterior supports, can be extended to a continuous beam with the number of spans equal to $2N$ by rotating the mode shape of the N-span beam by 180 degrees. This notion is clearly illustrated in Figure 2.12.

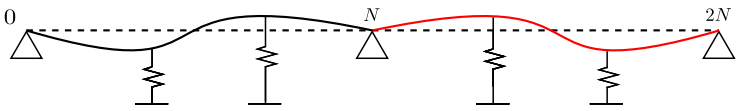

Figure 2.12: Spatial periodicities of mode shapes in continuous beams with elastic supports.

Lin [1962] notes that neither the boundary conditions or continuities (deflection and slope) are violated and the dynamic characteristics of the extended $2N$-span continuous beam remain the same of the original N-span beam. Hence, the corresponding modal frequency is unchanged. Furthermore, Lin [1962] notes that the same reasoning may apply to other types of exterior supports, but this might not guarantee a spatial periodicity.

In the numerical examples of Lin [1962], the interior boundary conditions were

considered to be identical with k_1 depicting the vertical stiffness and k_2 depicting the rotational stiffness at each support. The exterior supports are hinged, as discussed earlier. The number of spans in each concentrated group is expected to be equal to the number of spans (6), however, when the vertical stiffness is low and the rotational spring is completely rigid, only 5 frequencies were computed in each cluster.

Lin [1962] also deduced that as the vertical and rotational stiffness approaches infinity each span becomes independent of each other and each cluster of frequencies approaches only a single value. Lastly, and perhaps most critical to this work, Lin [1962] concludes that if there are numerous continuous spans, the boundary conditions of the exterior spans do not materially affect the interior spans, and therefore, any supporting conditions at the exteriors will be acceptable.

More recently, Saeedi and Bhat [2011] investigated the cluster of natural frequencies in multi-span beams using constrained characteristic functions. In the study, Saeedi and Bhat [2011] acknowledges that the method proposed by the likes of Frýba [1996] whereby a multi-span beam is divided into single span beams is more accurate as an exact solution can be obtained. However, this might generate a large problem when dealing with multi-span beams of a high number due to the compatibility constraints at the supports. Saeedi and Bhat [2011] therefore proposes diving the continuous beam into single-spans with forces acting on the supports. Although the approach is similar to that of Frýba [1996], fewer mathematical operations are required as the conditions such as the continuity at supports no longer need to be satisfied.

In one of the case studies presented by Saeedi and Bhat [2011] numerical solutions of the dimensionless frequencies for a simply supported continuous beam with six equal spans are compared to that of Lin [1962]. The agreement between the two studies is excellent, the results are tabulated in Table 2.3. Mode shapes of the first concentrated cluster of natural frquencies is also shown in Figure 2.13. Saeedi and Bhat [2011] also supports the study by Lin [1962] by noticing that all the odd-numbered mode shapes are anti-symmetric with respect to the beam centre, and the even number modes are symmetrical.

FEM has also become a tool capable of calculating natural frequencies and mode shapes of continuous beams. The advantages of this method, as reported by Rieger [1986], include the ability to solve large structural dynamics problems using high speed computers. This implies that continuous, multi-span beams which may have been highly inefficient to solve analytically, can be solved faster, and to a good degree of accuracy. Although this method is widely known, most of the work on multi-span, continuous beam-type structures have focused heavily on analytical

Table 2.3: Natural frequencies for six-span beam. $\beta^4 = \frac{\rho A \omega^2}{EI}$ [Saeedi and Bhat, 2011].

Mode	$\beta\frac{L}{6}$ [Lin, 1962]	$\beta\frac{L}{6}$
1	π	3.1416
2	3.260	3.2605
3	3.557	3.5564
4	3.926	3.9266
5	4.296	4.2975
6	4.601	4.6014
7	2π	6.2832
8	6.409	4.4098
9	6.708	6.7076
10	7.068	7.0685
11	7.462	7.4295
12	7.726	7.7269

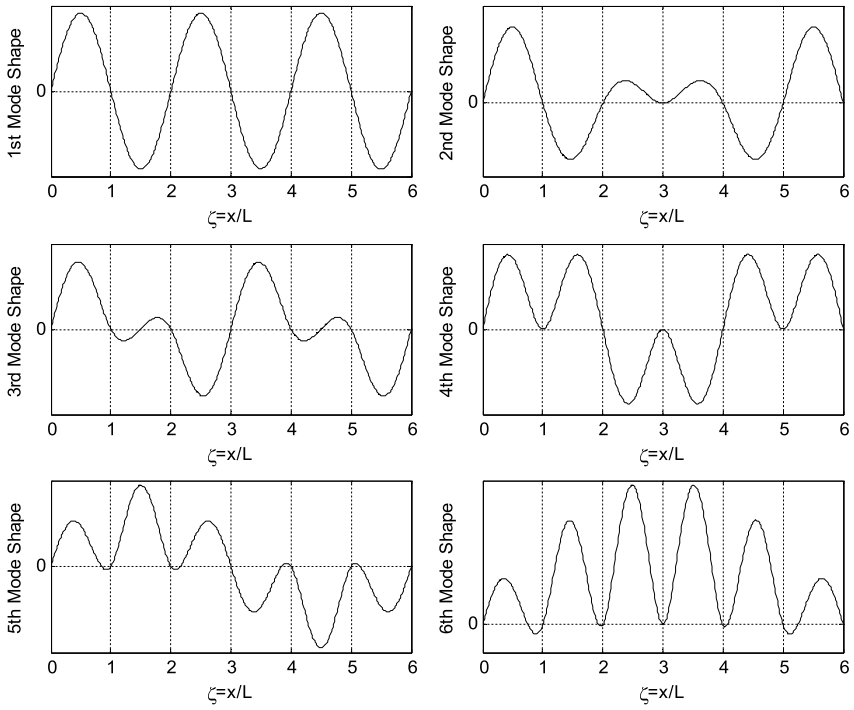

Figure 2.13: Normalized mode shapes 1 – 6 for a six span continuous beam, where ζ is the non-dimensionalised beam span parameter [Saeedi and Bhat, 2011].

procedures, as opposed to the newer numerical approach. Where FEM has been applied, it has generally been done as a comparison to experimental works such as Ambient Vibration Testing (AVT) or Forced Vibration Testing (FVT). The reason was not explicit in the literature which was reviewed for this work, however, some authors did acknowledge that the analytical approach is preferred as it can be applied in practice, during the early stages of design. Furthermore, the application of FEM requires knowledge of the numerical procedure and the solvers designed for certain problems.

2.4.2 Dynamic response to moving loads

Ichikawa et al. [2000] reinforces the notion that, although the dynamic behaviour of railway bridges subjected to moving loads or masses has been investigated for over a century, most of the investigations have only considered single-span simply supported beams. The investigations which were found in literature explored only analytical methods of calculating the dynamic response to moving loads or masses. Nonetheless, some interesting findings were made. A succinct summary of the moving load problem on continuous beams is provided by Johansson et al. [2013].

In two of the case studies in Johansson et al. [2013], the response of a three-span continuous beam caused by a moving load is solved using modal analysis and compared to the results from a FE model. Normally, modal analysis is solved numerically, which can have certain shortfalls. Contrastingly, Johansson et al. [2013], presented an exact closed-form solution to solve the equations of motion. The first case-study considered a bridge with three equal 20 m spans. The central span was twice as stiff as the outer two spans and the bridge was exposed to a single moving point force travelling at 34 m/s. The second case-study involved a haunched concrete beam with span lengths of 18 m, 24 m and 18 m with a four-axle moving vehicle travelling at 50 m/s. The results of the case studies are shown in Table 2.4 and Figures 2.14 to 2.19.

Johansson et al. [2013] obtained excellent agreement between the closed-form derivation and the results from the FE model. Further to this, Ichikawa et al. [2000] conducted a similar investigation for a moving mass travelling along a beam. The main purpose of the study was to investigate the inertial effect of the mass. Ichikawa et al. [2000] considered a continuous beam with two to four spans, based on the following assumptions,

i. The beam obeys Euler-Bernoulli beam theory and linear elasticity.

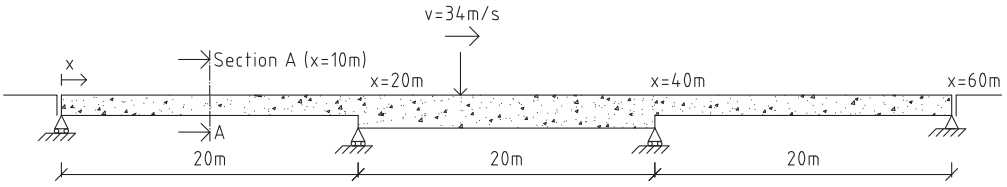

Figure 2.14: Three span continuous beam investigated in case-study 1 [Johansson et al., 2013].

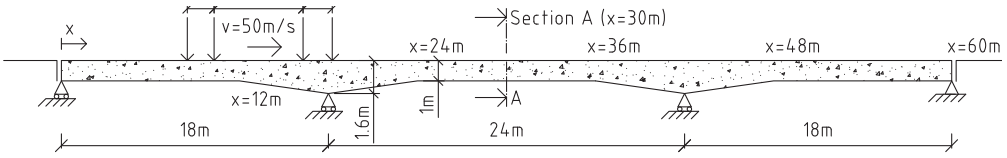

Figure 2.15: Three span continuous beam investigated in case-study 2 [Johansson et al., 2013].

Table 2.4: Natural frequencies from case-study 1 & 2 [Johansson et al., 2013].

	Case-study 1		Case-study 2	
Mode	$f_{n,analytical}$ [Hz]	$f_{n,FEM}$ [Hz]	$f_{n,analytical}$ [Hz]	$f_{n,FEM}$ [Hz]
1	6.204	6.204	3.839	3.839
2	7.581	7.581	8.149	8.150
3	11.974	11.974	13.622	13.622
4	24.207	24.210	21.678	21.687
5	26.439	26.443	24.976	24.976

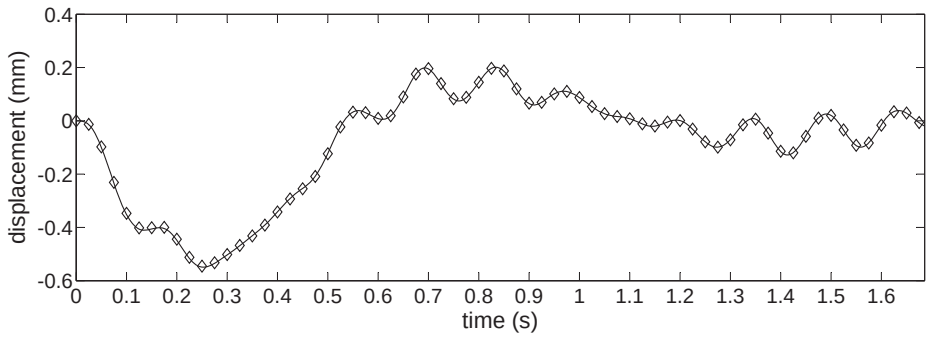

Figure 2.16: Displacement time history at mid-span of the first span of case-study 1. (–) Analytical, ◊ FEM [Johansson et al., 2013].

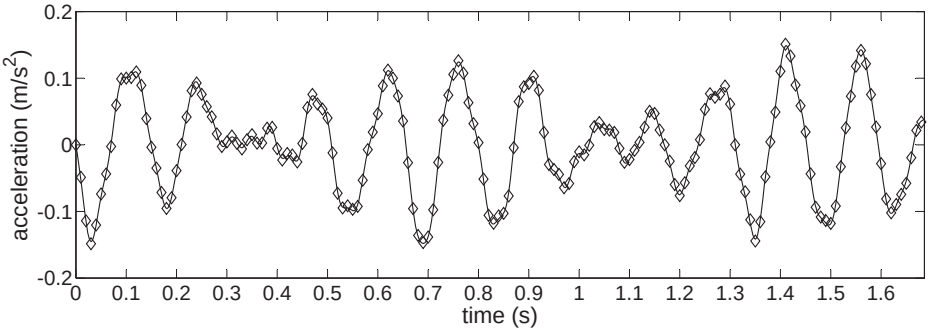

Figure 2.17: Acceleration time history at mid-span of the first span of case-study 1. (–) Analytical, ◊ FEM [Johansson et al., 2013].

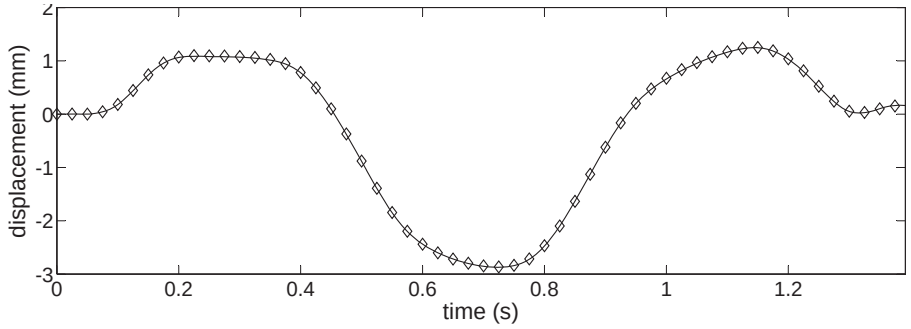

Figure 2.18: Displacement time history at mid-span of the first span of case-study 2. (–) Analytical, ◊ FEM [Johansson et al., 2013].

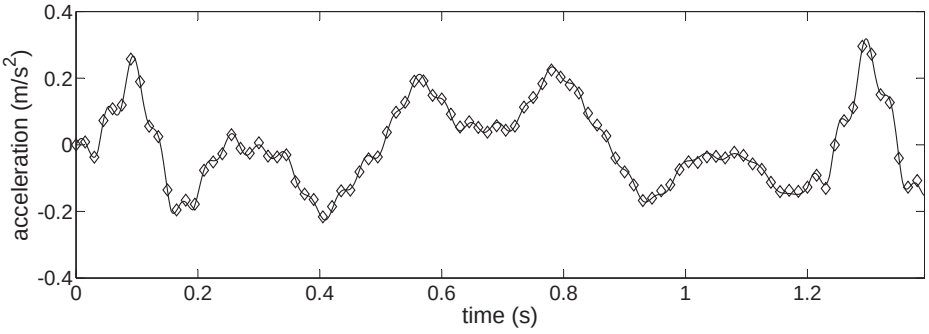

Figure 2.19: Acceleration time history at mid-span of the first span of case-study 2. (–) Analytical, ◊ FEM [Johansson et al., 2013].

ii. The moving mass remains in contact with the beam.

iii. The initial condition of the moving mass is that it is located at the left-hand end of the beam.

For the study, velocity was non-dimensionalised and the mass ratio was defined as the mass of the moving load to the mass of the first bridge span. Ichikawa et al. [2000] made the following interesting findings,

i. The inertia of the moving mass had a greater influence on the second and successive spans.

ii. For low values of the dimensionless ratio up to 0.5 the difference between the moving forces and moving mass did not differ significantly.

iii. The dynamic amplification factor at the mid-span of the first span was not influenced by the total number of beam spans (from two to four) and was not affected up to the velocity ratio of 0.5. When exceeding 0.5, higher mass ratios resulted in higher amplification factors.

iv. The amplification factor was generally low up to a velocity ratio of 0.9 in the second span of each model. When exceeding that, the amplifications were greater compared to that of the first span and also increased as the mass ratio increased.

Building on this, Ebrahimi et al. [2015] explored the vibration of a multi-span beam excited by a moving oscillator. Instead of idealising the moving load as a force or mass, a moving mass is coupled to the bridge as a single degree of freedom (SDOF) through a non-rigid connection with spring of stiffness k and dashpot of damping c. The oscillator is assumed to traverse the beam at a velocity v. This model is illustrated in Figure 2.20.

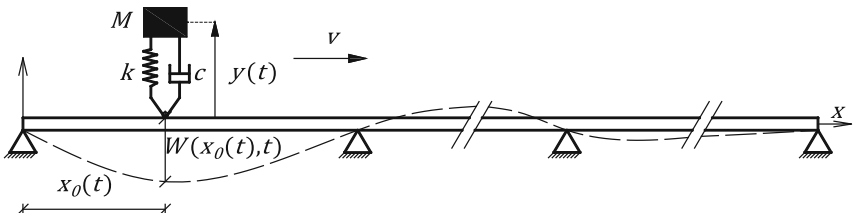

Figure 2.20: Idealisation of the SDOF model proposed by Ebrahimi et al. [2015].

Ebrahimi et al. [2015] illustrates his series-based solution to the problem by example, assuming a multispan beam having uniform spans of 20 m with flexural rigidity $EI = 1.96 \times 10^9 Nm^2$ and mass per unit length $\rho A = 10000\ kg/m$. The oscillator is assumed to be undamped; η, γ and α are considered to normalise the frequency, mass and speed [Ebrahimi et al., 2015]:

$$\eta = \frac{\omega_{OS}}{\omega_0}$$

$$\omega_{OS} = \sqrt{\frac{k}{m}}$$

$$\omega_0 = \frac{\pi^2}{L_1^2}\sqrt{\frac{EI}{\rho A}}$$

$$\gamma = \frac{M}{\rho A L_1}$$

$$\alpha = \frac{v}{u}$$

$$u = \frac{\pi}{2L_1}\sqrt{\frac{EI}{\rho A}}$$

Ebrahimi et al. [2015] compared the dynamic response of a four span beam at the midpoint of the second span with that of Ichikawa et al. [2000]. Very good agreement was achieved between the two studies - the results of which are shown in Figure 2.21. Furthermore, Ebrahimi et al. [2015] conducted parametric studies of the dynamic amplification factor (DAF) of beams with one, two, three and four spans for a range of velocity parameters from $0 < \alpha \leq 2$; normalised moving oscillator frequencies of $\eta = 0.10, 0.60, 1.00, 1.25, 2.00, 5.00$, and inertia parameters $\gamma = 0.1, 0.2, 0.3$ and 0.4. The parameter associated to the moving oscillator frequencies η can essentially be interpreted as the spring stiffness of the oscillator, where the lower bound value of $\eta = 0.10$ translates to a low stiffness, this was compared to the moving force model of Ichikawa et al. [2000]. For a high value of $\eta = 10$ the spring is infinitely stiff, this was compared to the moving mass model of Ichikawa et al. [2000]. The other parameters are straightforward. The results of the study by Ebrahimi et al. [2015] is presented through the DAF for the various cases in Figures 2.22 to 2.25.

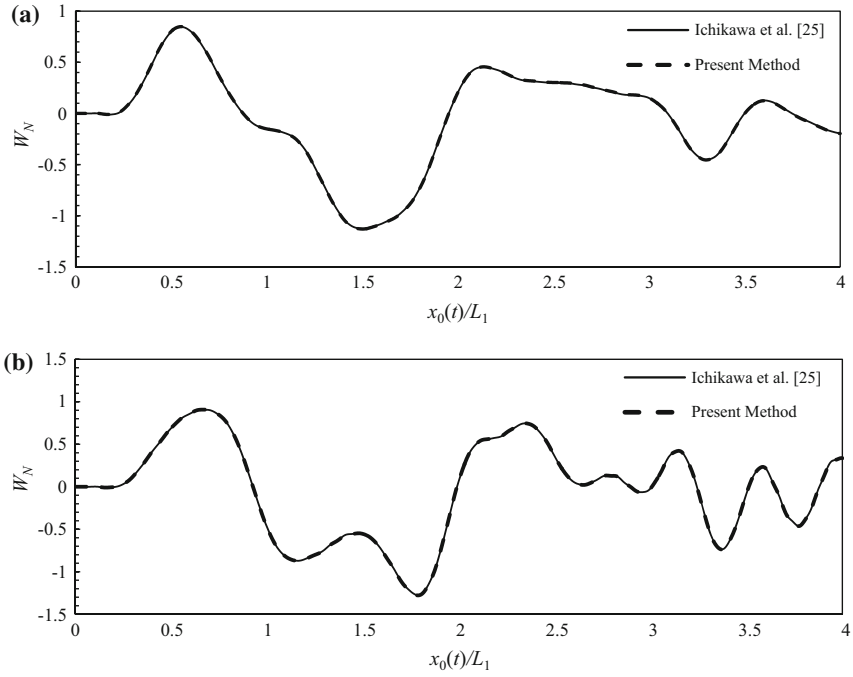

Figure 2.21: Comparison of dynamic response between Ebrahimi et al. [2015] and Ichikawa et al. [2000] at midpoint of second span of four span beam.

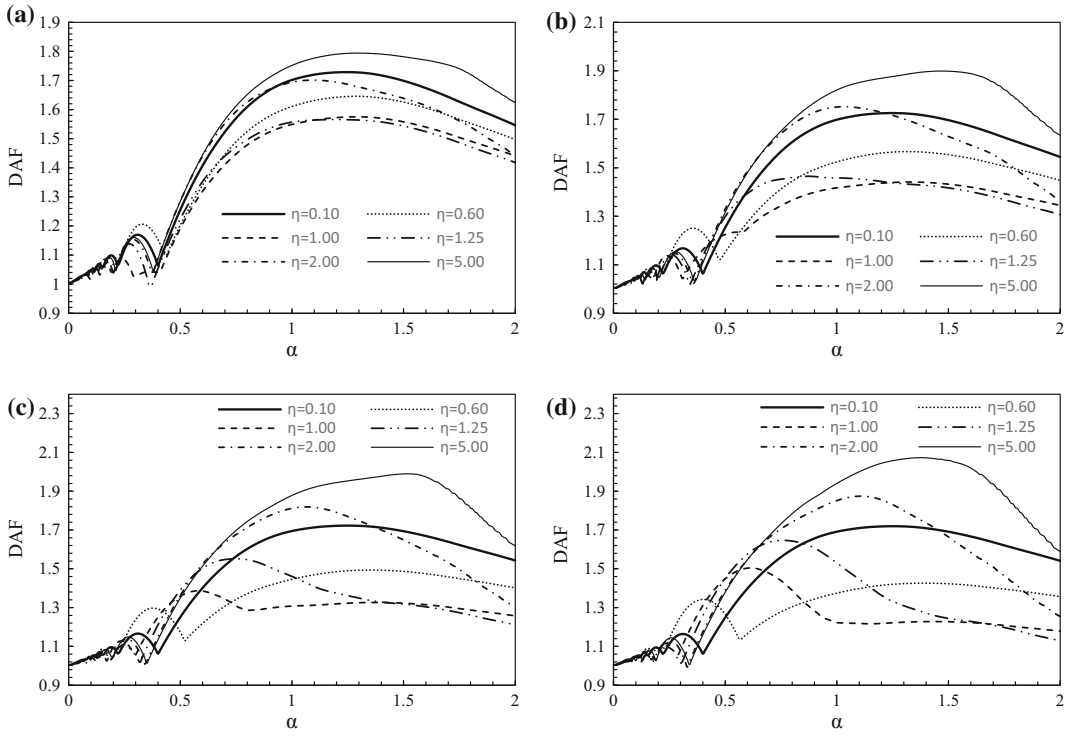

Figure 2.22: Normailsed maximum dynamic amplification factor for a single span beam. (a) $\gamma = 0.1$, (b) $\gamma = 0.2$, (c) $\gamma = 0.3$ and (d) $\gamma = 0.4$ [Ebrahimi et al., 2015].

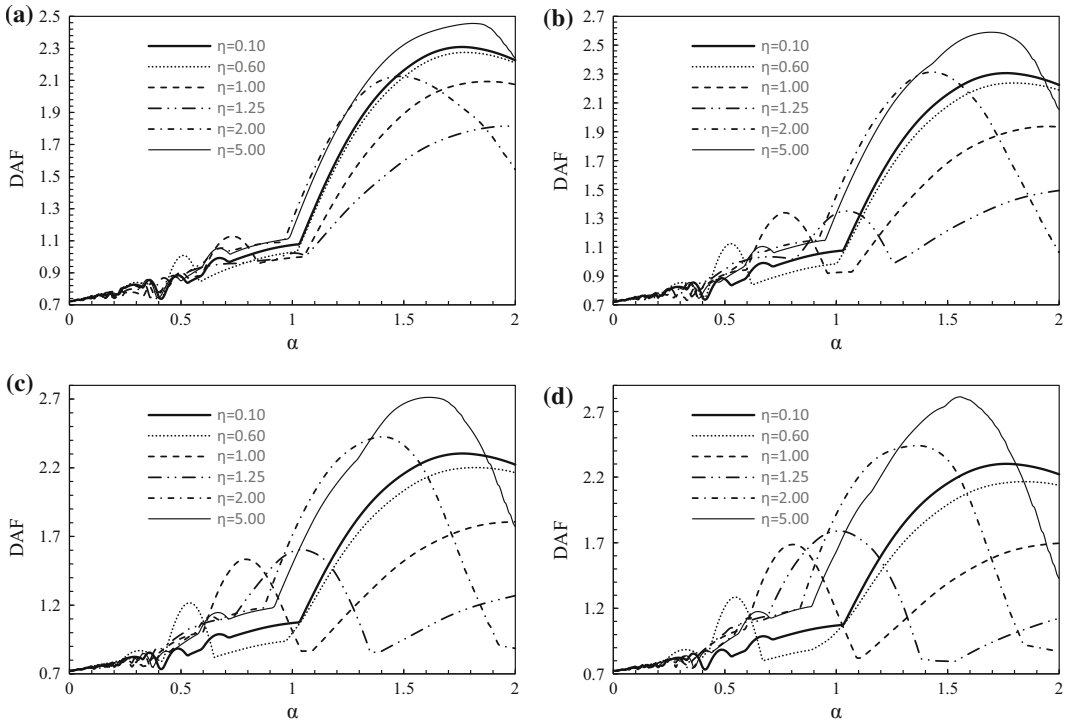

Figure 2.23: Normalised maximum dynamic amplification factor for a two span beam. (a) $\gamma = 0.1$, (b) $\gamma = 0.2$, (c) $\gamma = 0.3$ and (d) $\gamma = 0.4$ [Ebrahimi et al., 2015].

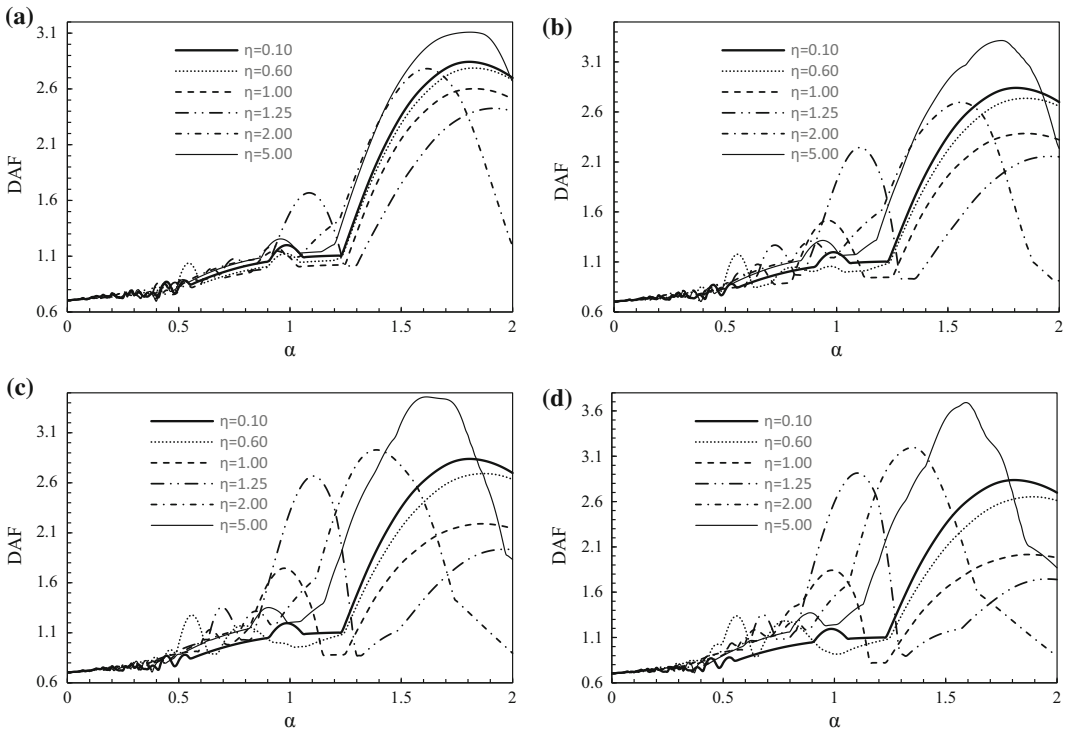

Figure 2.24: Normalised maximum dynamic amplification factor for a three span beam. (a) $\gamma = 0.1$, (b) $\gamma = 0.2$, (c) $\gamma = 0.3$ and (d) $\gamma = 0.4$ [Ebrahimi et al., 2015].

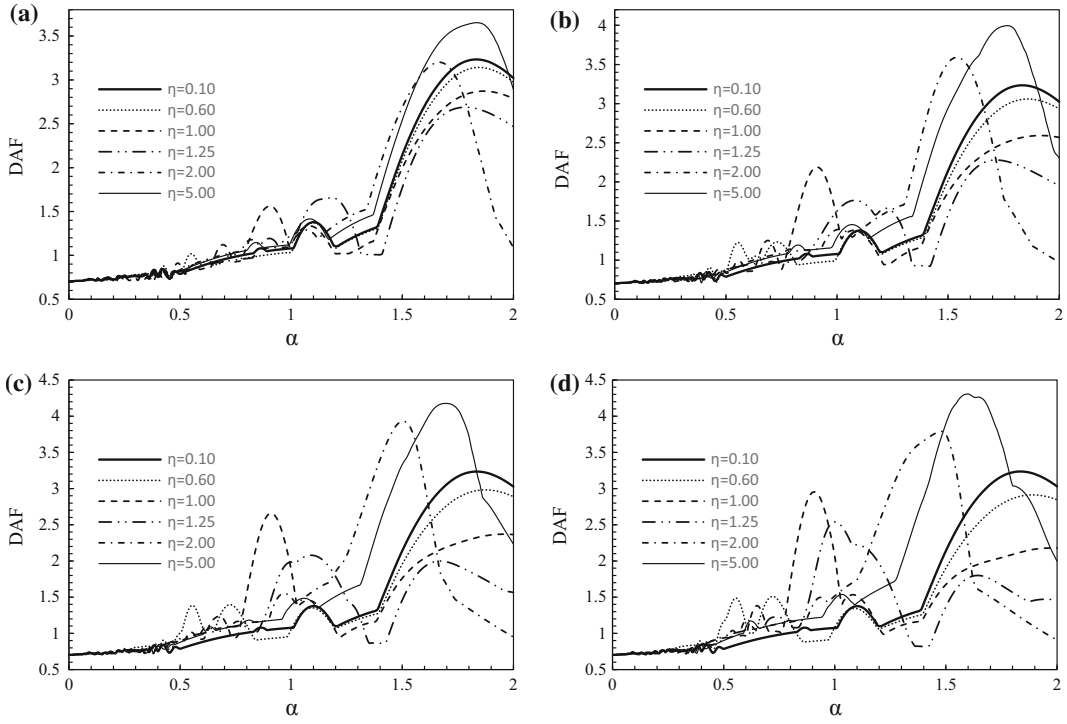

Figure 2.25: Normailsed maximum dynamic amplification factor for a four span beam. (a) $\gamma = 0.1$, (b) $\gamma = 0.2$, (c) $\gamma = 0.3$ and (d) $\gamma = 0.4$ [Ebrahimi et al., 2015].

In summary, the interesting findings from these results from Ebrahimi et al. [2015] are as follows:

i. For all number of spans the DAF is not affected by the stiffness of the oscillator spring when the velocity parameter $\alpha < 0.2$.

ii. There was a considerable difference in the dynamic response between the single span beam and the multi-span beams. For the single span beam the amplification increases exponentially from approximately $\alpha = 0.4$ and the maximum DAF is generally for the moving oscillator with low stiffness ($\eta = 0.10$). In the case of the multispan beams the DAF increases significantly only when the velocity parameter $\alpha > 1$ and the maximum amplification is generally for the oscillator with the higher normalised frequency of $\eta = 5.00$.

iii. Interestingly, for the multispan beams, the peak amplification was obtained for the intermediate oscillator stiffness ratios of $\eta = 0.60, 1.00, 1.25, 2.00$ for the velocity parameter within $0.40 \leq \alpha \leq 1.25$.

iv. Lastly, for beams with three and four spans, the DAF for the different spring stiffness values are more variable between the velocity parameters of $0.5 \leq \alpha \leq$

1.5.

Ebrahimi et al. [2015] concludes with the important observation that the DAF rises considerably as the number of spans increase. However, this does not necessarily imply that the response of the bridge in terms of displacement has increased, as the maximum static response might be significant lower. The study, in general, provides good insight into the dynamic response of continuous beams. The numerical example is on a smaller scale in terms of the size of beam and span length than that of a large scale railway bridge carrying heavy haul traffic. The results which show that the low stiffness oscillator does not necessarily produce the conservative result of a high amplification and the high stiffness oscillator the lower bound amplification is also in contrast to most of the other literature which implies that the moving forces approach is conservative.

These above mentioned studies show the status quo regarding the dynamic performance of continuous beam-type structures exposed to moving forces or masses. All of these studies have focused on analytical procedures to solve the problem of a moving force or mass on a beam, however, FE modelling has often been used to support their investigations. The lack of research in this area is clearly evident, this being one of the motivating factors for this research.

2.5 Concluding remarks

The problems associated with the dynamics of railway bridges were broadly defined into two categories: those with high speed rail and those with heavy haul rail. The literature review shows a substantial amount of research which has been carried out on high speed rail since it's evolution, however there is a lack of investigations on HH railway bridges. The problems of high speed rail tend toward safety concerns and the possibility of resonance, whereas this is still likely (yet improbable) in heavy haul railway bridges, excessive vibrations may lead to destabilisation of the ballast, higher maintenance costs and fatigue implications. Also, there is a lack of guidance from codes of practice as to how heavy rail traffic with long trains should be accounted for in design.

Moving forces, masses and interaction type load models which are generally used for research purposes were reviewed. The concentrated forces load model which represents the axle load of a train is easy to model and good results have been achieved at non-resonant speeds. The disadvantage of the model is that it does

not consider the inertial forces of the train, which the interaction models do. The interaction load models have not been warranted at non-resonant speeds as it is shown that, generally, precise results can be achieved with the simple concentrated loads prescribed in the codes or distributed loads discussed in some of the other literature. Above this there are other challenges which the model faces. It requires a number of parameters which are not easily accessible and it is computationally expensive.

Lastly, investigations which consider multi-span beam type structures were reviewed. The dynamic properties of continuous beam-type structures were discussed and investigations which focus on analytical methods to solve the problem of moving forces or masses on a beam were reviewed. From these it is clear that there is a shortfall of research on the specific problem of continuous, multi-span girders and on heavy rail traffic (especially considering the additional mass of trains). These particular issues are the underlying factors which motivate this study.

Based on this review further work in the dynamic properties and response of continuous, multi-span bridges carrying a long sequence of moving heavy loads is needed. This dissertation will therefore focus on, firstly, conducing a parametric study of a continuous, box-girder type bridges with a number of different span configurations and for trains travelling at different speeds. Secondly, a case-study will be conducted whereby results for the dynamic properties and response of the first 11-span segment of the ORV from a numerical model is compared to some experimental measurements and analytical data which has been presented by other authors. The following chapter will outline the methodology of the research in light of these aims.

Chapter 3

Methodology

3.1 Introduction

This thesis is divided into two two main parts. Firstly, a numerical investigation of continuous multi-span railway bridges is conducted as a parametric study. Different bridge configurations will be defined and their dynamic properties and response calculated and analysed. Secondly, a case-study will be conducted. This will involve modelling an 11-span continuous girder of the ORV and extracting dynamic properties and response to moving train loads. These will be compared to measurements and analytical data from other authors.

In this chapter the problem which this thesis aims to address is defined, along with the scope of works. The approach to conduct this work is also presented, including, details of the the FEM software package and work flow, properties of the bridge and train which are to be modelled, and details of the numerical analysis method used.

3.2 Problem

As was shown in the literature review, the problem of dynamics of continuous beam-type structures is complex. There has been numerous investigations into both the dynamic properties (mode shapes and natural frequencies) and response to moving loads. In the context of railway bridges there is substantial research of the dynamics to short spanned railway bridges, especially in response to high speed trains. There is, however, clearly a lack of information regarding the dynamics of multi-span, continuous, railway bridges which are trafficked by heavy loads.

The problem, therefore, this thesis addresses is firstly the dynamic properties and response of a large-scale, continuous girder with a single track. The dynamic

properties of these type of structures become even more complex as the number of continuous spans increase, due to the cluster of modes in the concentrated zone. This work will look at a number of multi-span, continuous bridge configurations and analyse how the natural frequencies and mode shapes change as the number of spans increase. The same will be done in terms of there dynamic response to a moving load. The dynamic response parameters of particular interest will be limited to the displacement time history and acceleration time history. Further to this, a case-study on the ORV is also conducted. The ORV is the longest bridge of its kind in South Africa, and is trafficked by very long trains with high axle loads at low-moderate speeds. Some experimental and analytical work has already been done by other authors, and information such as natural frequencies, mode shapes and some displacement and acceleration data is available to compare to values calculated by the numerical model.

The ORV does not have a completely uniform cross-section so determining its dynamic properties and response precisely through analytical methods is challenging. The fact that the bridge is very large also makes the problem very difficult to solve. The Finite Element Method was therefore chosen as a critical tool to assist in addressing this problem.

3.3 Scope of thesis

The numerical investigation of the multi-span, continuous bridge configurations entail the determination of the natural frequencies and mode shapes, and the response of the different configurations to moving loads at different speeds. Only the vertical behaviour of the bridge is of interest to this research. The geometry of the cross-section of the girder remained constant, and was based on the box-girder of the ORV. The length of spans investigated were 40 m, 45 m and 50 m. The span – height ratio of 1:12 of the 45 m ORV span was kept constant, and the height of the box-girder for the 40 m and 50 m spans were therefore reduced and increased, respectively, by changing the height of the webs. The ORV is a straight, level bridge and therefore all bridge configurations analysed were also modelled as level and straight.

No track system was modelled on the bridge, and the axles of the train was assumed to act directly on the bridge. Modelling a ballasted track itself is a complex procedure. There are numerous track models which require a number of input parameters, such as the mass density, stiffness and damping of ballast. This information was not available, and is difficult to estimate. Modelling a track system on such a large-scale

bridge would also increase the computational cost beyond the available computing power.

Modelling the pier supports was also avoided. Only the vertical behaviour of the bridge deck is of interest to this work, and the piers have little impact on this. Including the piers would also increase the computational cost, as the FE program would also calculate the lateral behaviour of the bridge. The abutments and supports were therefore modelled using simple supports with the relative degrees of freedom fixed.

The load train model which was used in the calculation of dynamic response of the bridge was based on a fully loaded series of four-axle CR-13 wagons which run on the ORV's rail line. The load model was based on the moving concentrated forces model which was discussed in the review. Each axle of the wagon was represented by a concentrated load, and the spacing between forces was defined as the same distance as the spacing on the CR-13 wagon. An empty train was not considered for this investigation, and the forces due to the driving locomotives was also ignored. In each train consist which operates on the ORV there is normally less than one locomotive per 100 wagons, and the affect of the locomotives are therefore considered to be insignificant to the dynamics of the bridge. The dynamic response calculation was limited to a length of only 30 wagons (a train of approximately 320 m) due to computational cost. Horizontal forces such as braking and acceleration was also ignored, and as the bridge is completely straight transverse forces were also ignored.

Acceleration and displacement time histories were determined for speeds ranging from 20 km/h to 100 km/h, in 20 km/h intervals. This interval is quite broad considering that HH trains travel at speeds lower than 100 km/h and the maximum permissible speed on the ORV is limited to 50 km/h. The range from 20 km/h to 100 km/h was therefore chosen purely for research purposes. To account for the effect of train mass, the moving forces load model was also run with the mass of the train lumped equally at the nodes of the bridge. In summary, the parameters which have been discussed here have been summarised in Table 3.1.

Table 3.1: Summary of parameters which were investigated.

Description	Parameters investigated
Span lengths	40 m, 45 m, 50 m
No. of continuous spans	1 – 10
Speeds	20 km/h – 100 km/h in 20 km/h intervals
Mass of train	With and without lumping the mass of train (10 t/m) at the nodes

3.4 Finite Element model

The commercial FEM software package SOFiSTiK was used for the numerical modelling of the bridge and train loading. The work-flow which was used to solve this problem was divided into the following four main steps:

i. Material definition.

ii. Defining cross-section & geometry.

iii. Assigning the finite element, meshing & boundary conditions.

iv. Defining the train loading.

The material properties, cross-section and geometry of the bridge was extracted from the available information (constructions drawings, research papers and presentations from Busatta and Moyo [2015], Kuys [2009] & Ngwenyama et al. [2013]) of the ORV and modelled in SOFiSTiK. The loading in the numerical model was also derived from the trains which are currently commissioned to operate on the bridge. The precise parameters which were used in the final model is described below.

3.4.1 The bridge

The FEM model of the bridge was limited to the deck only. Other aspects such as the piers and foundations were not applicable to this investigation, and therefore omitted. The reason for this is that this study is only concerned with the vertical behaviour of the bridge, the transverse behaviour and sway is not considered and the piers and founding conditions, which is assumed to have little influence on the

vertical response, can therefore be ignored. This also allows faster computational time due to a smaller model. Inputs to SOFiSTiK Structural Desktop (SSD) are given below.

3.4.1.1 Material

The bridge was modelled using the definition of a single material. Continuous, multi-span girders are normally constructed out of reinforced concrete (RC) or PSC. In this investigation, the reinforcing materials were ignored, and the mass density of the material defined in SSD was assumed to account for the mass reinforcing material. The normal reinforcement and presetressing tendons also has flexural stiffening effect, this was accounted for in the elastic modulus. Material properties of the bridge are defined in Table 3.2.

Table 3.2: Material properties of FE model.

Property	Symbol	Value
Nominal strength	f_{ck}	40 MPa
Self-weight	γ	24 kN/m^3
Mass Density	ρ	2300 kg/m^3
Elastic Modulus	E	36 GPa
Poisson's ratio	ν	0.2

3.4.1.2 Cross-section & geometry

The graphical user interface (GUI), SOFiPLUS, was used to model the cross-section and geometry of the bridge. A uniform box-girder cross-section with overall dimensions of 3800 mm in height and 5500 mm in width was used. The thickness of the web, top flange and bottom flange is 350 mm, 700 mm and 650 mm respectively. A sketch showing all dimensions is given in Figure 3.1.

These cross-sectional dimensions are based on the 45 m span length of the ORV. The effect of different span lengths will also be studied by increasing and decreasing the span length by 5 m to 40 m and 50 m. The span – height ratio of 1:12 will remain constant. For the 40 m and 50 m span models only the height of the webs will be adjusted, the thickness of the top and bottom flanges will remain as shown in Figure 3.1. Cross-sectional properties are given in Table 3.3.

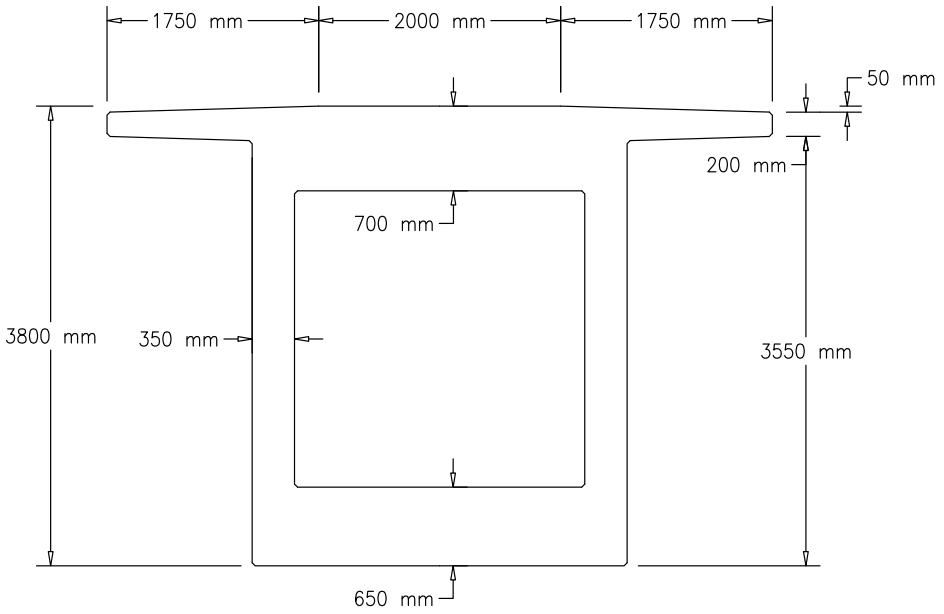

Figure 3.1: Bridge cross-section for the 45 m span length.

Table 3.3: Properties of three different cross-sections investigated.

Property	Symbol	40 m Span	45 m Span	50 m Span
Height	h	3.38 m	3.80 m	4.22 m
Area	A	6.16 m^2	6.45 m^2	6.75 m^2
Moment of inertia	I	9.46 m^4	12.73 m^4	16.57 ^{4}
Mass per unit lentgh	m	14 170 kg/m	14 835 kg/m	15 525 kg/m

3.4.1.3 Finite elements & boundary conditions

The bridge was modelled as a series continuous spans using 3D beam elements, with the positive x-axis along the length of the bridge, the y-axis in the transverse direction and the z-axis vertically upwards, opposite to the gravitational direction. The boundary condition of the first abutment at the start of the bridge deck was fully fixed except for rotation about the y-axis which was released. All subsequent supports were modelled similarly, but also releasing the longitudinal translation degree of freedom (x-axis). A boundary condition for the other abutment was not required because only 10 spans continuous spans were modelled for the numerical study, this was increased to 11 for the case-study. The other 12 spans were not

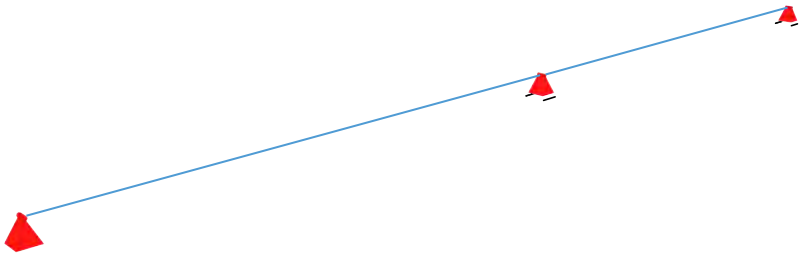

Figure 3.2: Idealisation of the two span FE model.

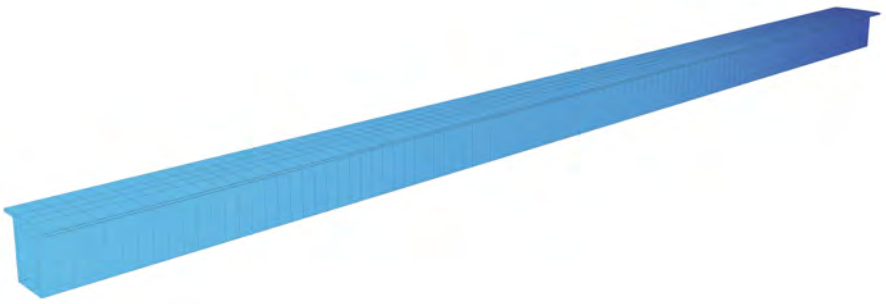

Figure 3.3: FE model of the bridge deck.

modelled due to joints on either side of the 12^{th} span, making the drop span and rest of the bridge act independently of the first 11-span continuous section. An example of the two span FE model is shown in Figure 3.2 and 3.3.

3.4.1.4 Damping

A critical damping ratio, ζ, of 1 % was assumed for this investigation. This value was based on the recommendation of UIC [2009] for prestressed concrete with spans greater than 20 m in length.

3.4.2 Train loading

The train was modelled using a set of moving concentrated forces. Each bogie, which has two axles, has been idealised as two concentrated forces 1.83 m apart. The distance between the second axle of the first bogie and the first axle of the second bogie is 4.66 m. The layout of forces is based on the type CR-13 wagons which are currently in operation on the ORV.

The wagons have a gross weight of 120 tonnes when fully loaded, this translates to

an axle load of roughly 290 kN. The electric locomotives which power the train weigh slightly less (190 kN – 220 kN) and the diesel ones approximately the same as the fully loaded wagons. For trains up to 40 – 60 wagons diesel locomotives are normally used to power the train, above this electric or a combination of diesel and electric locomotives are used. Each bogie of the locomotives have three axles, compared to the wagon's two axles. These differences between the locomotives and wagons are not of interest to the actual train load model, but must be considered when comparing the FE model's response to measurements in the case-study. Figure 3.4 shows the idealisation of the concentrated forces model of a two wagon model.

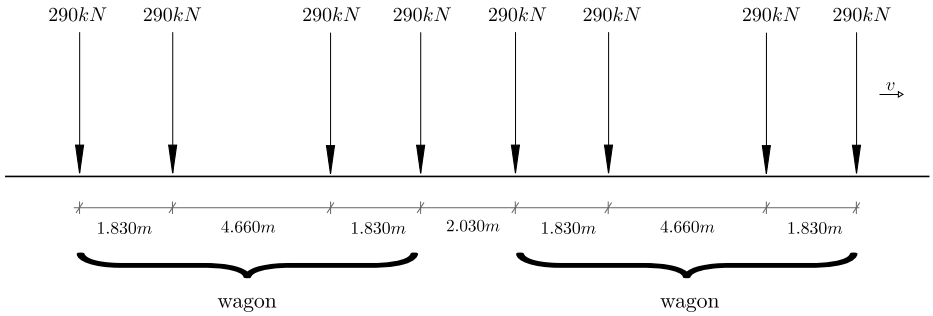

Figure 3.4: Idealisation of the moving forces load model for two wagons, based on the CR-13 wagon.

Two scenarios were investigated regarding the mass of the train. First, the mass of the train was ignored. The natural frequencies and mode shapes were obtained and the numerical model was simulated using only the axle load of the trains. Thereafter, the mass of the train was accounted for by lumping it equally at the nodes. This allows the natural frequencies to be obtained for the loaded case. The bridge's response was also simulated for this scenario. It can be expected that the structural response time histories for the second case may be affected by the inclusion of the mass for the entire time domain, however, it was not possible to define time-dependent lumped masses to avoid this.

3.5 Finite Element Method in SOFiSTiK

Below, a brief background of the linear dynamic theory which was used and applied in SOFiSTiK to solve this problem is described. The numerical solvers which were used to calculate the dynamic properties and response of the bridge configurations are also discussed.

3.5.1 Linear dynamic theory

For a single degree of freedom (SDOF) system the equilibrium equations can be solved analytically, but when the system becomes larger and loading becomes complex it becomes increasingly difficult to do this. In cases such as this, multi degree of freedom (MDOF) problems can be solved numerically using time-stepping methods and applying D'Alembert's principle which assumes a dynamic system to be in equilibrium at each time instant [Chopra, 2012]. Two evaluation methods can be used to solve the problem, these are: the direct integration method and mode superposition, the former was chosen for this particular study.

A railway train running on a track system is a complicated dynamical system. The entire system is comprised of many bodies, some of which are moving and some which are static. The system, therefore, has many degrees of freedom. The railway vehicle can be connected in various ways and the interface between the train and the bridge is continuously moving. The governing equation, assuming Euler-Bernoulli theory, is defined by the following partial differential equation [Frýba, 1996]:

$$EI\frac{\partial^4 v(x,t)}{\partial x^4} + \mu\frac{\partial^2 v(x,t)}{\partial t^2} + 2\mu\omega_d\frac{\partial v(x,t)}{\partial t} = f(x,t) \tag{3.1}$$

Where $v(x,t)$ is the vertical deflection of the beam at point x and time t, E is the modulus of elasticity, I is the moment of inertia, μ is the constant mass per unit length of beam, and $f(x,t)$ is the load at point x at time t.

In order to apply linear dynamic theory and apply this theory to this study it is assumed that, because the deflections are small in comparison to the size of the structure, the structure performs in a linear manner. Thus, loading and unloading will be in the elastic range. The system can be defined as a finite number of DOF, N, and can be solved in the time-domain and it is therefore valid to assume the system as discrete. We also assume the system to be time-invariant because the output does not explicitly depend on time, but also on other parameters such as the magnitude of the dynamic force. Applying FEM, the system can be defined as Chopra [2012]:

$$\mathbf{M}\ddot{d}(t) + \mathbf{C}\dot{d}(t) + \mathbf{K}d(t) = F(t) \tag{3.2}$$

Where:

- $\mathbf{M}$ is the mass matrix,

- $\mathbf{C}$ is the damping matrix,
- $\mathbf{K}$ is the stiffness matrix,
- $F(t)$ is the vector of external loads,
- d is the displacement vector, and
- $(\dot{})$ refers to the time derivative, $\frac{d}{dt}$.

The left-hand side of Equation 3.2 reserves the properties of the system while the right-hand side contains the external time-dependant forces the system experiences. When the geometry and material properties of the structure is known the mass matrix can be assembled easily. Assembling the damping and stiffness matrices are more challenging.

Damping is the energy dissipating process whereby a structures amplitudes diminishes with time. Sources of damping in vibrating structures include friction at steel connections, opening and closing of microcracks in concrete, and friction between the structure itself and nonstructural elements [Chopra, 2012]. For existing bridges the damping parameter can be calculated using the logarithmic decrement from vibration measurements. Generally, it is impractical, for a lack of budget and time, to do so and damping is therefore specified by numerical values [Chopra, 2012]. In the case of the design of new structures, damping and other properties cannot be measured. Here, previous experimental results can assist in estimating the damping ratio, values recommended by UIC [2009] can be used. As previously discussed, a critical damping ratio of $\zeta = 1\%$ was assumed for this study.

The stiffness matrix is dependent on the elastic modulus of the material and geometric properties of the structure. The elastic modulus can be measured experimentally or estimated based on the strength classification of the material. The geometry is generally known from engineering drawings or measurements. But when calculating the stiffness of an existing structure one must keep in mind that over time concrete strengthens resulting in a higher elastic modulus. There is also a possibility of material deterioration and cracks forming, which in turn can reduce the stiffness. The stiffness also depends on the reinforcing and prestressing steel, which was considered when choosing the elastic modulus for this investigation. The moment of inertia was calculated in SOFiSTiK based on the cross-sectional information which was defined.

The external forces are calculated based on the train load model which was defined,

and the train speed. In the FE model these forces are applied as nodal loads in order to solve Equation 3.2.

3.5.2 Modal analysis

A modal analysis (or Eigenvalue analysis as it is referred to in SOFiSTiK SSD) was used to determine the natural frequencies and mode shapes of the bridge in this thesis. Modal analysis as defined by Rieger [1986] is an analytical procedure which applies a transformation to the structural equations of motion to uncouple them. This allows the identification of the structural modes of vibration and their associated frequencies. The dynamic equation, Equation 3.2, can be solved for the free vibration of the structure:

$$\mathbf{M}\ddot{d}(t) + \mathbf{K}d(t) = 0 \tag{3.3}$$

Assuming a harmonic solution of the form $d = \phi \sin \omega t$, and differentiating this twice such that it can be substituted into Equation 3.3, the system becomes:

$$[\mathbf{K} - \omega^2 \mathbf{M}]\phi = 0 \tag{3.4}$$

From this system, the natural circular frequencies (ω) and the undamped mode shapes (ϕ) can be determined [Rieger, 1986]. These parameters are the basic dynamic properties of structural systems. Interpretively, ϕ is the shape at which the structure oscillates at the frequency of ω. When using FEM there are a number of solution methods. A wide array of these methods are discussed in Bathe [2005]. SOFiSTiK allows the user a choice of the following four solvers, which are also summarised in Table 3.4:

i. Method of Lanczos

ii. Simultaneous Vector Iteration

iii. Minimum Rayleigh Quotient

The Lanczos solver was used to determine the frequencies and mode shapes of bridge configurations in this study. The Lanczos method was also compared to the Vector Iteration algorithm, on occasion, to compare the frequencies and mode shapes,

Table 3.4: Overview of algorithms used to solve the Eigenvalue problem in SOFiSTiK.

	Vector iteration	Lanzos	Rayleigh
No. of Eigenvalues	Moderate	High	Few
Range of Eigenvalues	Ritz-step problematic	No problems	No problems
Multiple Eigenvalues	Yes	Yes	Yes
Missing Eigenvalues	Very rare	Rare	Very rare
Negative Eigenvalues	Yes	Does not work	Only positive
Memory requirement	Moderate	High	Small
Speed	Moderate	Fast	Variable

especially where missing eigenvalues were presumed. The two algorithms provided very similar and satisfactory results, however, the Lanczos method was generally faster and sufficient memory was available to use it for the larger geometrical models of 10 spans and the case-study of 11 spans.

3.5.3 Direct integration

Direct integration was used to solve the dynamic structural response of the bridge. In direct integration, the system in Equation 3.2 is integrated numerically using a step-by-step procedure over a finite time domain. Instead of trying to solve the system for all t, the aim of this procedure is to solve it at discrete time intervals, Δt apart [Bathe, 2005]. Direct integration is also based on the assumption that a variation of displacement, velocity and accelerations is within each time interval Δt.

When calculating the linear dynamic system using FEM, the time domain is commonly divided into constant time steps. Assuming the initial conditions of the system are known, the solution at the next time step is required. To determine the solution a general algorithm is developed. These algorithms can be classified in two groups, namely explicit methods and implicit methods. Explicit algorithms involve expressing the solution at the next time step in terms of the solution and its derivatives at the previous time step. Implicit algorithms are solved by defining the solution at the next time step as a function of the solution and its derivatives at the next time step, which results in an implicit equation which needs to be solved. When using these to solve dynamic problems explicit algorithms generally require very small time steps but are computationally inexpensive at each step. Implicit algorithms allow for a larger time step but are computationally expensive in comparison. Algorithms

generally adopted in programs such as SOFiSTiK include the Central Difference Method (explicit), the Wilson θ Method and the Newmark Method (implicit). A good account of these algorithms can be found in Bathe [2005].

The Newmark Method was used for this investigation, and the parameters as defined in Bathe [2005], $\gamma = \frac{1}{2}$ and $\beta = \frac{1}{4}$, was used. If other values for γ were chosen non-mechanical damping might be introduced into the problem. The values chosen guaranteed unconditional stability, irrespective of the time-step, however the time-step needs to be small enough to ensure the solution is accurate. For this reason a small time step of 0.001 s was chosen, unless otherwise stated.

3.6 Concluding remarks

This thesis investigates the problem of moving heavy loads on continuous, multi-span bridge configurations with varying number of spans and travelling at different speeds. The investigation has been divided into two parts. Firstly a purely numerical study of continuous bridges, and secondly a case study on the ORV. Aspects of the bridge and train loading were described in this chapter, and details regarding the numerical process used in the Finite Element program SOFiSTiK were described, along with valid assumptions and the work flow. Methods in which the governing equations are solved were also described. The following chapter will present the results and discussion of the numerical analysis.

Chapter 4

Results & discussion

4.1 Introduction

In this chapter the results of the numerical analysis are discussed. Firstly, the dynamic properties in the form of natural frequencies and mode shapes are discussed. Secondly, the dynamic response of different bridge configurations in terms of the displacement and accelerations at mid-spans, are calculated using the moving forces train model for two scenarios: (1) ignoring the additional mass of the heavy haul train; and (2) lumping the mass of the HH train at the nodes of the FE bridge models for the entire time domain investigated. Due to the shear volume of data produced by this investigation not all results are presented in the text, however, they have been included in the Appendices.

The aim of this analysis was to compare the dynamic properties of different bridge configurations of continuous, multi-span railway bridge in order to deduce some conclusions about the effect the number of continuous spans has on the natural frequencies and mode shapes and to compare the response of different spans in continuous railway bridges, to determine which spans may be critical in terms of maximum dynamic response.

4.2 Dynamic properties

4.2.1 Natural frequencies

The first ten vertical modes for the 40 m, 45 m and 50 m spans of the one, five and ten span models are shown in Tables 4.1 to 4.3. The cluster of frequencies in the concentrated zone, which always occurs when there is more than one continuous

span, has been highlighted in blue. The first 10 vertical frequencies for all models are attached in Appendix A of this dissertation.

The pattern of results presented in Tables 4.1 to 4.3 are as expected. Considering that a natural frequency for a SDOF system is defined as $f = \sqrt{\frac{k}{m}}$, when the added mass of the train is lumped at the nodes of the bridge a decrease in frequency is expected because an increase in mass per unit length occurs, and indeed occurs when analysing results. Similarly, an increase in span length, L, would decrease the stiffness k, and also decrease the expected natural frequency. This is also observed in the results.

Any natural frequency that appears in a bridge configuration (a certain cross-section, span length and number of spans), also appears in all bridge models which have a multiple of the number of spans and the same span length, but at a higher mode. As an example, the frequency of Mode 2 of the 40 m five span model with no added mass is 4.971 Hz. This frequency is also Mode 3 of the ten span model with the same span length and no added mass. The repetition of natural frequencies of symmetric bridges can be explained by analysing Equation 3.4 . Considering that $\mathbf{K}$ is a function of the length of the bridge and that $\mathbf{M}$ can be expressed as mass per unit length, and that there can be multiple solutions to Equation 3.4, natural frequencies can be repeated. However, for equilibrium to hold there must be a multiple of the corresponding mode shape, ϕ.

The first vertical natural frequency (fundamental frequency) for each of the different models is presented and compared in Table 4.4, for all 40 m, 45 m and 50 m span models. The frequencies are reported considering, firstly, only the mass of girder (M0) and secondly, the mass of the girder in addition to the mass of the fully loaded train (M1). By definition, when considering mass of the train, the frequencies which are reported are not real natural frequencies as the bridge would be experiencing an external load. The aim of adding the mass of the train as lumped nodal masses to the FE model was to determine what effect the considerable mass of a HH train could have on the dynamic properties of the bridge. These results show that the critical response of a railway bridge might not occur when the frequency of the trains axle loads is equal to the natural frequency of the bridge, but rather when the frequency of axle loads is equal to the frequency of a coupled train-bridge system, which is more challenging to determine.

The added mass of the train which was assumed to be 10 tonnes/m for a heavy haul train is significant. The mass constitutes more than a 20% decrease in the fundamental frequencies for each of the 40 m, 45 m and 50 m systems. The span

Table 4.1: Vertical natural frequencies [Hz] 1 to 10 for the one, five and ten span model with span lengths of 40 m. All frequencies in the concentrated zone are highlighted in blue.

Mode	One Span		Five Spans		Ten Spans	
	M0[1]	M1[2]	M0[1]	M1[2]	M0[1]	M1[2]
1	4.540	3.512	4.540	3.512	4.540	3.512
2	16.524	12.812	4.971	3.845	4.652	3.598
3	32.899	25.532	6.055	4.683	4.971	3.845
4	51.403	39.857	7.409	5.730	5.455	4.219
5	70.837	54.808	8.635	6.677	6.055	4.683
6	90.658	69.939	16.524	12.812	6.721	5.198
7	110.647	85.063	17.128	13.278	7.409	5.730
8	130.734	100.114	18.531	14.361	8.068	6.239
9	150.917	115.075	20.136	15.600	8.635	6.677
10	171.223	129.948	21.465	16.625	9.032	6.983

[1] Without added mass of train.

[2] With added mass of train.

Table 4.2: Vertical natural frequencies [Hz] 1 to 10 for the one, five and ten span model with span lengths of 45 m. All frequencies in the concentrated zone are highlighted in blue.

Mode	One Span		Five Spans		Ten Spans	
	M0	M1	M0	M1	M0	M1
1	4.074	3.181	4.074	3.181	4.074	3.181
2	14.891	11.656	4.464	3.485	4.176	3.260
3	29.784	23.344	5.445	4.251	4.464	3.485
4	46.713	36.600	6.674	5.210	4.903	3.827
5	64.561	50.503	7.791	6.081	5.445	4.251
6	82.796	64.616	14.891	11.656	6.050	4.723
7	101.189	78.747	15.450	12.091	6.674	5.210
8	119.655	92.823	16.746	13.102	7.273	5.678
9	138.178	106.823	18.232	14.261	7.791	6.081
10	156.77	120.745	19.469	15.224	8.154	6.364

[1] Without added mass of train.

[2] With added mass of train.

Table 4.3: Vertical natural frequencies [Hz] 1 to 10 for the one, five and ten span model with span lengths of 50 m. All frequencies in the concentrated zone are highlighted in blue.

Mode	One Span		Five Spans		Ten Spans	
	M0	M1	M0	M1	M0	M1
1	3.688	2.904	3.688	2.904	3.688	2.904
2	13.533	10.686	4.044	3.185	3.781	2.977
3	27.180	21.498	4.940	3.890	4.044	3.185
4	42.781	33.838	6.063	4.774	4.444	3.500
5	59.291	46.842	7.087	5.580	4.940	3.890
6	76.193	60.079	13.533	10.686	5.492	4.325
7	93.254	73.358	14.052	11.095	6.063	4.774
8	110.377	86.598	15.256	12.042	6.612	5.206
9	127.535	99.772	16.639	13.130	7.087	5.580
10	144.730	112.879	17.795	14.038	7.421	5.842

[1] Without added mass of train.

[2] With added mass of train.

Table 4.4: First vertical natural frequency, with and without added mass of the train, for each model.

Span Length	Without train mass	With train mass	Percentage decrease
40 m	4.540 Hz	3.512 Hz	22.64 %
45 m	4.074 Hz	3.181 Hz	21.92 %
50 m	3.688 Hz	2.904 Hz	21.26 %

length did not really impact the reduction, but the 50 m span length had a reduction in frequency which was 1.38% lower compared to the 40 m span length when adding the mass of the train. The mass of the bridge varies between 14 tonnes/m to 15.5 tonnes/m, and thus the live load – dead load ratios are large (between 0.71 and 0.65).

The critical wavelengths for speeds ranging from 20 km/h to 100 km/h were calculated based on equating the fundamental frequency of the bridge with the frequency of axles of the train, giving the following equation:

$$f_0 = \frac{v}{\lambda}$$

$$\lambda = \frac{v}{f_0} \tag{4.1}$$

Where:

- λ is the distance between axles of the train, defined as wavelength, in m.
- v is the speed of train in m/s.
- f_0 is the fundamental frequency of the bridge.

The values are presented in Table 4.5. At lower speeds of 20 km/h to 40 km/h wavelengths range from 1.23 m to 3.83 m. These wavelengths are short, and are likely to only coincide with the distance between axles of the same bogie. Due to the configuration of trains the distance between bogies are always larger than the distance between axles of the same bogey, thus vibration will not be a problem for any of the span lengths. At the moderate speeds of 60 km/h to 100 km/h wavelengths range from 3.7 m to 9.6 m, here vibration might be more problematic, depending on the precise configuration of axles and bogies. Table 4.6 presents the critical speeds at which resonance and sub-resonance occurs, for the fundamental frequencies of the bridge with and without the mass of the train. Sub-resonance can, by definition, occur when the frequency of the excitation is half of the frequency of the natural bridge frequency. This might result in an amplification of the bridge's response.

The numerical model of the bridge is able to determine all natural frequencies in the concentrated zones. As the number of spans increase the range of frequencies in the concentrated zone tend to increase, however, it is clear that the frequencies become more closely spaced. This was investigated by calculating the envelope of natural frequencies in the concentrated zone, defined as,

$$\Delta f = f_i - f_0 \tag{4.2}$$

Table 4.5: Critical wavelengths in m for all fundamental frequencies and for speeds ranging from 20 km/h to 100 km/h.

Speed	40 m span		45 m span		50 m span	
[km/h]	4.504 Hz	3.512 Hz	4.074 Hz	3.181 Hz	3.688 Hz	2.904 Hz
20	1.23	1.58	1.36	1.75	1.51	1.91
40	2.47	3.16	2.73	3.49	3.01	3.83
60	3.70	4.75	4.09	5.24	4.52	5.74
80	4.93	6.33	5.45	6.99	6.03	7.65
100	6.17	7.91	6.82	8.73	7.53	9.57

Table 4.6: Critical speeds at resonance and sub-resonance for all models.

Span length	f_0	Critical speed	
	[Hz]	v_R [km/h]	v_{SR} [km/h]
40 m	4.540	169.16	84.58
	3.512	130.86	65.43
45 m	4.074	151.80	75.90
	3.181	118.52	59.26
50 m	3.688	137.41	68.71
	2.904	108.20	54.10

Where:

- f_0 is the fundamental frequency.
- f_i is the natural frequency of the higher vibration mode in the first cluster of m natural frequencies f_n with $n = 1, 2, 3, ..., m$.

The result was plotted for each model, ranging from two spans to ten spans, in Figures 4.1 and 4.2.

These figures show that as the number of spans increase, the range of natural frequencies in the concentrated zone increases towards what appears to be a limiting value. The limiting frequency is approximately equal to the the fundamental frequency of the system. The accompanying values of such have been compared in Table 4.7.

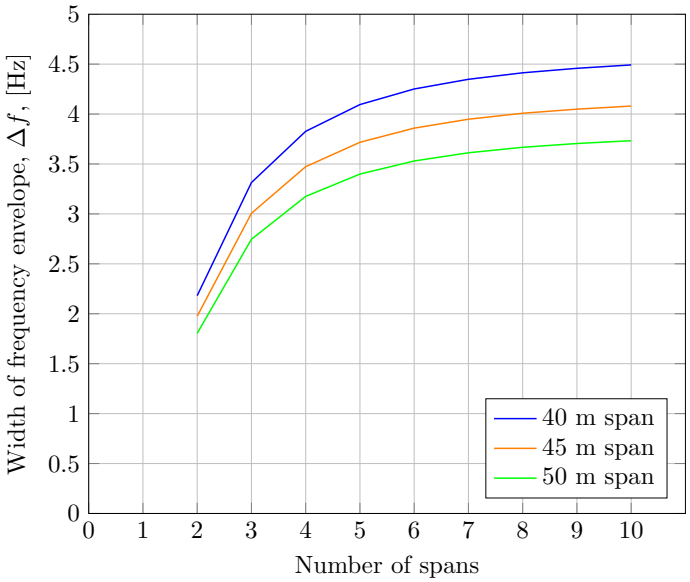

Figure 4.1: The relationship between the number of spans and the range of frequencies in the concentrated zone, Δf, for all models without the added mass of the train.

Table 4.7: Comparison of the fundamental frequency and the range of frequencies on the concentrated zone.

Span Length	With/ Without Added-mass	f_0 [Hz]	Δf of 10 Span Model [Hz]
40 m	M0	4.540	4.492
	M1	3.512	3.471
45 m	M0	4.074	4.080
	M1	3.181	3.183
50 m	M0	3.688	3.667
	M1	2.904	2.938

Frequencies for the second and third modes have also been plotted against the number of spans in Figure 4.3 for the 45 m span length model. From the results presented in Table 4.7 and these figures, it is clear that as the number of spans increase the change in frequency becomes very small for both modes.

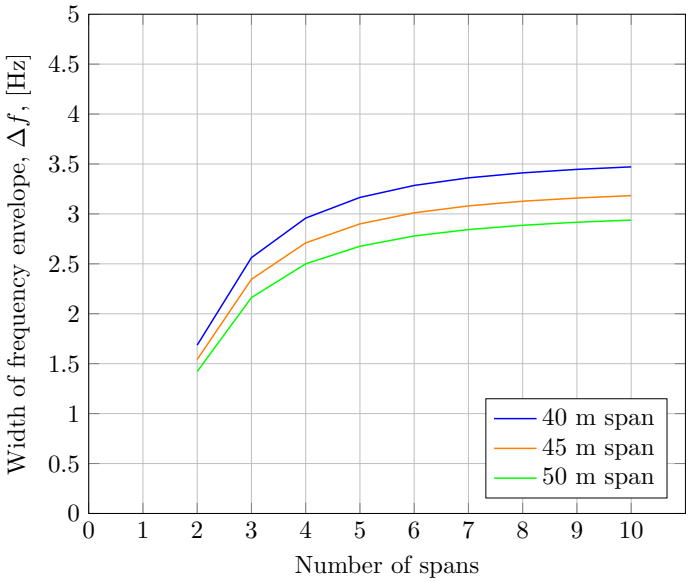

Figure 4.2: The relationship between the number of spans and the range of frequencies in the concentrated zone, Δf for all models with the added mass of the train lumped at the nodes of the FE model.

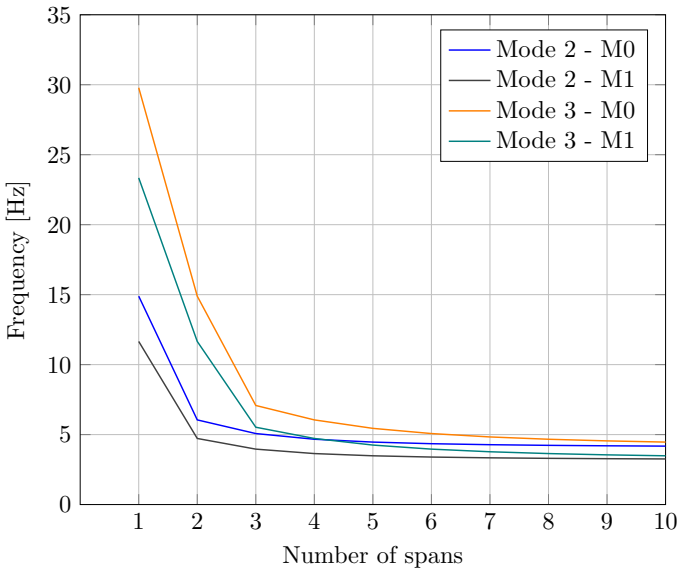

Figure 4.3: Frequencies of the second and third mode plotted against the number of continuous spans for 45 m span length.

4.2.2 Mode shapes

Mode shapes were exported from SOFiSTiK for all models ranging from single-span to ten spans, for each span length (40 m, 45 m and 50 m), without and with the added mass of the train. In summary, mode shapes one to five for the one, five and ten span model with 45 m span lengths are shown in Figure 4.4. Mode shapes six to

ten is also shown shown for the ten span model.

Mode shapes of continuous beams can be calculated analytically, the solutions of which are trivial (see Frýba [1996]). Mode shapes calculated in the FE model are in agreement with those found in literature, and it can therefore be considered that the models are verified with respect to performing like a continuous bridge would. Adding mass or changing the length of the span had no effect on the mode shape, however the following was observed:

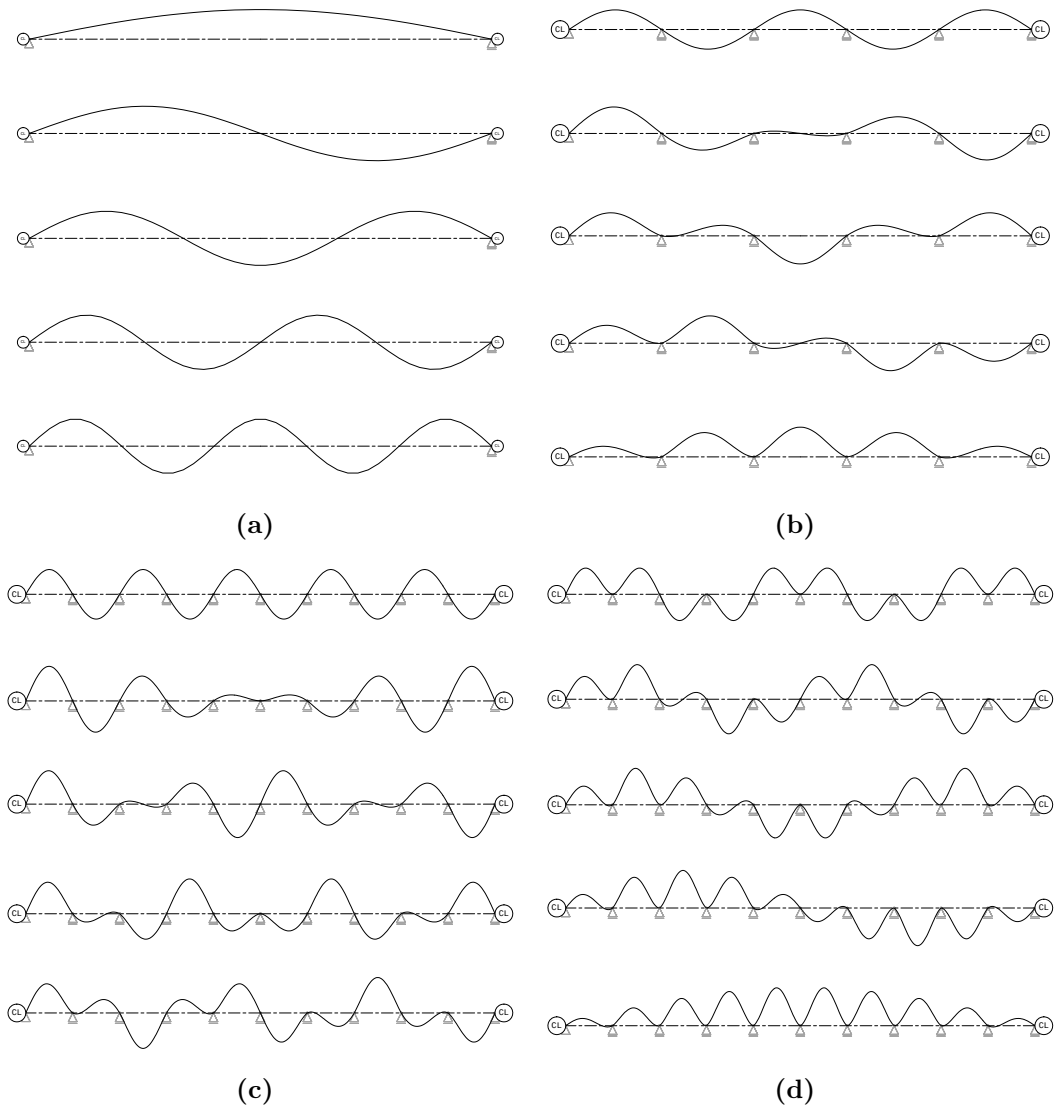

Figure 4.4: Mode shapes obtained from the FE model

(a) Mode shapes 1 – 5 for the 45 m single span model.

(b) Mode shapes 1 – 5 for the 45 m five span model.

(c) Mode shapes 1 – 5 for the 45 m ten span model.

(d) Mode shapes 6 – 10 for the 45 m ten span model.

- Adding mass of the train decreased the natural frequencies of each mode by approximately 20 %. The displacements associated with each mode of vibration also decreased by approximately the same amount.
- Increasing span length from 40 m to 50 m resulted in an increases mass per unit length and therefore a decrease of frequency. Modal displacements also subsequently decreased.
- As the number of spans increase the mode shapes in the cluster become more challenging to predict.
- Spatial periodicities, such as those described by Lin [1962], are clearly present.

As discussed earlier, any natural frequency which appears in a bridge configuration also appears in all bridge models which have a multiple of the number of spans and the same span length, but at a higher mode. In these cases multiples of the mode shapes are also repeated. The example of 45 m five span and ten span model is referred to in Figure 4.5. The top two mode shapes are mode 2 from the 5 span model, the mode shape on the bottom of Figure 4.5 is mode 4 from the 10 span model.

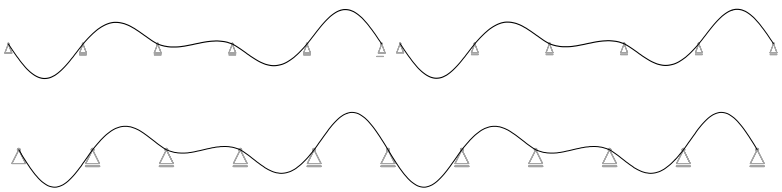

Figure 4.5: Mode shape two from five span model compared to mode 5 from the ten span model.

From these results it is clear that the dynamic behaviour of continuous, multi-span railway bridges becomes more complex as the number of spans increase due to nature of the frequencies in the concentrated zone and how closely they are spaced for bridges with numerous spans. It is also apparent that the lower the fundamental frequency of the system, the more closely spaced the frequencies are. The additional mass of a HH train, when lumped at the nodes of the bridge, results in a significant decrease in the natural frequencies. This method, however, is not perfect in determining the natural frequencies of a bridge when trafficked, because the actual train-bridge system comprises a train signal and not an ambient signal as the model assumes.

4.3 Dynamic response

Nodal displacements and accelerations, in reaction to the moving forces train model described in the previous chapter, were calculated using SOFiSTiK's DYNA program. Complete displacement time-histories and acceleration time histories were calculated for the node at (or closest to) mid-span for each span, for each of the models and for train speeds varying from 20 km/h to 100 km/h in 20 km/h intervals.

4.3.1 Displacement

First observations showed that varying train speeds up to 100 km/h generally had little to no influence on the magnitudes of the deflections. This might be due to the fact that the investigation only considered only speeds in multiples of 20 km/h, and therefore some speeds at which a more significant dynamic amplification occur were missed. At higher speeds, the difference in displacement magnitudes were only significant for the models up to three span lengths, thereafter the displacement magnitudes tend toward a constant magnitude. Displacement time histories for the mid-span node of the first bridge span for the one, two to three and eight to ten span models at a train speed of 60 km/h are shown in Figure **??**. Similarly, the time history of the centre node of the last span of the eight, nine and ten span models is shown in Figure 4.8.

Increasing the span length from 40 m to 45 m and subsequently 50 m increases the displacements by approximately 2 mm for each 5 m increase. Similarly, adding the train mass as nodal masses generally had little influence on the displacement time history, except for the 45 m span models. In this case, the additional mass resulted in a small, yet clear, excitation of the bridge at 60 km/h. The time displacement history for this particular case is shown in Figure 4.9(a).

Whereas the displacements were not critical (largest) in the central spans of the multi-span models, their time histories tell an interesting story. This has been shown by plotting the displacement at the centre-most node of the most central span of the three, five, seven and nine span models in Figure 4.11.

The comparison of displacement time histories in Figure 4.6 shows that, for a single span that is simply supported, the displacement is approximately 14 mm (downward) while the train is travelling over the bridge. For the two span model, the displacement reaches a maximum of 10 mm at 2.7 s. At this point in time the fist axle of the

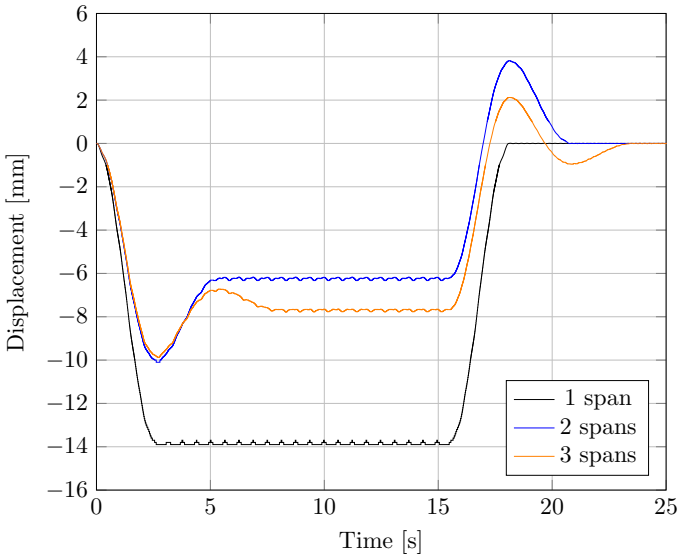

Figure 4.6: Displacement time history of the first mid-span node for one, two and three span 45 m models and a train speed of 60 km/h. The added mass effect of the train has not been considered.

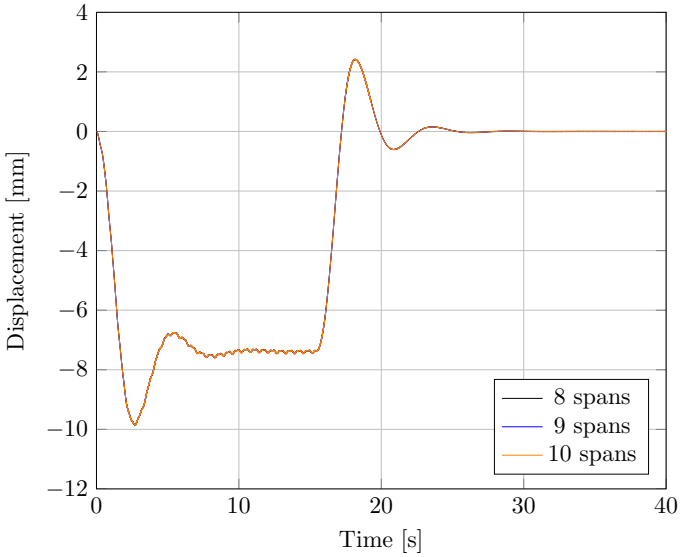

Figure 4.7: Displacement time history of the first mid-span node for eight, nine and ten span 45 m models and a train speed of 60 km/h using the moving forces load model. The added mass effect of the train has not been considered.

train reaches the second span, and counteracts the displacement at mid-span of the first span and the displacement remains at -6 mm while both spans are loaded. The last axle of the train reaches the first node of the bridge at 15.4 s, from when the negative displacement starts to increase to zero. At 15.1 s the last axle leaves the first span, and the displacement of the first mid span node becomes positive, essentially due to the lift up of the axle loads on the second span. At approximately 18 s the

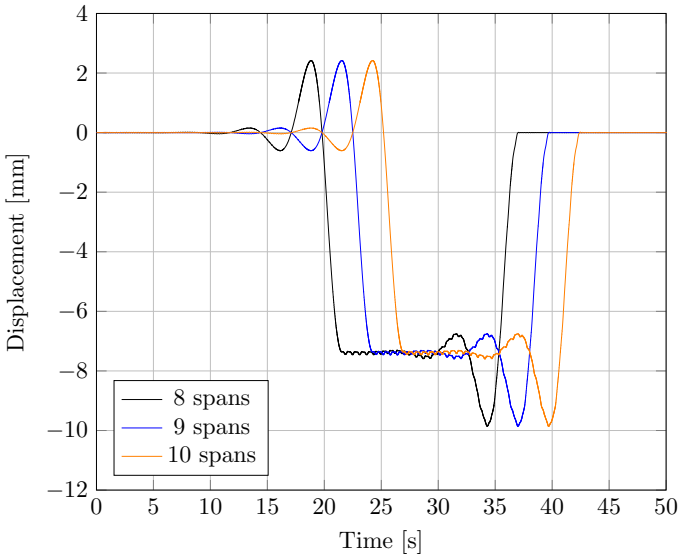

Figure 4.8: Displacement time history of the last mid-span node for eight, nine and ten span 45 m models and a train speed of 60 km/h using the moving forces model. The added mass effect of the train has not been considered.

displacement reaches a maximum positive displacement of 4 mm. The last axle of the train leaves the two span bridge at 20.8 s.

A similar phenomenon occurs for the three span model, except the displacement of the first mid-span node is now counteracted by the second span and abetted by the third span. The displacement while all three spans are trafficked is now closer to -8 mm and the positive displacement of the first span is only 2 mm while the end of the train is travelling over the second span. The same reversal of displacement occurs when the last axle leaves the first span. However, there is another smaller reversal (between 19.5 s and 22.5 s) once the last moving axle leaves the second span.

Considering only displacement histories from the two and three span model the following nuances can be drawn. Up to the instant where the first axle reaches the end of the first span the displacement history is almost identical, while the train begins to pass over the second span the displacement starts to tend toward the displacement of the two span model, but at 5.4 s when the train reaches the third span the displacement begins to decrease toward -8 mm. Over the remaining time history difference in displacement is approximately 2 mm between the two models.

When comparing the displacement time histories of the first mid-span node of the eight, nine and ten span model under the same conditions, it can clearly be seen that they are identical in Figure 4.7. Upon further investigation it showed that after the number of spans increase to greater than four the displacement time histories

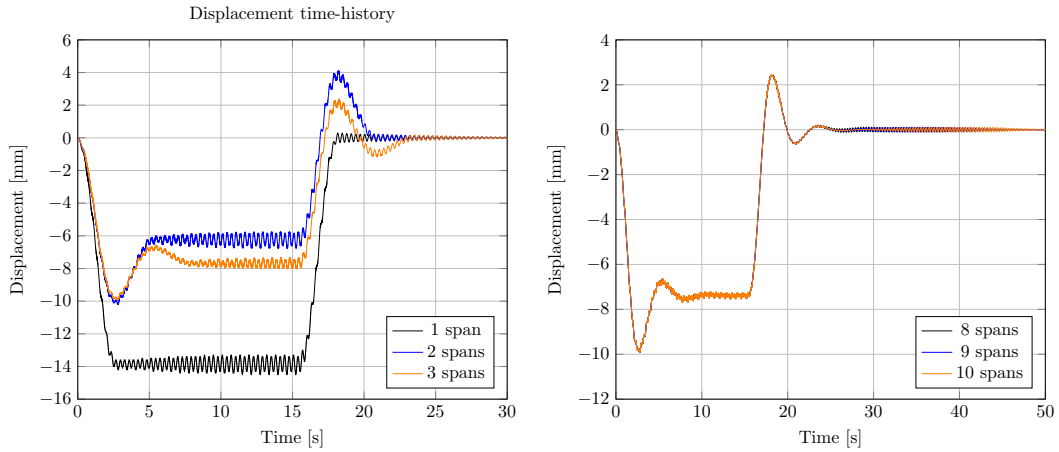

(a) 1, 2 and 3 spans. **(b)** 8, 9 and 10 spans.

Figure 4.9: Displacement time history of the first mid-span node for one, two and three span vs the eight, nine and ten span 45 m models and a train speed of 60 km/h. The mass of train is lumped at the nodes of the FE model.

in fact become almost identical. The maximum downward displacement is still approximately 10 mm and the maximum positive displacement is just greater than 2 mm. The same result is shown for the other most critical node, the mid span of the last span, in Figure 4.8 (the offset in the time domain is due to the overall length of bridge being different in the eight, nine and ten span model).

Similar to Figure 4.6 and 4.7, the displacement time histories have been shown for the model which has included the mass of train in Figure 4.9. In Figure 4.9(a) resonant vibrations are clear for the one, two and three span model. In this particular case, the fundamental mode is excited at the sub-resonant speed of 59.2 km/h. The effect of increasing the number of spans is similar to that of the model which did not consider the mass of the train. The displacement histories are again identical for the eight, nine and ten span model (Figure 4.9(b)), however the vibration effect is hardly noticeable. The significance of this is that it supports the presumption that the bridges with more continuous spans vibrate less than those with fewer spans. Because these models hold the same properties in the form of mass per unit length, stiffness and damping – the reduction in vibration might be attributed to the cancellation effect of modes which are closely spaced in the concentrated cluster for continuous, multi-span bridges.

Figure 4.11 shows the displacement time histories for the mid-span node of the centre most span of the three, five and seven span models for span length of 45 m and train speed of 60 km/h. What is most prevalent, initially, is the effect of sub-resonance in the results which have considered the added mass of the train in

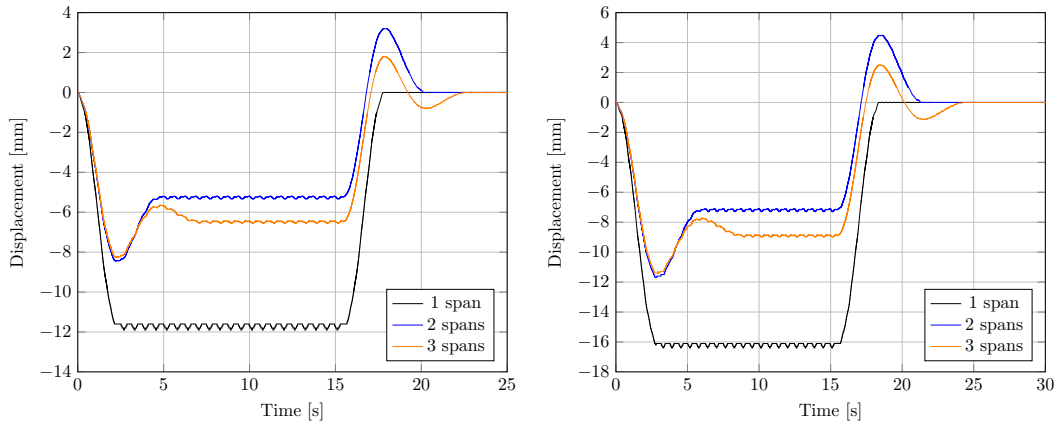

(a) 40 m spans. **(b)** 50 m spans.

Figure 4.10: Displacement time history of the first mid-span node for one, two and three span 40 m and 50 m models and a train speed of 60 km/h using the moving forces load model. The mass of the train was lumped at the nodes over the entire time domain.

Figure 4.11(b). The centre-most node of the three span model vibrates more than that of the five and seven span model – supporting the earlier result that showed models with more continuous spans vibrate less. Secondly, as expected, there is a clear difference in the time domain due to the different total length of bridge in each of the three, five and seven span model. More critically is the stress reversal observed. Depending on the number of spans, before the train reaches the span which the node of interest is situated on, there is a fluctuation between positive and negative displacements. Essentially, the large axle loads from a heavy train induces a "kick-up" effect. Whereas these displacements are much smaller than the largest displacement over the time domain (when the actual train has just entered or left the span) the moments induced may still be significant such that it might cause damage or influence fatigue behaviour of the bridge. This effect begins when the train is as much as four spans from the node.

Lastly, displacements were always maximum at the centre of the first and last span of the the multi-span models with more than three spans. As an example, the maximum displacement at mid-span of the first and last span are compared to the maximum displacement at mid-span of any of the central spans, at a train speed of 60 km/h and without considering the mass of the train, has been presented in Table 4.8 below. It is also interesting to note that as the number of spans increased from greater than 3 all the way to 10 spans that there was no significant change in the maximum displacements.

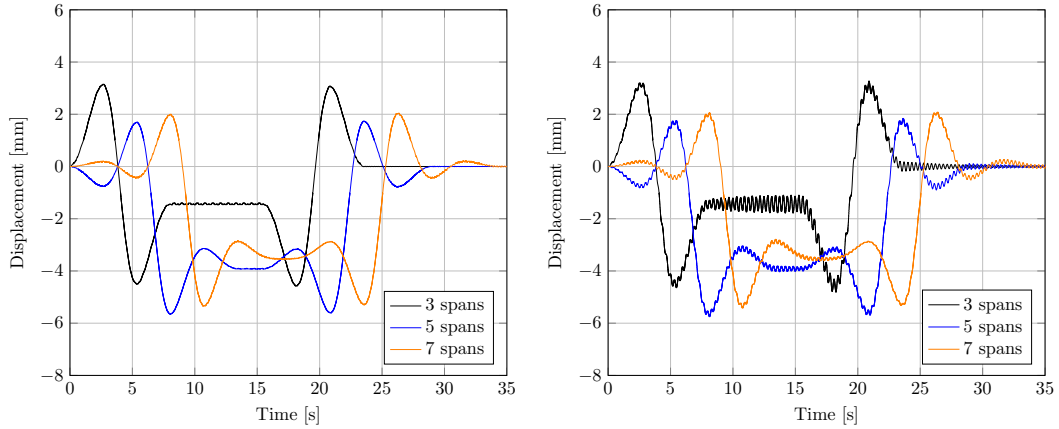

(a) Without train mass.

(b) With train mass lumped at the nodes over the entire time domain.

Figure 4.11: Displacement-time history of the first mid-span node for one, two and three span 40 m and 50 m models and a train speed of 60 km/h using the moving forces model.

4.3.2 Acceleration

The acceleration time histories tell a somewhat similar story to the displacements, whereby, the critical spans in terms of maximum accelerations were generally the first and last spans of the multi-span models. Time histories for the mid-span node of the one and ten span, 45 m span length models are shown in Figure 4.12 and 4.13. Figure 4.14 shows the acceleration time histories of spans two to five of the ten span model with added mass and a train speed of 60 km/h.

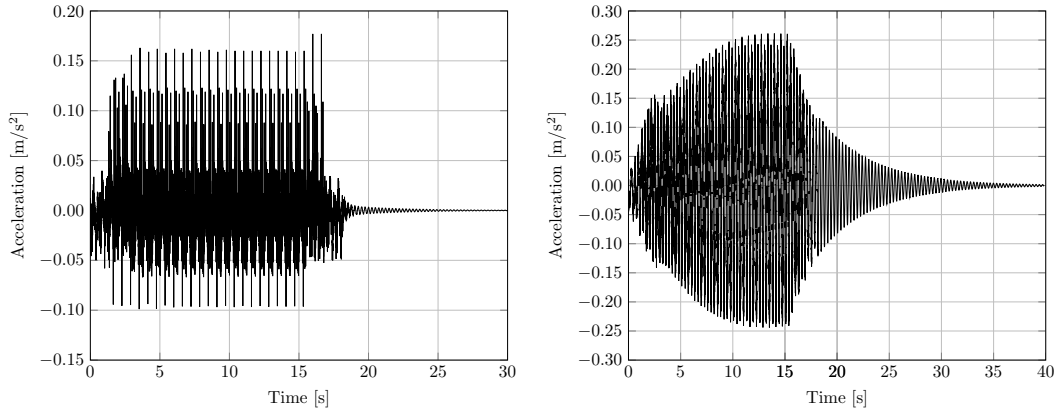

(a) Without added mass of train.

(b) With added mass of train.

Figure 4.12: Acceleration time history of single span, 45 m span length model for train speed of 60 km/h.

Table 4.8: Maximum displacements at the mid-span of the first and last span, compared to the maximum displacement of the central spans, at a train speed of 60 km/h and without adding the mass of the train to the model.

No. of spans	First span $u - z_{max}$ (mm)	Central spans $u - z_{max}$ (mm)	Last span $u - z_{max}$ (mm)
3	-9.880	-4.583	-9.883
4	-9.849	-5.773	-9.856
5	-9.855	-5.657	-9.858
6	-9.862	-5.650	-9.861
7	-9.825	-5.657	-9.876
8	-9.853	-5.648	-9.859
9	-9.858	-5.648	-9.858
10	-9.855	-5.653	-9.864

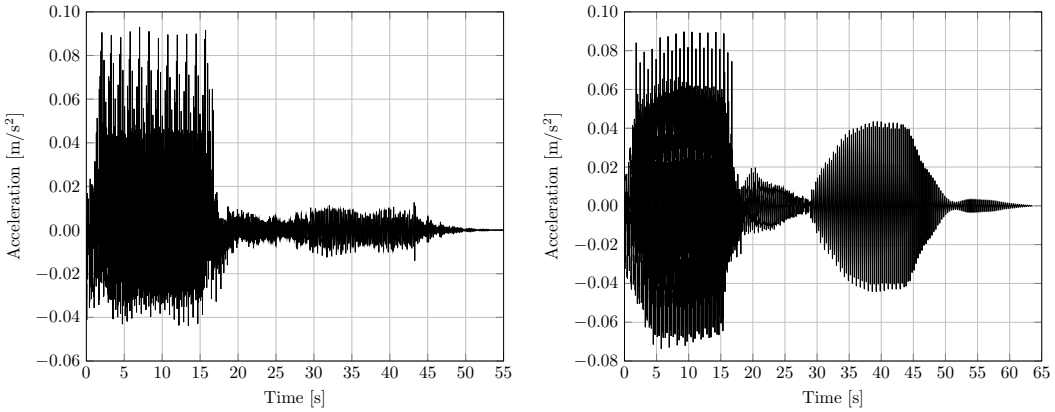

(a) Without added mass of train. **(b)** With added mass of train.

Figure 4.13: Acceleration time history of ten span, 45 m span length model for train speed of 60 km/h.

The maximum acceleration for the single span, 45 m span length model is 0.17 m/s^2 and 0.26 m/s^2 for the model without and with the mass of the train, respectively. The critical sub-resonant speeds are 75.90 km/h and 59.26 km/h, the latter being relatively close to the 60 km/h which was used in the FE model. The effect of this is clear in Figure 4.12(b) where resonant vibrations can be seen. The last axle of the train crosses the node of interest at 16.75 s, where after the damping of the bridge comes in to effect.

The acceleration time histories shown in Figure 4.13 are for the first mid span node

of the ten span model. While the train occupies the first span between 0 s and approximately 18 s the accelerations range from -0.04 m/s^2 to 0.08 m/s^2. Between 18 s and 42.4 s when the last axle of the train leaves the bridge the vibrations are relatively low at the first mid span node. When the mass of the train is included in the model, a similar phenomenon occurs over the first 18 s, except the accelerations range between -0.07 m/s^2 to 0.08 m/s^2. Resonant vibrations are still apparent in the vibration of the first mid span node, but only after the last axle of the train has left the fifth span of the bridge at 28.9 s. This may be a numerical effect and requires further investigation. The magnitude of acceleration ranges from -0.04 m/s^2 to 0.04 m/s^2 over the time the train is still on the bridge, until it leaves the last span.

In Figure 4.14, the acceleration time histories of the mid span node of the second to fifth span is shown for the ten 45 m span model, with mass of train included and at a train speed of 60 km/h. Resonant vibrations are less clear but still apparent in spans two and three, and to a much lesser degree in the fourth and fifth spans. Magnitudes of accelerations are also generally less than those in the first span.

The magnitudes of accelerations in the one span model are significantly greater than those of the ten span model. Resonant vibrations is clearly identifiable in Figure 4.12(b), and noticeable (to a much smaller degree and magnitude) in Figure 4.13(b). Possible trends relating the maximum acceleration with the number of spans of the model was further investigated by plotting Figures 4.15 and 4.16.

The highest calculated acceleration is 0.51 m/s^2 which occurred at midspan of the single span 50 m model with no added mass and at a train speed of 100 km/h. The lowest acceleration calculated was 0.02 m/s^2, and this occurred on a number of the multi-span models with 50 m span lengths, and at speeds of 20 km/h to 40 km/h.

At low speeds of 20 km/h to 40 km/h the difference in acceleration between the models with different number of spans is low. As speeds increase the maximum accelerations increase and the variation in spread of the maximum accelerations is higher. This is apparent in all models (with different span lengths and with and without the mass of the train considered). This supports the assumption that bridges with continuous spans have lower peak deck accelerations, as the approach adopted by *Eurocode* (EN 1991-2) [2003].

The general trend of an increase in acceleration as the train speed increases was also observed. Resonance was not observed in the range of speeds investigated but sub-resonance was noted in the 45 m span model with the added mass of the train included. For this particular case the fundamental frequency was calculated to be

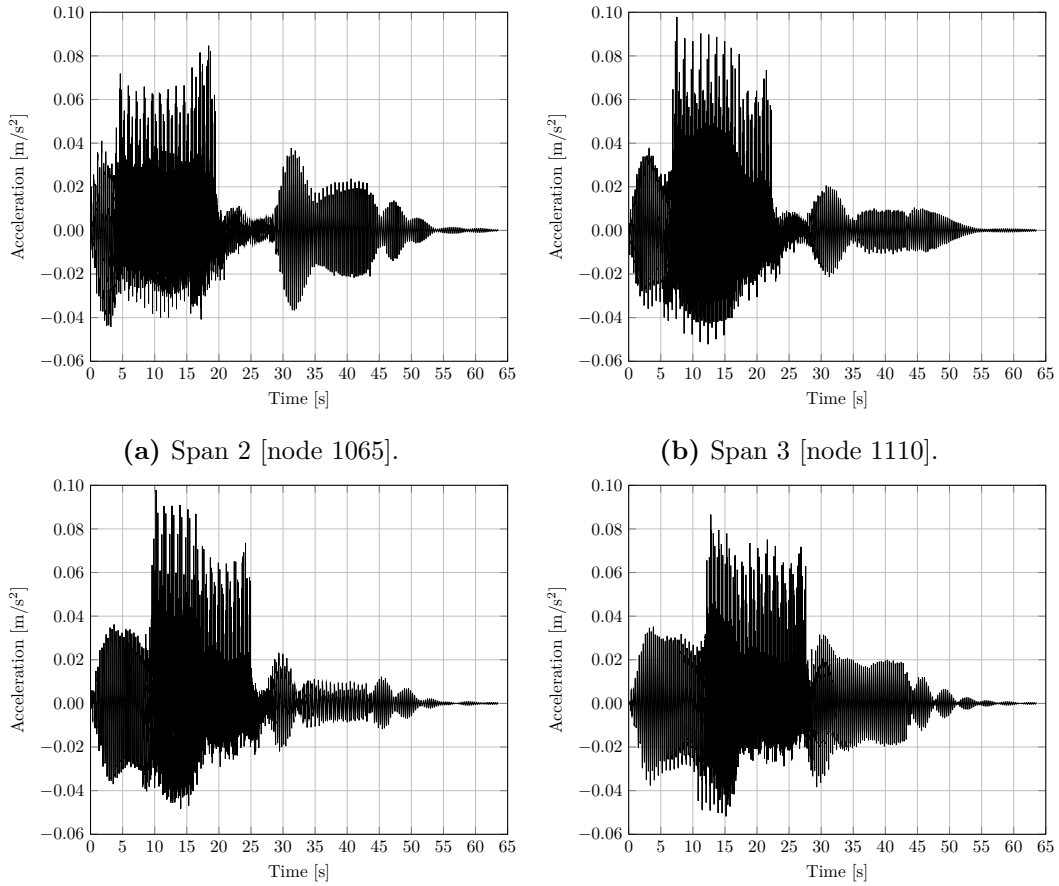

(a) Span 2 [node 1065].

(b) Span 3 [node 1110].

(c) Span 4 [node 1154].

(d) Span 5 [node 1198].

Figure 4.14: Acceleration time history for midspan node of spans two to five for the 45 m, 10 span model at train speed of 60 km/h with added mass of the train included in the FE model.

3.181 Hz, and the critical speed for resonance to occur is 118.52 km/h. Sub-resonance occurs at 59.26 km/h, which is very close the speed of 60 km/h where the peak in acceleration can be observed in Figures 4.15 and 4.16.

As the span length increased from 40 m to 45 m and 50 m, the difference in accelerations at low speeds was not really distinguishable. However, as speeds increased past 60 km/h it was clear that with each span length increase the maximum acceleration increased. The increase in maximum acceleration for models with fewer continuous spans was more significant in comparison to models with more continuous spans.

The maximum accelerations of the the mid-span node of the first span and last span are almost identical. This is likely due to the symmetry of the model, and the idealisation of the moving forces model. The maximum accelerations show an

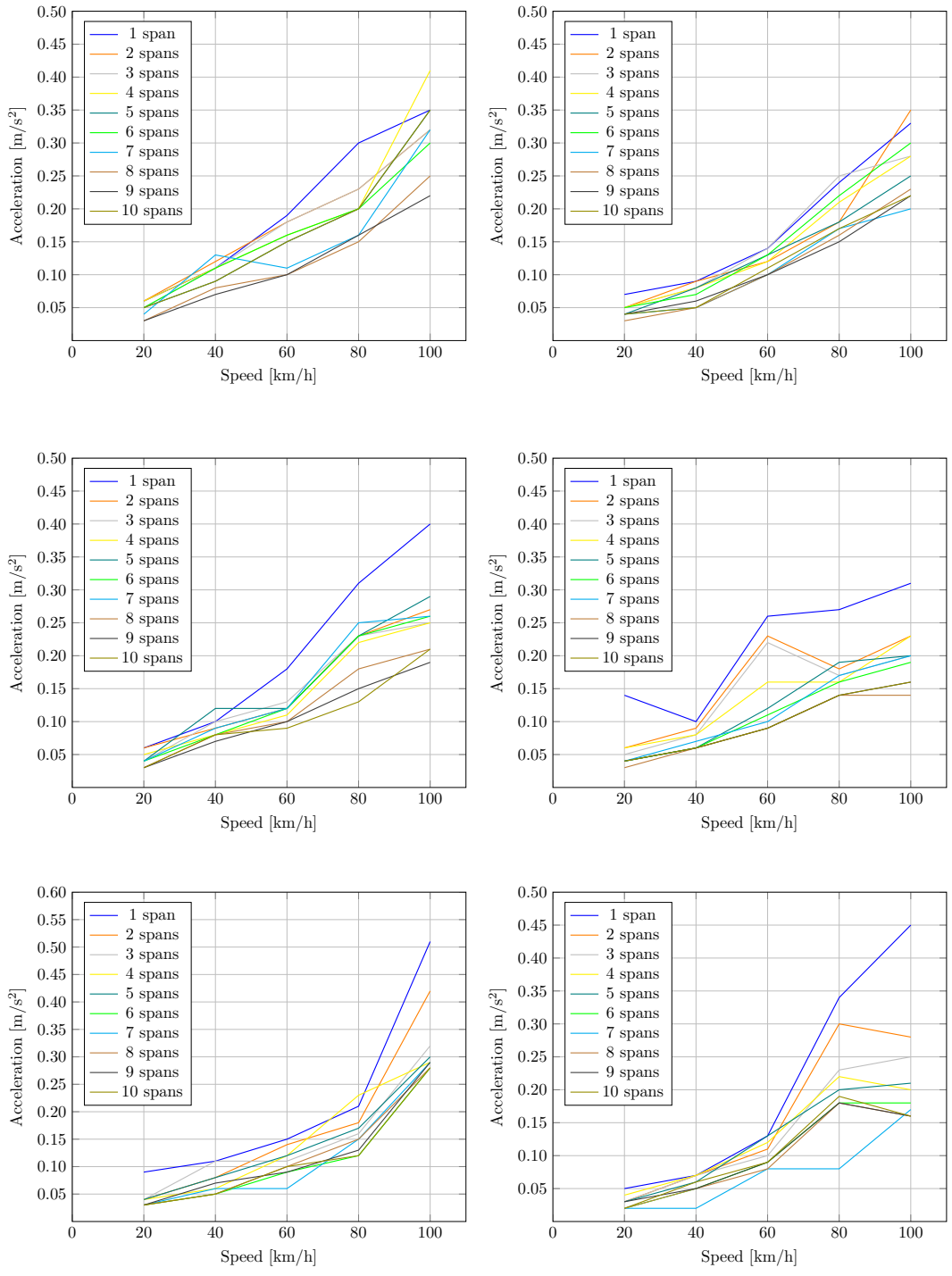

Figure 4.15: Maximum acceleration of the mid-span node of the first bridge span for the 40 m, 45 m, and 50 m (top to bottom) without and with the mass of the train (left column and right column).

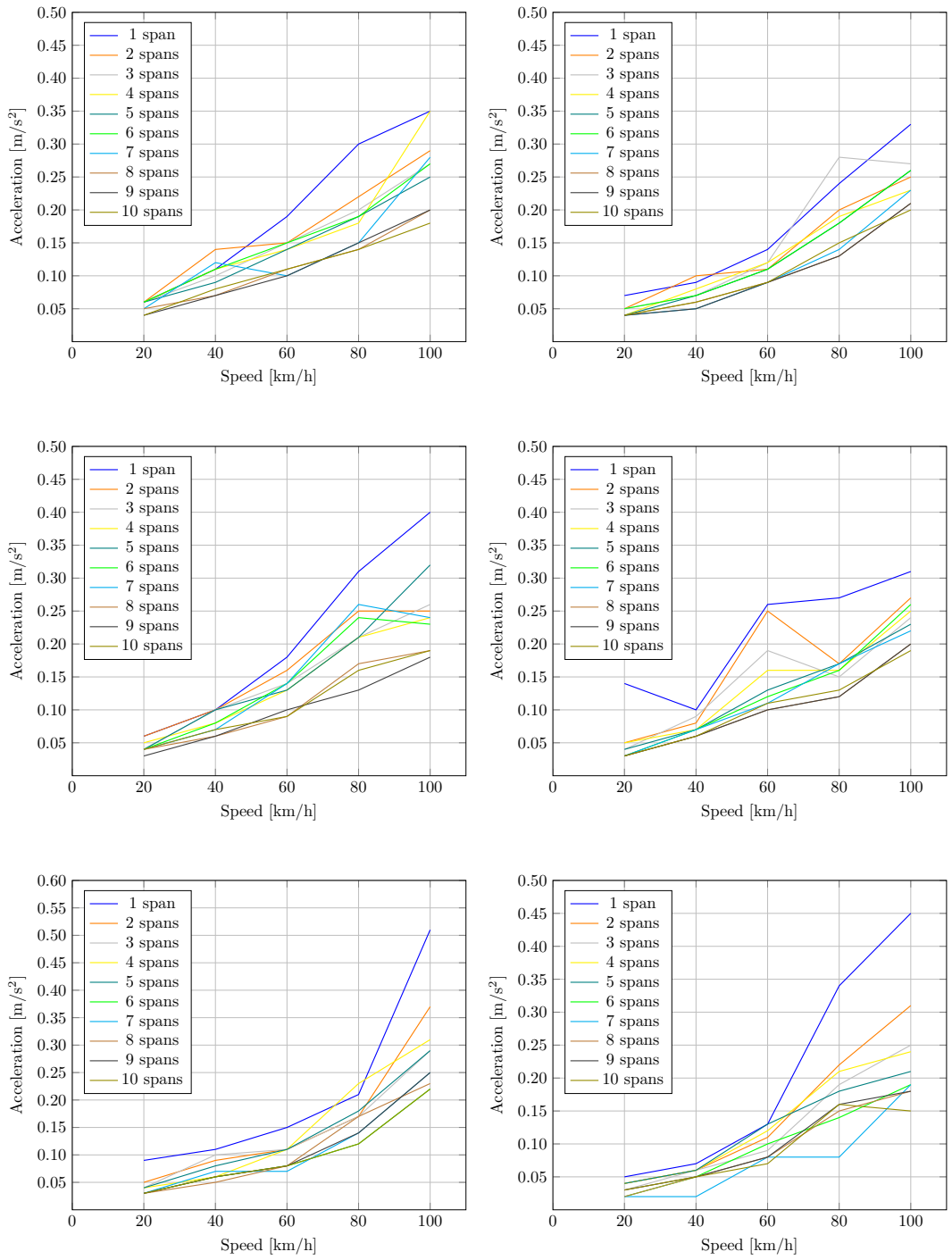

Figure 4.16: Maximum acceleration of the mid-span node of the last bridge span for the 40 m, 45 m, and 50 m (top to bottom) without and with the mass of the train (left column and right column).

increase over the speeds which were investigated. As the number of spans increase the maximum accelerations decrease. At low to moderate speeds of 20 km/h to 60 km/h the decease is much smaller in comparison to the accelerations at 100 km/h.

4.4 Chapter summary

The numerical analyses resulted in some interesting findings about both the dynamic properties, and the response the model has to the moving concentrated force model. The natural frequencies and mode shapes were calculated for bridge models ranging from one span to ten continuous spans, for span lengths of 40 m, 45 m and 50 m. Adding the mass of a fully loaded train by lumping it at the nodes of the model was also investigated.

The natural frequencies and mode shapes were presented in summary only, while the full results is attached in Appendix A & B. When the mass of the heavy haul train was accounted for by lumping at the nodes of the model there was a drastic decrease in natural frequencies of approximately 20 %. Spatial periodicities in natural frequencies and mode shapes were observed and the nature in which mode shapes change when the number of continuous spans of a multi-span bridge was also observed.

The single span model had the highest maximum displacement and acceleration for all the models. The critical nodes, in terms of displacements and accelerations, were generally found to be the centre node of the first and last span of the multi-span models. For the number of spans greater than three, there was no significant differences in the maximum displacement, whereas for the acceleration there was a general, yet small, decrease at low to moderate speeds as the number of spans increased. The decrease becomes larger as the speeds approached 100 km/h.

Chapter 5

The Olifants River Viaduct: a case study

The parametric investigation of the previous chapter is extended further in this chapter by conducting a case-study of the ORV. The existing ten-span model with 45 m span lengths has been extended to eleven spans, with the as-built geometry identical to the local and global geometry of the ORV shown on the construction drawings. Results from the case-study will be compared to analytical and experimental investigations which have been conducted by other authors, however, the number of railway trains investigated in the case study was also limited to 40 due to computational power.

The location and history of the bridge is presented first, followed by aspects of the bridge and trains. Thereafter the study's results are presented, and compared to the available analytical results and experimental data.

5.1 Location and history

The ORV is situated on the 861 km Sishen-Saldanha rail export line – the second longest heavy haul railway line in the world [Kuys, 2009]. The line is primarily used to transport iron ore from mines in the Sishen area of the Northern Cape, South Africa, to export at the port of Saldanha on the West Coast. The line is a single track, narrow gauge (1067 mm) with crossing loops at 40 km intervals. The line was constructed in the early 1970s and was completed in 1976. In 1977 it was transferred to the current operator, Transnet Freight Rail, a parastatal which was known as South African Railways and Harbours at the time.

Since the bridge's inauguration in the 1970s the mining areas around Sishen have expanded. This, along with the increasing demand and competition from foreign markets have led Transnet Freight Rail (TFR), the owners and operators of the line,

Figure 5.1: The 861 km Iron Export line which runs between Sishen and Saldanha, South Africa.

to progressively increase the capacity of the line. An operational plan was sanctioned by TFR whereby railway traffic was increased by [Kuys, 2009]:

i. Increasing the axle loads of the wagons.

ii. Increasing the length of the train by adding additional wagons.

iii. Increasing the operating speed of trains.

iv. Adding new crossing loops on the line.

The above-mentioned actions arising from the increasing demand on heavy haul rail infrastructure such as the ORV, particularly increasing the axle load and number of trains, may have consequences on the structural performance of the bridge, even though the ORV was initially designed for a 30 t axle load – trains initially operated with 26 t axles. The aim of this study, and including the analytical and experimental work conducted by other authors as a bigger project, is determining the response of the bridge with the 30 t axle loads using the current FE model and comparing it to available measured and analytical data. Thereafter, recommendations on the future improvement of the model shall be made.

5.2 The bridge

The viaduct consists of a pre-stressed concrete (PSC) box-girder. The original engineering drawings indicate that concrete used in the structure is of class H20 and has a 28 day cube compressive strength of 41 MPa. Normal reinforcing bars used in the deck consisted of both "R" and type "Y" reinforcement with characteristic yield strengths of 250 MPa and 450 MPa respectively. Prestressing cables of type KA 40 with a cross-sectional area of 1600 mm^2 and a strength of approximately 1600 MPa were used to longitudinally post tension the deck.

Figure 5.2: A global perspective of the Olifants River Viaduct.

The viaduct was constructed using the incrementally launched method. Prestressing of the deck was done in three stages:

1. In the shutter before launching, at a compressive cube strength of 28 MPa.
2. Between the shutter and the abutment, at a compressive cube strength of 33 MPa.
3. When the deck is in its definitive position.

The viaduct totals 1035 m in length, separated in to 23 spans equally spaced at 45 m. The first 11 spans from either abutment is continuous, before the expansion joint which is located on either edge of span 12 (the central span), making the span simply supported. This essentially translates to one 495 m long continuous girder, one simply supported 45 m span and another 495 m long girder.

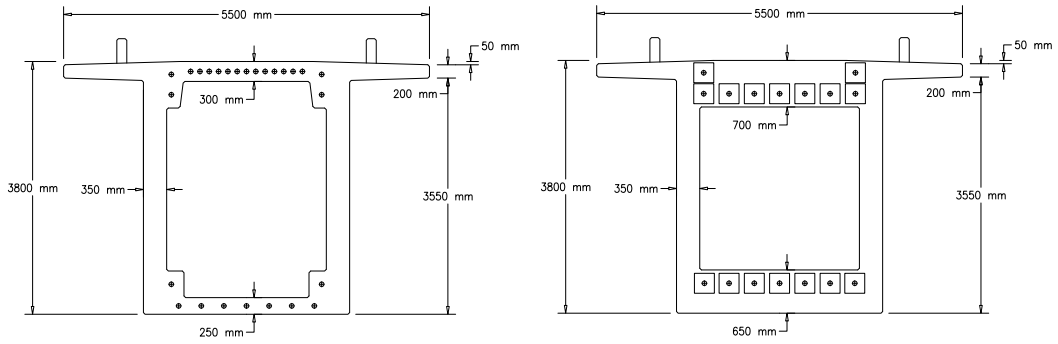

(a) Deck cross-section at midspan **(b)** Deck cross-section at piers

Figure 5.3: General configuration of the deck cross-sections

The box-girder type cross-section of the deck is 3.800 m in height and 5.500 m in width and is kept constant along the length of the entire viaduct. The thickness of the web is also constant at 0.350 m along the length of the viaduct. The thickness of the top and bottom flanges vary, depending on the location in the span. The thickness of the top flange is 0.300 m, this increases to 0.700 m near the supports and at mid-span. The thickness of the bottom flange is 0.250 m and this increases to 0.650 m near the supports and at mid-span. The increasing thickness is to allow the prestressing cables to be anchored.

The girder is supported by 22 reinforced concrete H-shaped piers of heights varying between 17.850 m (Pier 1) and 51.500 m (Pier 10). The cross-sectional width of each pier is 4.600 m, while the thickness of the flanges and webs are 0.500 m and 0.400 m respectively. The cross-sectional height varied along the length of the pier from 2.400 m at the top at a grade of 3.5 : 100. Each pier has a capping of 0.700 m, except for the piers supporting the drop span where the thickness increases to 1.200 m.

The first four piers in the Saldanha side and the first three piers in the Sishen side of the viaduct are founded on spread footings while the central 15 piers are founded on either Benoto 300 $\times$ 300 mm piles or 559 mm diameter cased driven piles.

5.3 The train

Prior to 2007 a 216 wagon head-end powered train operated on the Ore Line [Ngwenyama et al., 2013]. The head-end trains could not cope with the increasing demand and in 2007 a new freight train based on Radio-Distributed Power (RDP) was commissioned. RDP trains allow locomotives to power the train from intermediate

points, and in comparison to head-end powered trains, in-train forces are reduced and train brake propagation is improved [Ngwenyama et al., 2013].

The rolling stock has changed over the past four decades. At present locomotives 15E, 34D and 43E are in operation. The attributes of each locomotive is summarised in Table 5.1. The most common wagon type, CR-13, is fitted with Scheffel self-steering bogeys [Kuys, 2009]. The wagon has a gross weight of 20 tonnes when empty and 120 tonnes when loaded. This equates to a static load of 300 kN per an axle. The total length of the three wagon rakes is approximately 3.85 km and the total length of the train becomes approximately 4.1 km when including the four locomotive consists, making this the longest heavy haul train in the world.

Table 5.1: Characteristics of locomotives currently in operation.

	Class 15E	Class 34D	Class 43D
Manufacturer	Toshiba	GE	GE
Designed max. speed	90 km/h	100 km/h	100 km/h
Bogies	2	2	2
Axles per bogie	2	3	3
Axle mass	30 000 kg	18 850 kg	21 630 kg

Figure 5.4: A consist of one class 15E locomotive and a class 43D locomotive.

A 40 wagon train consisting of type CR-13 wagons was only considered for comparison with the analytical results. The total train length is approximately 410 m and the number of axles equal to 160 at 30 tonnes/axle. Locomotives were ignored because,

firstly, they only make up a small number of contributing axle loads compared to the overall length of the train, and secondly their mass is not significantly different from a fully loaded CR-13 wagon. The train configuration for the comparison with events which the monitoring system recorded are described for each particular event in section 5.5.2.

5.4 Modal Analysis

5.4.1 Finite element modal analysis

A numerical modal analysis was conducted on the first 11 spans of the girder on the Sishen side of the bridge. This 11-span section acts independently to the rest of the bridge due to the joints on either side of the 12^{th} span (the drop span). The same material properties used in the parametric study was used in the case-study, except for the material stiffness which was increased to 39 GPa. The stiffness was increased due the age of the bridge and the fact that there is normal and prestressing steel in both the longitudinal and vertical direction of the girder. The FE model was meshed into 4.5 m beam elements such that each span contained 10 beam elements.

The numerical modal analysis was conducted using the Inverse Vector Iteration approach. The mass matrix was assembled diagonally in Sofistik. The first 11 natural frequencies and mode shapes are presented in Table 5.2 and Figure 5.5 respectively. These 11 modes make up the first concentrated zone of the 11-span continuous section until the drop span on the Sishen side of the ORV.

The fundamental frequency from the numerical FE analysis is 4.091 Hz, while the last frequency in the concentrated zone was calculated to be 8.717 Hz. These 11 natural frequencies in the concentrated zone are closely spaced over a range of only 4.626 Hz. The mode shapes observed for the case-study is in agreement with the observations made in the parametric investigation in the previous chapter. The mode shapes are perfectly symmetric about the centre point of the 11-span girder for all odd modes, and can therefore be mirrored about a vertical plane at mid-span. On the other hand, even modes are rotated by 180 degrees about the same point.

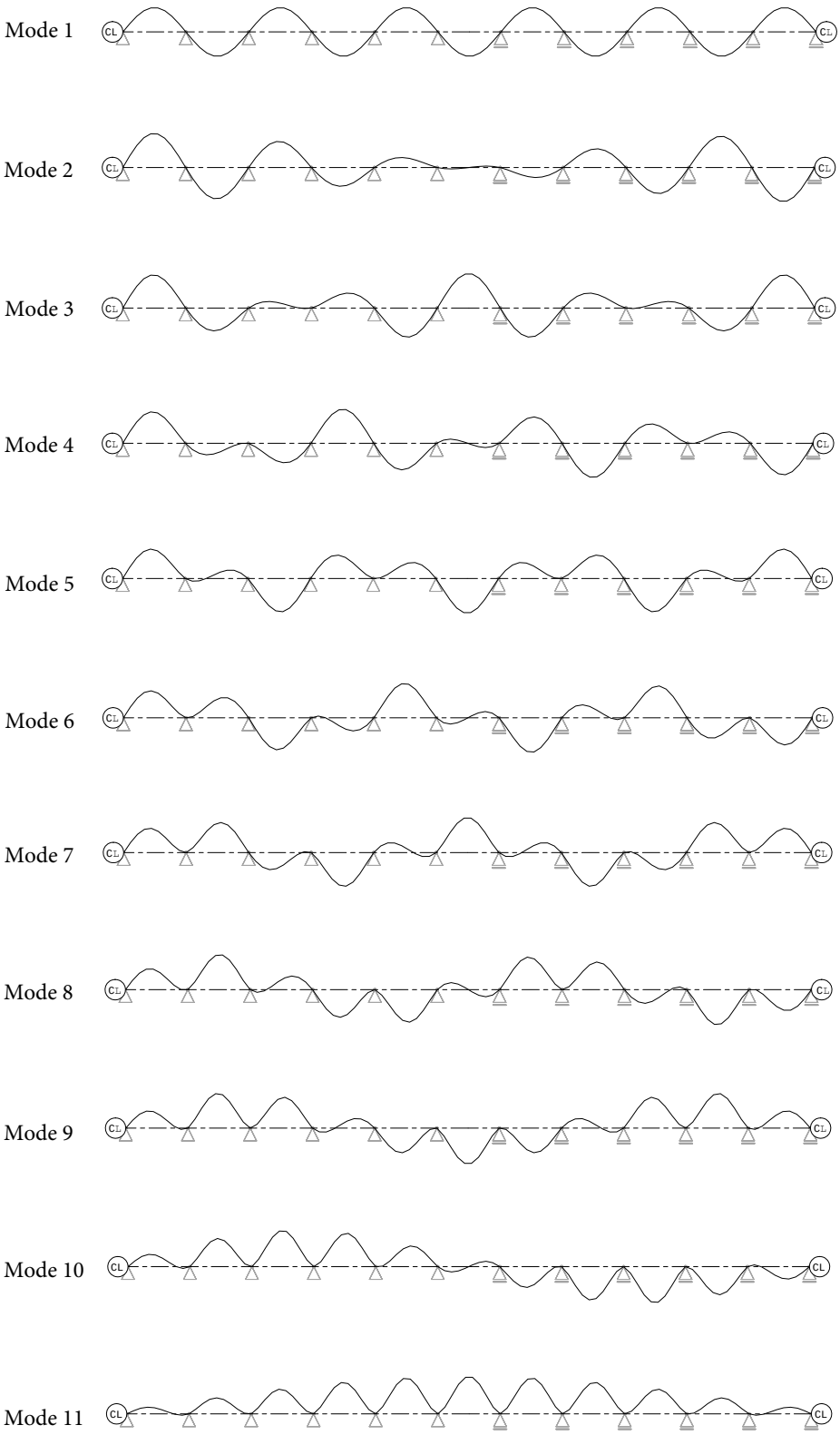

Figure 5.5: The first 11 vertical mode shapes of the FE model.

Table 5.2: Natural frequencies for the first 11 modes for the FE model.

Mode	f_{FE} [Hz]
1	4.091
2	4.184
3	4.452
4	4.864
5	5.382
6	5.972
7	6.601
8	7.263
9	7.839
10	8.356
11	8.717

5.4.2 Comparison with analytical and experimental results

Experimental work on the ORV was ongoing at the time this dissertation was carried out, and only limited data was available. Thus far, the initial experimental test was conducted on only a single girder, and a follow up test was conducted on the first six spans. The results show that the first vertical mode of vibration was measured to be 4.075 Hz.

While the results from the FE model and the analytical investigation can be compared relatively well because they are based on similar assumptions, the same is not true for the experimental results of the actual girder. The inherent differences, such as the presence of a ballasted track and complex (imperfect) boundary conditions make this comparison complicated. In the future, once experimental investigations have been completed with satisfactory results the FE model can be validated, and a more thorough comparison can be conducted. The first natural frequency of 4.075 Hz does, introspectively, appear to be close to the fundamental frequency of the FE model.

The analytical investigation conducted by Kabani and Moyo [2014] assumed the following parameters: E = 39 GPa, I = 9.58 m^4 and ρA_L = 26060 kg/m and 13 820 kg/m for a loaded and unloaded train-bridge system respectively. The natural frequencies of the first 11 modes of vibration of the FE model and the analytical investigation are compared in Table 5.3, where

$$\Delta f = \frac{f_{FE} - f_{analytical}}{f_{FE}} \tag{5.1}$$

and the value is presented as a percentage (%).

Table 5.3: Natural frequencies for the first 11 modes for the FE model and analytical investigation.

Mode	Without mass of train			With mass of train		
	f_{FE} [Hz]	$f_{analytical}$ [Hz]	Δf [%]	f_{FE} [Hz]	$f_{analytical}$ [Hz]	Δf [%]
1	4.091	4.09	0.02	2.997	2.90	3.24
2	4.184	4.19	-0.14	3.066	2.97	3.13
3	4.452	4.47	-0.40	3.262	3.17	2.82
4	4.864	4.90	-0.74	3.563	3.47	2.61
5	5.382	5.44	-1.08	3.942	3.86	2.08
6	5.972	6.06	-1.47	4.373	4.30	1.67
7	6.601	6.740	-2.11	4.833	4.78	1.10
8	7.263	7.430	-2.30	5.296	5.27	0.49
9	7.839	8.11	-3.46	5.736	5.45	5.43
10	8.356	8.70	-4.12	6.113	6.17	-0.93
11	8.717	9.12	-4.62	6.376	6.67	-4.61

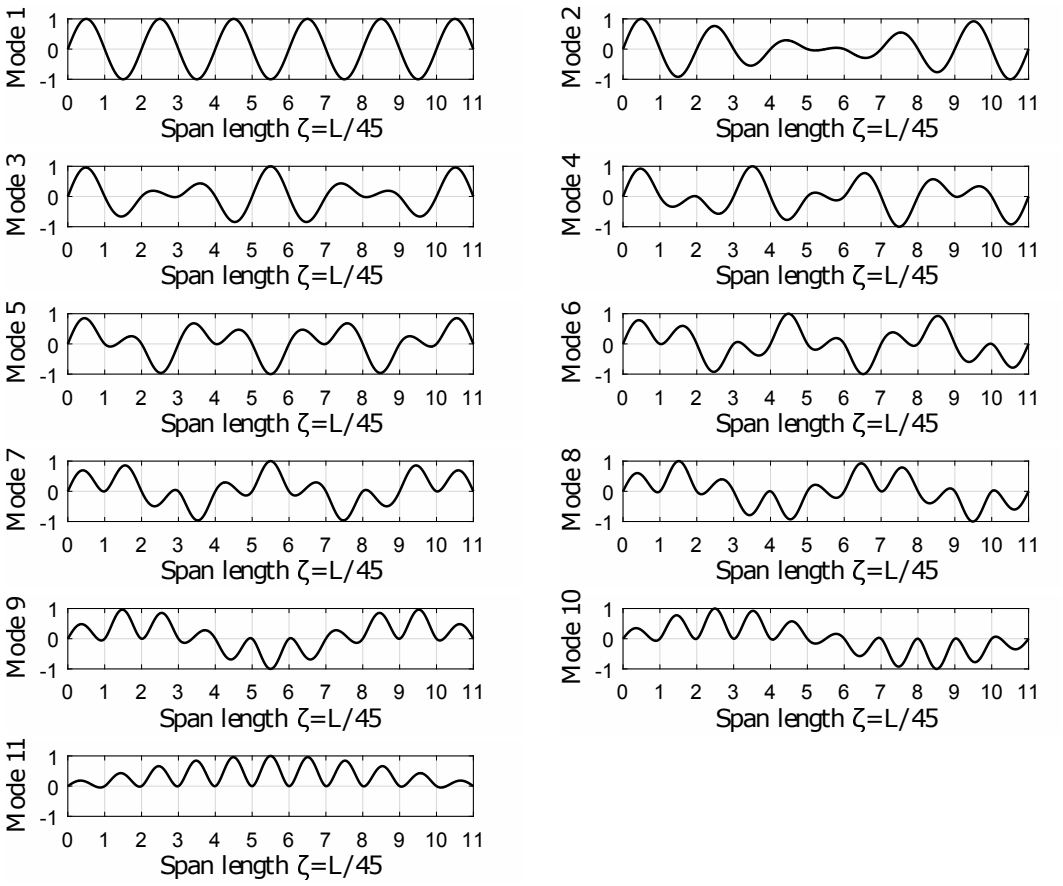

Figure 5.6: The first 11 vertical mode shapes of the analytical solution presented by Kabani and Moyo [2014].

Mode shapes from the FE model and the analytical study are in full agreement with one another (Figure 5.5 and 5.6). The natural frequencies in the first concentrated zone which are presented in Table 5.3 are also in good agreement. The difference in frequencies varies from 0.02 % for mode 1 to 4.62 % for mode 11. When the bridge is loaded there is a greater discrepancy in frequencies, however, there is still agreement of frequencies to a reasonably good degree. Difference in frequencies range from 3.24 % for mode 1 to -4.61 % for mode 11, while the greatest difference of 5.43 % occurs for mode 9.

5.5 Train-induced dynamic response

5.5.1 Finite element dynamic analysis

Simulations were conducted with the same moving forces load models described in Chapter 3 to determine displacement and acceleration time histories at mid-span of certain spans. Each span of the 11-span girder was again mesed into 4.5 m beam elements. The Newmark Method was used for this investigation, and the parameters as defined Bathe [2005], $\gamma = \frac{1}{2}$ and $\beta = \frac{1}{4}$, was used. The values chosen guaranteed unconditional stability, irrespective of the time step, however the time-step needs to be small enough to ensure the solution is accurate. For this reason a time step of 0.001 s was chosen, unless otherwise stated.

Displacement and acceleration time histories are shown in Figure 5.7 for span 23 (the 1st span on the Sishen side of the bridge).

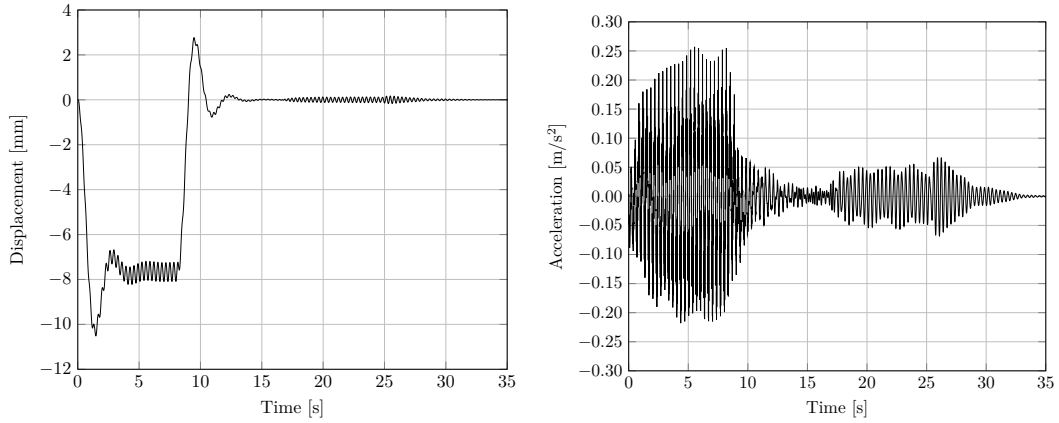

(a) Displacement. **(b)** Accelertion.

Figure 5.7: Displacement and acceleration time histories of the mid-span node of span 23 and for a train speed of 111 km/h.

5.5.2 Comparison with analytical and experimental results

Displacement and acceleration time histories are presented, and where the data is available, compared to results from the analytical model. Figure 5.8 and 5.9 show the comparison of displacement time histories for the centre node of span 23 (the first span on the Sishen side of the viaduct) and span 20 (the fourth span on the Sishen side of the viaduct).

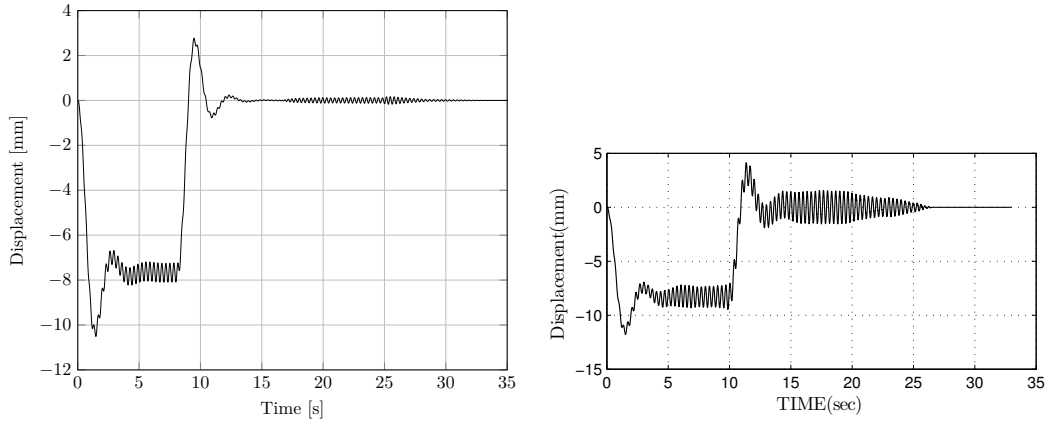

(a) FE model. **(b)** Analytical solution.

Figure 5.8: Comparison of FE and analytical displacement time history at the centre of span 23 at resonant speed of 111 km/h for the FE model and 108 km/h for the analytical model.

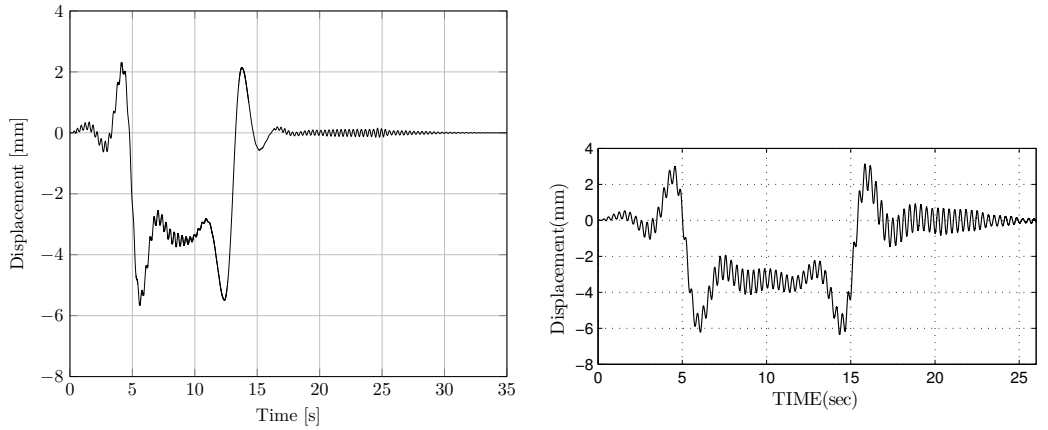

(a) FE model. **(b)** Analytical solution.

Figure 5.9: Comparison of FE and analytical displacement time history at the centre of span 20 at resonant speed of 111.67 km/h for the FE model and 103.27 km/h for the analytical model.

For the FE model, the first frequency when the mass of train is included in the model (2.997 Hz) translates to a critical speed of 111.67 km/h at resonance, and a sub-resonant speed of 55.83 km/h. The first frequency of the loaded bridge obtained from the analytical study was marginally lower than that of the FE model, this translated to a speed of 103.27 km/h and 51.63 km/h at resonance and sub-resonance, respectively.

The comparison of the time displacements of the FE model and the analytical investigation is generally very good in Figure 5.8, particularly over the time while

the train is travelling over the node of interest. The only significant difference is seen once the last axle of the train passes the node and enters the adjacent span, the vibration is almost not visible in the FE model. This is due to the technique of lumping the mass of the train at the nodes in the FE model, whereas, in the analytical study the axle loads were modelled as moving masses and is therefore expected to perform much more similarly to the real structure.

Displacements of mid-span of span 20 of the FE model and analytical solution [Figure 5.9] also have a good degree of similarity. The behaviour of the displacement of the mid span is near identical while first axle of the train leads up to span 20. Over the remainder of the time domain while the bridge is trafficked, the movement of the node is still similar, however, the vibration effect is significantly lower in the FE model.

Figure 5.10 shows the displacement history of the centre node of span 23 and span 20 at the sub-resonant speed of 55.83 km/h. The graph shows a much smoother displacement history for both nodes. The only vibration that is noticeable [to a very small degree] is between 5 s and 15 s in Figure 5.10(a). Over that period the bridge is fully loaded [i.e., first axle has left the end of the bridge and the last axle has yet to reach the start of the bridge].

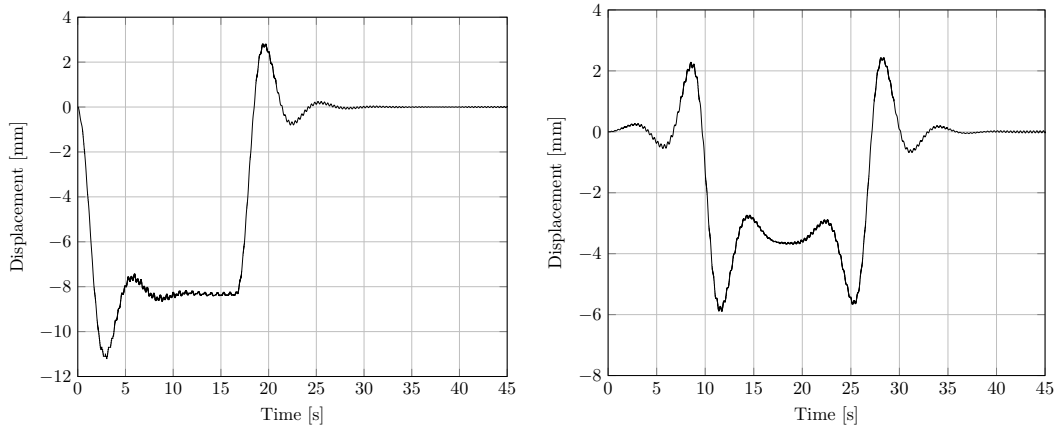

(a) Span 23 [end span]. **(b)** Span 20.

Figure 5.10: FE model displacement time history of mid-span of span 23 and span 20 at sub resonant speed of 55.83 km/h.

Accelerations for the same nodes are presented in Figures 5.11 [at the critical resonance speed] and 5.12 [at sub-resonance]. At the critical resonant speed, the maximum acceleration in span 23 was calculated to be 0.26 m/s^2 compared to 0.15 m/s^2 for span 20. For sub-resonance, maximum accelerations were much lower at

-0.07 m/s^2 for span 23 and 0.06 m/s^2 for span 20.

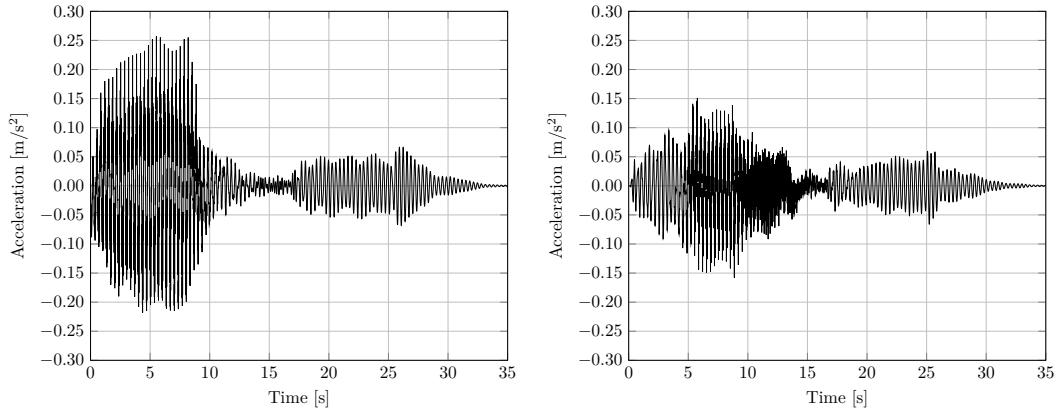

(a) Span 23 [end span]. **(b)** Span 20.

Figure 5.11: FE model acceleration time history of mid-span of span 23 and span 20 at resonant speed of 111.67 km/h.

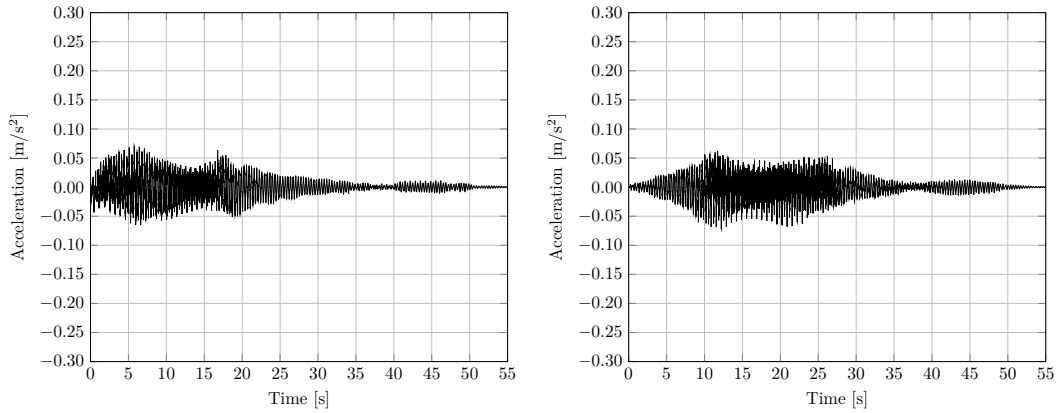

(a) Span 23 [end span]. **(b)** Span 20.

Figure 5.12: FE model acceleration time history of mid-span of span 23 and span 20 at sub resonant speed of 55.83 km/h.

Resonant phenomenon is only clear in Figure 5.11(a), between 0 s and 8 s when the first span of the bridge is being trafficked by the moving load at 108.67 km/h. The vibrations in span 20 are much lower than that of span 23, and resonant vibrations is not distinguishable in the acceleration time history. At the sub-resonant speed the accelerations are very low and no resonance is visible. These results support the finding that accelerations, like displacements, are greater in end spans compared to the central spans of the bridge. This is most likely due to the high stiffness of the interior spans of the continuous bridge, which was also discussed in the results of the numerical investigation in Chapter 5.

Acceleration time histories measured by Busatta and Moyo [2018] using a permanent monitoring system which is installed on the viaduct at span 20 is presented and compared to FEM acceleration time histories in Figure 5.13 and 5.14. A Wheel-Impact-Monitoring & Weight-In-Motion (WIM-WIM) system installed on the track on span 21 provided data of two trains with known configurations of locomotives and wagons, as well as their static masses. The WIM-WIM system is installed on a carefully maintained rail segment, and if irregularities are noticed they can generally be attributed to the wheels or suspension of the vehicle Busatta and Moyo [2018].

The train configurations of the two events were:

i. A 15E and 43D locomotive, with 38*CR13+CR14*CR14+1*CR17+1*CR9 wagons.

ii. A 15E and 43D locomotive, with 41*CR13+CR13*CR14+5*CR17 wagons.

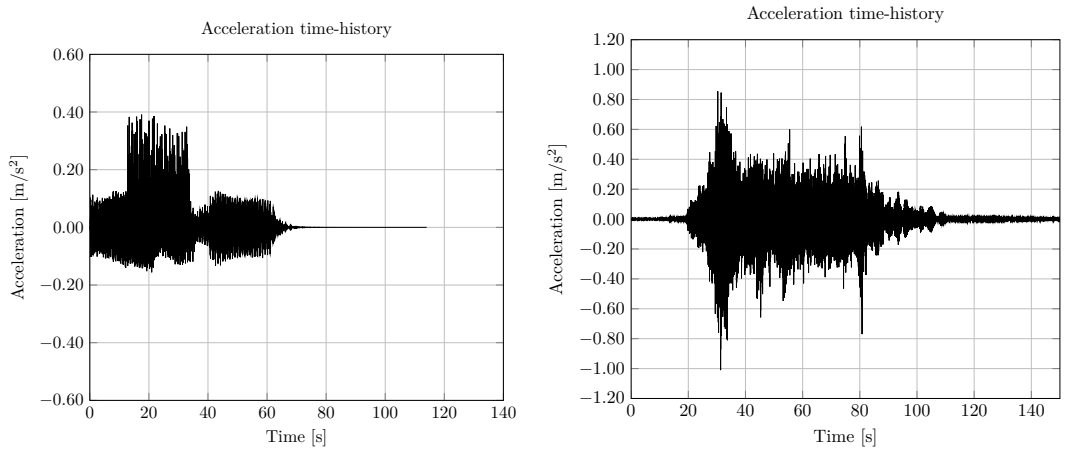

(a) FEM **(b)** Measured

Figure 5.13: Comparison of FEM and measured acceleration time histories at mid-span of span 20 with train configuration (i) at a speed of 44.4 km/h.

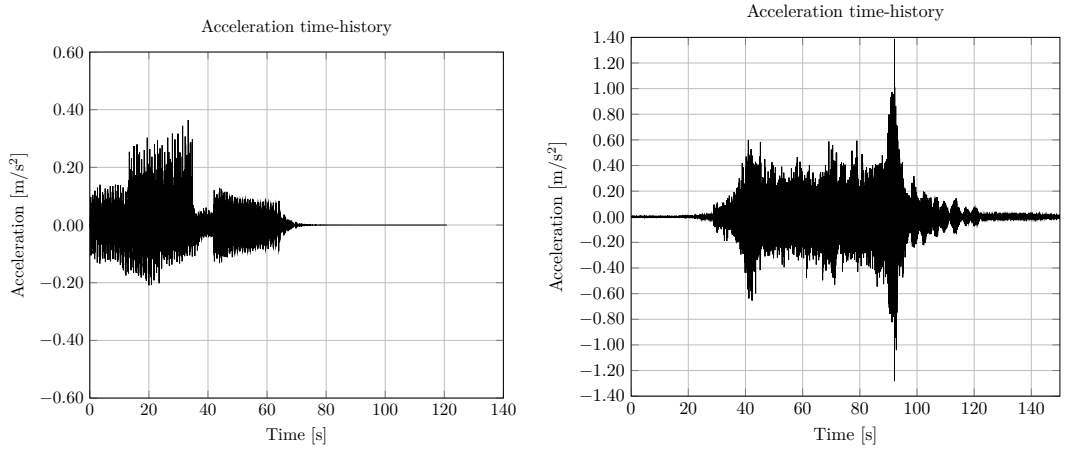

(a) FEM **(b)** Measured

Figure 5.14: Comparison of FEM and measured acceleration time histories at mid-span of span 20 with train configuration (ii) at a speed of 44.6 km/h.

The correlation between the FEM and measured acceleration time histories is not good. Sampling for the measured time histories began before the first axle of the train entered the viaduct, resulting in an offset in the time domain between the two comparisons. The factors which contribute to the measured performance, which include the track system and irregularities have not been considered in the FEM model, and the model has not been validated. Nonetheless, the results of this work generally shows that the FEM model is, firstly, a good starting point to further this study, and secondly, has provided valuable insight into the performance of continuous, multi-span railway bridges.

Chapter 6

Conclusion & future work

The objective of this research was to investigate, numerically, the dynamic properties and response of continuous, multi-span railway bridges under the traffic of long heavy haul trains. This chapter summarises the work, provides concluding remarks on the major findings and recommends future work which may build on this research.

6.1 Summary

Dynamic problems associated with railway bridges can broadly be defined into two categories: those associated with high speed trains and those associated with heavy haul trains. The factors which influence these problems, and which were of particular interest in this research, were the mass, rigidity and span length of the bridge, and the length and speed of the train travelling on the bridge. When designing a bridge for dynamic effects, two possible methods can generally be applied. Either the structure is designed for static loads, and dynamic effects are accounted for using an amplification factor. Alternatively, a full dynamic analysis whereby the bridge and train is modelled and the response is simulated using, for example, a numerical method like the Finite Element Method.

There exists a "grey" area in design codes when designing for special structures such as a multi-span, continuous railway bridge which experiences dynamic effects from very long heavy haul trains travelling at low to moderate speeds. When the design process for *Eurocode* (EN 1991-2) [2003] is applied to a scenario such as this, a detailed dynamic analysis is not warranted and the structure may be designed using the dynamic amplification factor. The primary concern of this is that the additional mass of the train in conjunction with amount of axles at constant spacings may affect the dynamic behaviour of the structure such that accelerations and displacements become problematic. This was the underlying motivating factor for this research.

The work that was reviewed in preparation for this study showed that the majority of investigations around the dynamic behaviour of railway bridges involved high speed trains. These studies involved the analysis and assessment of bridges at speeds which may result in resonance. Different load models, such as the moving forces, sprung-mass and full vehicle-bridge interaction model, were also investigated. These studies were generally conducted on smaller, single span and simply supported bridges. Research on continuous, multi-span beam type structures were limited to analytical methods to calculate response.

The aim of this research was therefore to investigate the dynamic properties (natural frequencies and mode shapes) of multi-span, continuous railway bridges. The Finite Element program SOFiSTiK was used to conduct a numerical modal analysis to extract the dynamic properties for a range of bridge configurations ranging from 1 – 10 spans, with span lengths of 40 m, 45 m and 50 m. The dynamic response to a heavy haul train was also investigated by modelling the train as a sequence of moving forces. Accelerations and displacements at the mid-span for all bridge configurations were calculated for train speeds from 20 km/h to 100 km/h, in 20 km/h intervals. Lastly, a case-study was conducted on the Olifants River Viaduct. The dynamic properties was calculated numerically, and compared to available results from an analytical study and experimental measurements obtained using ambient vibration testing. Concluding remarks on all of the above is made in the following section.

6.2 Concluding remarks

Natural frequencies and mode shapes were obtained for all bridge configurations. Frequencies were also obtained for a bridge assumed to be fully loaded by four-axle wagons which weigh 120 kN/ wagon. The mass was equally lumped at the nodes of the FE bridge model. The natural frequencies of the bridge resulted in critical speeds in excess of 100 km/h for the particular train investigated, however, sub-resonant speeds fell within the range of speeds which were investigated.

The natural frequency of any mode which was identified in a bridge configuration with certain span length and number of spans was also identified in the configuration which has the same span length but a multiple of the number of spans, but at a higher mode. This meant that the each of the modes identified in the single span models are always the first mode in each of the concentrated clusters of natural frequencies which are observed for beam type structures.

For continuous beam-type structures which have the concentrated clusters of natural frequencies, it is known that the number of frequencies in the concentrated zone is equal to the number of spans. As the number of bridge spans increase the concentration of clusters increase, but is limited by the first frequency of the next concentrated zone. It appeared as if, as the number of spans increase the frequencies were limited to an envelope approximately equal to the first natural frequency of the bridge. This was further supported by showing that as the number of spans increase frequencies decrease, and in fact, with the addition of each additional span the decrease is less.

The mode shapes of beam type models are trivial for beams with only a few spans. Literature showed that the mode shapes are easily obtained analytically. The mode shapes which were calculated numerically was in agreement with what was found in literature, up to mode six. Higher modes were not obtained in literature and therefore cannot be compared. It was also observed that as the number of continuous spans increase, the mode shapes in the concentrated zone becomes more and more intricate. For bridges with odd number of spans it was found that mode shapes were symmetric about the centre of the bridge and anti-symmetric about the centre for even spans. Contrastingly, for bridges with an even number of spans, the odd modes were anti-symmetric and the even modes were symmetric about the centre of the bridge.

Displacement and acceleration time histories were calculated at mid-span of all bridge configurations at speeds ranging from 20 km/h to 100 km/h. There was no evidence that speed affected the maximum displacement, however, there was a clear indication that as the speed increases, the peak deck acceleration also increased. The response showed that, generally, displacements and accelerations were highest in the first and last span of the multi-span bridges.

When comparing the displacement time history at mid-span of the first span in models which had less than four spans, the difference in displacements were distinguishable. However, when the number of spans were greater than four, a difference in time histories were not observed. In general, the magnitudes of displacements were not affected as the number of spans increased from four spans upwards.

The maximum accelerations which were extracted from the acceleration time histories showed that for speeds less than or equal to 40 km/h the peak deck acceleration was very low and there was very little difference between the peak deck acceleration of all models with different number of spans. As speed increased the peak accelerations increased much faster for models which had fewer spans. The highest accelerations

at 100 km/h were obtained from models with one, two or four spans. The lowest accelerations obtained were from either of the eight, nine or ten span models.

As the span length increased from 40 m to 45 m and 50 m, the difference in accelerations at low speeds was not really distinguishable. However, as speeds increased past 60 km/h it was clear that with each span length increase the maximum acceleration increased. The increase in maximum acceleration for models with fewer continuous spans was more significant in comparison to models with more continuous spans.

The case-study showed an excellent agreement of results between the FEM model and the analytical investigation. Due to the FE model not being validated and not accounting for important aspects such as the track system and irregularities, the correlation between the measured and numerical results were not good. The FE model did not accurately predict the response of the bridge after the train has left the bridge as the mass of the train remained lumped at the nodes in the time domain. Some of these challenges may be addressed in future work.

6.3 Future work

Based on the literature reviewed for this study, it is evident that there is a lack of research into the dynamics of continuous, multi-span railway bridges and especially those carrying special traffic such as very long heavy haul trains. There is a need for both experimental and numerical work in this area. Based on the drawbacks and findings of this thesis, the following issues may be addressed in the future:

i. The Finite Element of the model should include or account for the dynamic properties of the track system, including the rail, sleepers and ballast. This might include additional studies of the track to determine material properties and characteristics of the ballast, sleepers and rail. Finite Element programs such as SOFiSTiK also allow for an investigation into the effect irregularities in the rail might have on the dynamic response of the bridge, however, this might not be of worth for assessment purposes. A full validation process of the FE model should also be done, once more experimental data from the bridge becomes available.

ii. An all encompassing load model of heavy haul trains should be developed, whereby the model is capable of accounting for the mass and suspension of the

vehicle. This will require additional information from the locomotive and wagon manufacturers, as well as additional computing power which can simulate the more robust vehicle model in reasonable time.

iii. The lateral response of the bridge should also be considered in the FE model by including the piers of the bridge.

References

K.-J. Bathe. *Finite Element Procedures*. Prentice Hall, New Jersey, 2005. ISBN 0133014584.

L. Bjorklund. *Dynamic Analysis of a Railway Bridge subjected to High Speed Trains*. PhD thesis, Royal Institute of Technology, 2004.

F. Busatta and P. Moyo. Vibration monitoring of a large scale heavy haul railway viaduct. In *MATEC Web of Conferences*. EDP Sciences, 2015.

F. Busatta and P. Moyo. Assessing the performance of a heavy haul railway viaduct through monitoring traffic loads and dynamic effects. experimental vibration analysis for civil structures. 2018.

W.-F. Chen and L. Duan. *Bridge Engineering Handbook*. CRC Press, Boca Raton, 1999. ISBN 978-0-8493-7434-0.

T. K. Cheung, F. T. K. Au, D. Y. Zheng, and Y. S. Cheng. Vibration of multi-span non-uniform beams under moving loads by using modified beam vibration functions. 228(3):455–467, 1999.

A. Chopra. *Dynamics of structures*. Prentice Hall, fourth edition, 2012. ISBN 0444890459.

R. W. Clough and J. Penzien. *Dynamics of structures*. Computers & Structures, Inc., third edition, 2003.

Department of Mineral Resources. Mineral Statistical Tables. Technical report, Pretoria, 2015.

M. Ebrahimi, S. Gholampour, H. J. Kafshgarkolaei, and I. M. Nikbin. Dynamic behavior of a multispan continuous beam traversed by a moving oscillator. *Acta Mechanica*, 226:4247–4257, 2015.

Eurocode (EN 1991-2). *Eurocode 1: Actions on structures - Part 2: Traffic Loads on bridges*, volume 2. Brussels, 2003.

J. Fish and T. Belytschko. *A First Course in Finite Elements*. Wiley, 2007. ISBN 9780470035801.

L. Frýba. *Dynamics of Railway Bridges*. Telford, London, second edition, 1996. ISBN 0-7277-2044-9.

F. Gabaldón, J. Arribas, J. Goicolea, and F. Riquelme. *Dynamic Analysis of Structures Under High Speed Train Loads : Case Studies in Spain*, volume 1. Taylor & Francis, London, 2009.

J. M. Goicolea, J. Domínguez, J. A. Navarro, and F. Gabaldon. New Dynamic Analysis Methods for Railway Bridges in Codes IAPF and Eurocode 1. page 43, 2002.

M. Ichikawa, Y. Miyakawa, and A. Matsuda. Vibration Analysis of the Continuous Beam Subjected to a Moving Mass. *Sound and Vibration*, 230(3):493–506, 2000.

C. Johansson, C. Pacoste, and R. Karoumi. Closed-form solution for the mode superposition analysis of the vibration in multi-span beam bridges caused by concentrated moving loads. *Computers and Structures*, 119:85–94, 2013. ISSN 0045-7949.

M. Kabani and P. Moyo. Impact factors on heavy haul rail lines using monitoring data. 2014.

G. Kumaran, D. Menon, and K. K. Nair. Dynamic studies of railtrack sleepers in a track structure system. *Journal of Sound and Vibration*, 268(3):485–501, 2003. ISSN 0022460X.

W. C. Kuys. Ore Line Capacity Expansion: Conceptual Design of the Railway Line to Increase Capacity. In *9th International Heavy Haul Association Conference*, volume 85, pages 1722–1731, 2009.

J. W. Kwark, E. S. Choi, Y. J. Kim, B. S. Kim, and S. I. Kim. Dynamic behavior of two-span continuous concrete bridges under moving high-speed train. *Computers and Structures*, 82:463–474, 2004. ISSN 00457949.

Y. K. Lin. Free Vibrations of a Continuous Beam on Elastic Supports. *International Journal of Mechanical Sciences*, 4:409–423, 1962.

L. Mao and Y. Lu. Critical Speed and Resonance Criteria of Railway Bridge Response to Moving Trains. *Journal of Bridge Engineering*, 18:232, 2011. ISSN 1084-0702.

D. Martino. Train-Bridge Interaction on Freight Railway Lines. Master's thesis, KTH Royal Institute of Technology, 2011.

J. D. Ngwenyama, P. N. Naidoo, and J. M. Mulder. 5 Years of Operational Experience and Lessons Learnt with the on South Africa' s Iron Ore Line. In *10th International Heavy Haul Association Conference*, pages 796–803, 2013.

N. F. Rieger. The Relationship Between Finite Element Analysis and Modal Analysis. *Sound and Vibration*, 20:16–31, 1986.

C. Rigueiro, C. Rebelo, and L. S. da Silva. Influence of ballast models in the dynamic response of railway viaducts. *Journal of Sound and Vibration*, 329:3030–3040, 2010.

K. Saeedi and R. B. Bhat. Clustered natural frequencies in multi-span beams with constrained characteristic functions. *Shock and Vibration*, 18:697–707, 2011.

Sofistik AG. SOFiSTiK 2016: VERiFiCATiON MANUAL. Technical report, Oberschleissheim, 2015.

M.-K. Song, H.-C. Noh, and C.-K. Choi. A new three-dimensional finite element analysis model of high-speed trainbridge interactions. *Engineering Structures*, 25 (13):1611–1626, 2003. ISSN 01410296.

UIC. UIC Leaflet 776-2. Design requirements for rail-bridges based on interaction phenomena between train, track and bridge. Technical report, International Union of Railways, 2009.

D. Van Der Meulen and F. Möller. Competitiveness and Sustainability of Railways. 2012.

T.-L. Wang, D. Huang, and M. Shahawy. Dynamic Response of Multigirder Bridges. *Journal of Structural Engineering*, 118(8):2222–2238, 1993.

H. Xia and N. Zhang. Dynamic analysis of railway bridge under high-speed trains. *Computers and Structures*, 83:1891–1901, 2005.

Appendices

Appendix A

40 m Span(s)

	One Span		Two Spans		Three Spans		Four Spans		Five Spans		Six Spans		Sever Spans		Eight Spans		Nine Spans		Ten Spans	
	M0	M1	M0	M1	M0	M1	M0	M1	M0	M1	M0	M1	M0	M1	M0	M1	M0	M1	M0	M1
Mode 1	4.540	3.512	4.54	3.512	4.54	3.512	4.54	3.512	4.54	3.512	4.54	3.512	4.54	3.512	4.54	3.512	4.54	3.512	4.54	3.512
Mode 2	16.524	12.812	6.721	5.198	5.645	4.366	5.196	3.845	4.971	3.845	4.844	3.747	4.766	3.686	4.714	3.646	4.678	3.618	4.652	3.598
Mode 3	32.899	25.532	16.524	12.812	7.854	6.074	6.721	4.683	6.055	4.683	5.645	4.366	5.378	4.16	5.196	4.019	5.066	3.918	4.971	3.845
Mode 4	51.403	39.857	19.339	14.984	16.524	12.811	8.367	5.73	7.409	5.73	6.721	5.198	6.24	4.826	5.897	4.561	5.645	4.366	5.455	4.219
Mode 5	70.837	54.808	32.899	25.532	18.014	13.962	16.524	6.677	8.635	6.677	7.855	6.074	7.213	5.578	6.721	5.198	6.345	4.908	6.055	4.683
Mode 6	90.658	69.939	35.425	27.467	20.633	15.983	17.43	12.812	16.524	12.812	8.791	6.797	8.156	6.307	7.578	5.861	7.103	5.494	6.721	5.198
Mode 7	110.647	85.063	51.403	39.857	32.898	25.53	19.338	13.278	17.128	13.278	16.524	12.812	8.888	6.873	8.367	6.47	7.854	6.074	7.409	5.73
Mode 8	130.734	100.114	53.336	41.327	34.216	26.54	21.185	14.361	18.531	14.361	16.954	13.143	16.524	12.811	8.953	6.923	8.52	6.589	8.068	6.239
Mode 9	150.917	115.075	70.837	54.808	36.589	28.36	32.898	15.6	20.136	15.6	18.015	13.963	16.845	13.058	16.524	12.812	8.998	6.958	8.635	6.677
Mode 10	171.223	129.948	72.211	55.852	51.399	39.853	33.689	16.625	21.465	16.625	19.339	14.984	17.671	13.696	16.772	13.003	16.524	12.811	9.032	6.983

45 m Span(s)

Mode 1	4.074	3.181	4.074	3.181	4.074	3.181	4.074	3.181	4.074	3.181	4.074	3.181	4.074	3.181	4.074	3.181	4.074	3.181	4.074	3.181
Mode 2	14.891	11.656	6.05	4.723	5.074	3.961	4.667	3.644	4.464	3.485	4.349	3.395	4.278	3.34	4.231	3.303	4.199	3.278	4.176	3.26
Mode 3	29.784	23.344	14.891	11.656	7.08	5.526	6.05	4.723	5.445	4.251	5.074	3.961	4.832	3.773	4.667	3.644	4.55	3.552	4.464	3.485
Mode 4	46.713	36.6	17.493	13.685	14.891	11.656	14.891	11.656	6.674	5.21	6.05	4.723	5.614	4.382	5.302	4.139	5.074	3.961	4.903	3.827
Mode 5	64.561	50.503	29.784	23.344	16.269	12.73	15.729	12.309	7.791	6.081	7.08	5.526	6.496	5.071	6.05	4.723	5.709	4.457	5.445	4.251
Mode 6	82.796	64.616	32.173	25.195	18.694	14.621	17.493	13.685	14.891	11.656	7.933	6.192	7.354	5.74	6.828	5.33	6.397	4.994	6.05	4.723
Mode 7	101.189	78.747	46.713	36.6	29.784	23.344	29.784	23.344	15.45	12.091	14.891	11.656	8.022	6.261	7.547	5.891	7.08	5.526	6.674	5.21
Mode 8	119.655	92.823	48.584	38.038	31.033	24.311	30.534	23.925	16.746	13.102	15.289	11.966	14.891	11.656	8.082	6.308	7.687	6	7.273	5.678
Mode 9	138.178	106.823	64.561	50.503	33.279	26.051	32.173	23.195	18.232	14.261	16.269	12.73	15.188	11.887	14.891	11.656	8.123	6.34	7.791	6.081
Mode 10	156.77	120.745	65.916	51.542	46.713	36.6	33.739	26.407	19.469	15.224	17.493	13.685	15.951	12.482	15.12	11.835	14.891	11.656	8.154	6.364
	One Span		Two Spans		Three Spans		Four Spans		Five Spans		Six Spans		Sever Spans		Eight Spans		Nine Spans		Ten Spans	

50 m Span(s)

	One Span		Two Spans		Three Spans		Four Spans		Five Spans		Six Spans		Sever Spans		Eight Spans		Nine Spans		Ten Spans	
	M0	M1	M0	M1	M0	M1	M0	M1	M0	M1	M0	M1	M0	M1	M0	M1	M0	M1	M0	M1
Mode 1	3.688	2.904	3.688	2.904	3.688	2.904	3.688	2.904	3.688	2.904	3.688	2.904	3.688	2.904	3.688	2.904	3.688	2.904	3.688	2.904
Mode 2	13.533	10.686	5.492	4.325	4.601	3.623	4.23	3.331	4.044	3.102	3.939	3.102	3.874	3.051	3.832	3.017	3.802	2.994	3.781	2.977
Mode 3	27.18	21.498	13.533	10.686	6.434	5.066	5.492	4.325	4.94	3.623	4.601	3.623	4.38	3.449	4.23	3.331	4.123	3.247	4.044	3.185
Mode 4	42.781	33.838	15.951	12.589	13.533	10.686	6.863	5.404	6.063	4.325	5.492	4.325	5.093	4.011	4.809	3.787	4.601	3.623	4.444	3.5
Mode 5	59.291	46.842	27.18	21.498	14.814	11.694	13.533	10.686	7.087	5.066	6.434	5.066	5.9	4.646	5.492	4.325	5.18	4.079	4.94	3.89
Mode 6	76.193	60.079	29.447	23.271	17.071	13.469	14.312	11.299	13.533	5.683	7.218	5.683	6.686	5.264	6.204	4.885	5.809	4.574	5.492	4.325
Mode 7	93.254	73.358	42.781	33.838	27.18	21.498	15.951	12.589	14.052	10.686	13.533	10.686	7.3	5.747	6.863	5.404	6.434	5.066	6.063	4.774
Mode 8	110.377	86.598	44.593	35.244	28.366	22.425	17.551	13.847	15.256	10.977	13.903	10.977	13.533	10.686	7.355	5.79	6.991	5.505	6.612	5.206
Mode 9	127.535	99.772	59.291	46.842	30.497	24.091	27.18	21.498	16.639	11.694	14.814	11.694	13.809	10.903	13.533	10.686	7.393	5.821	7.087	5.58
Mode 10	144.73	125.916	60.626	47.874	42.781	33.838	27.893	22.055	17.795	12.589	15.951	12.589	14.518	11.461	13.746	10.854	13.533	10.686	7.421	5.842
	M0	M1	M0	M1	M0	M1	M0	M1	M0	M1	M0	M1	M0	M1	M0	M1	M0	M1	M0	M1
	One Span		Two Spans		Three Spans		Four Spans		Five Spans		Six Spans		Sever Spans		Eight Spans		Nine Spans		Ten Spans	

Appendix B

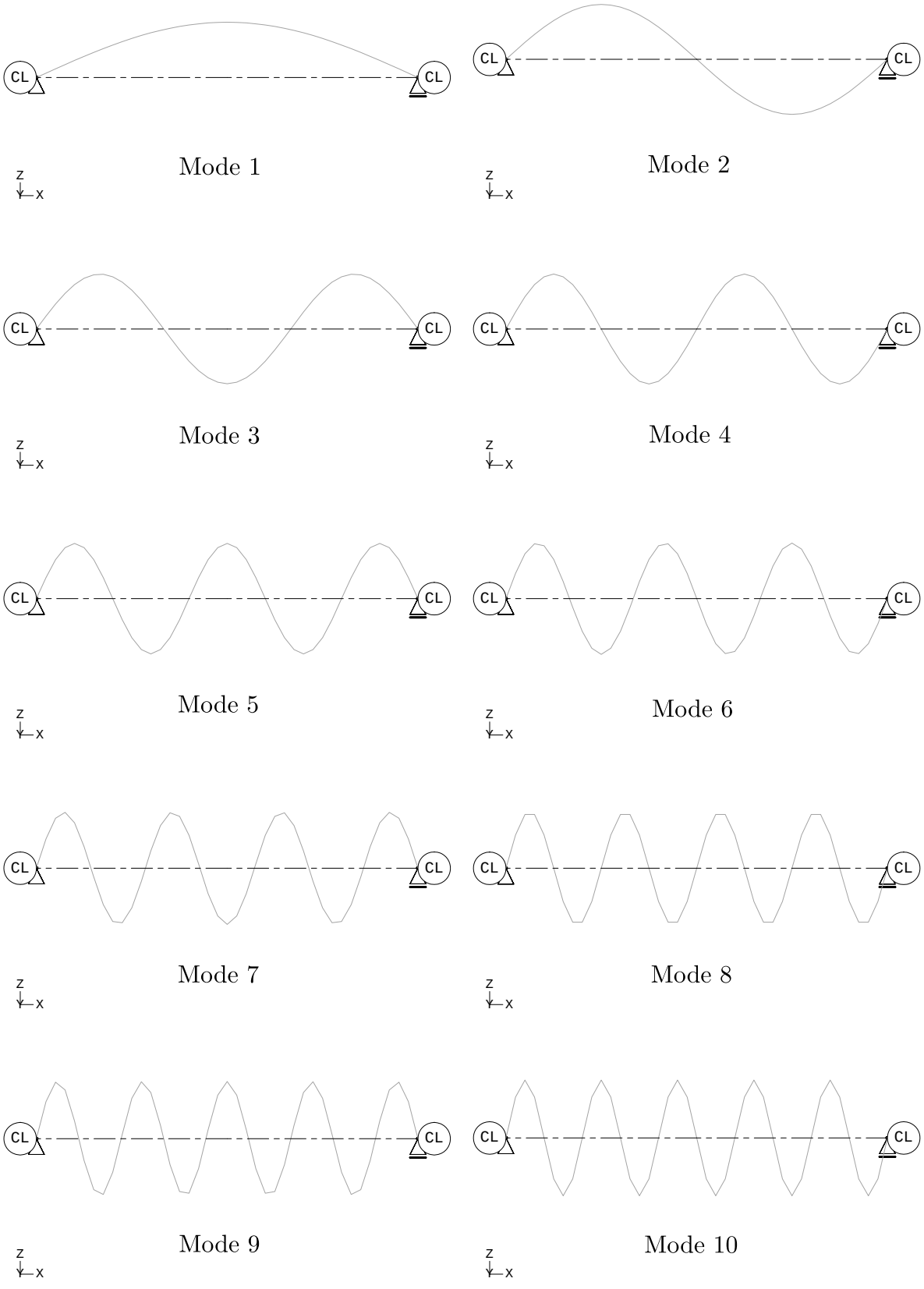

Figure B.1: Mode shapes 1 – 10 for the single span bridge.

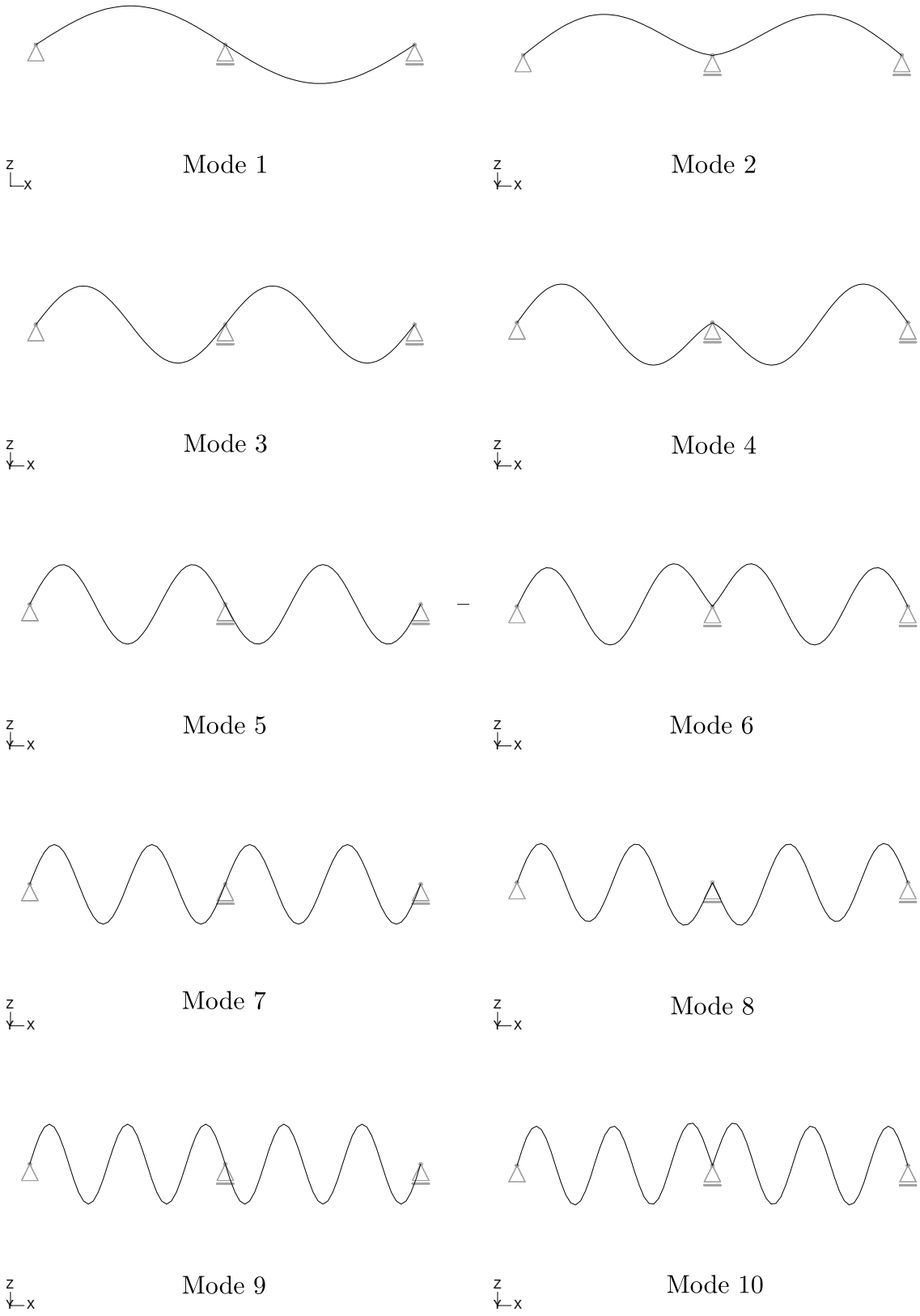

Figure B.2: Mode shapes 1 – 10 for the two span bridge.

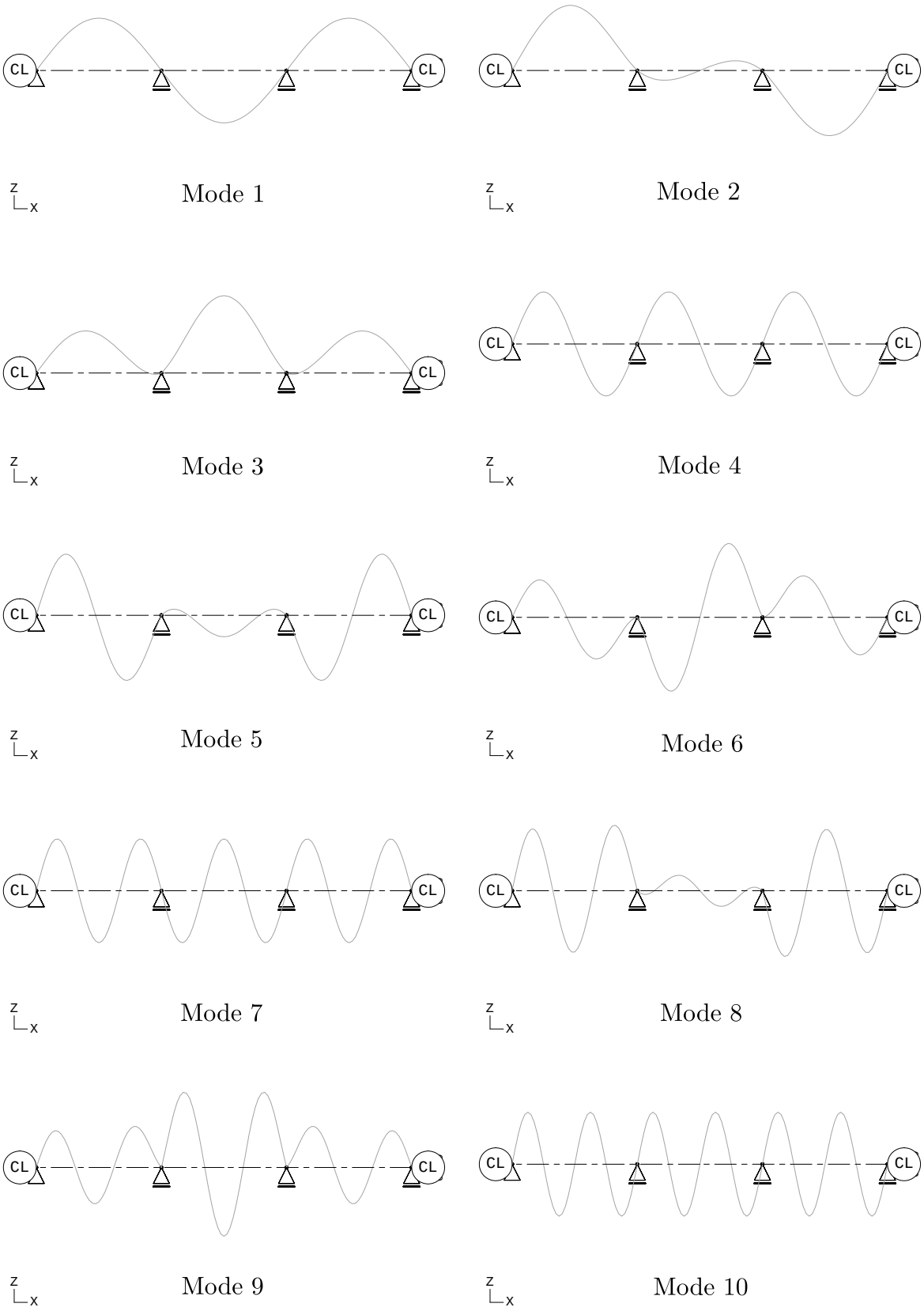

Figure B.3: Mode shapes 1 – 10 for the three span bridge.

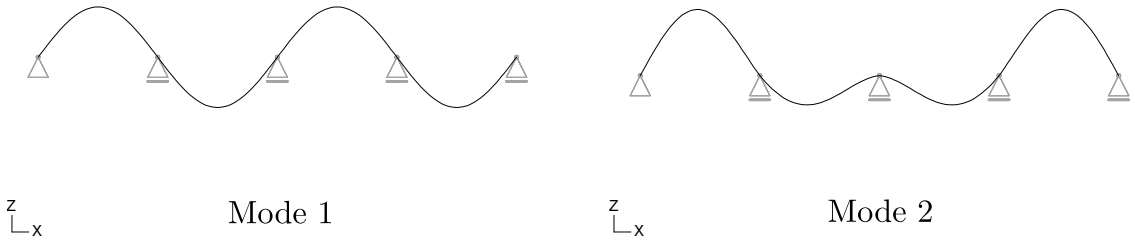

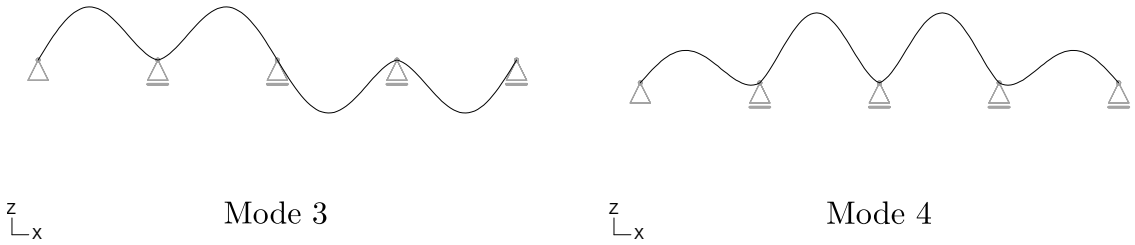

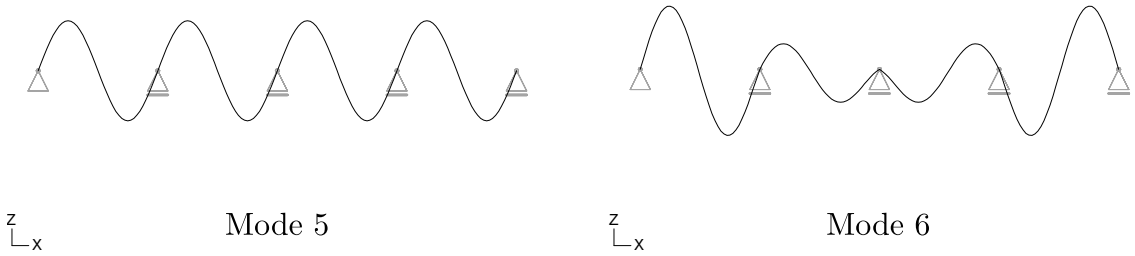

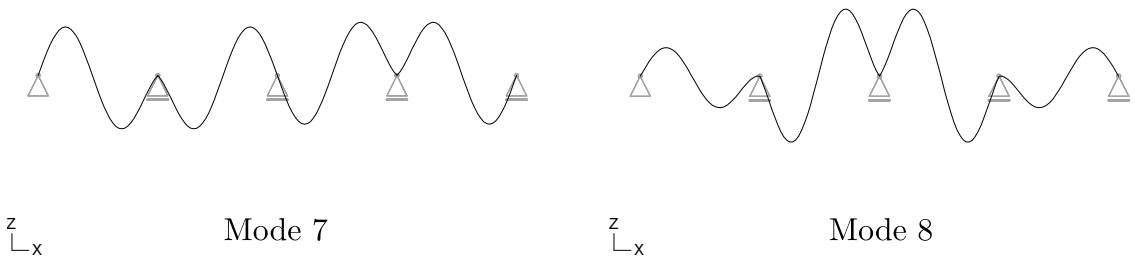

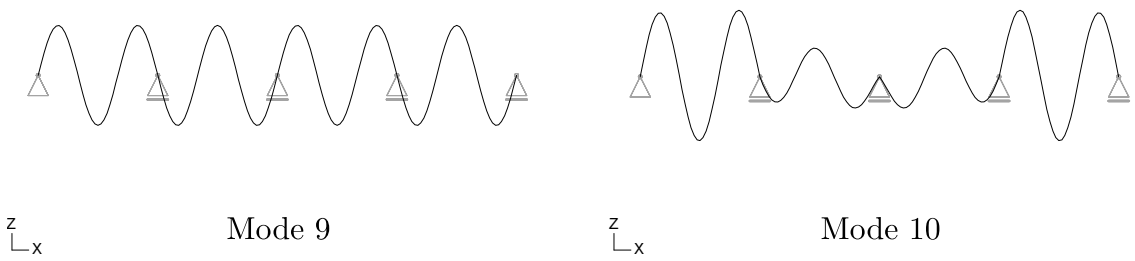

Figure B.4: Mode shapes 1 – 10 for the four span bridge.

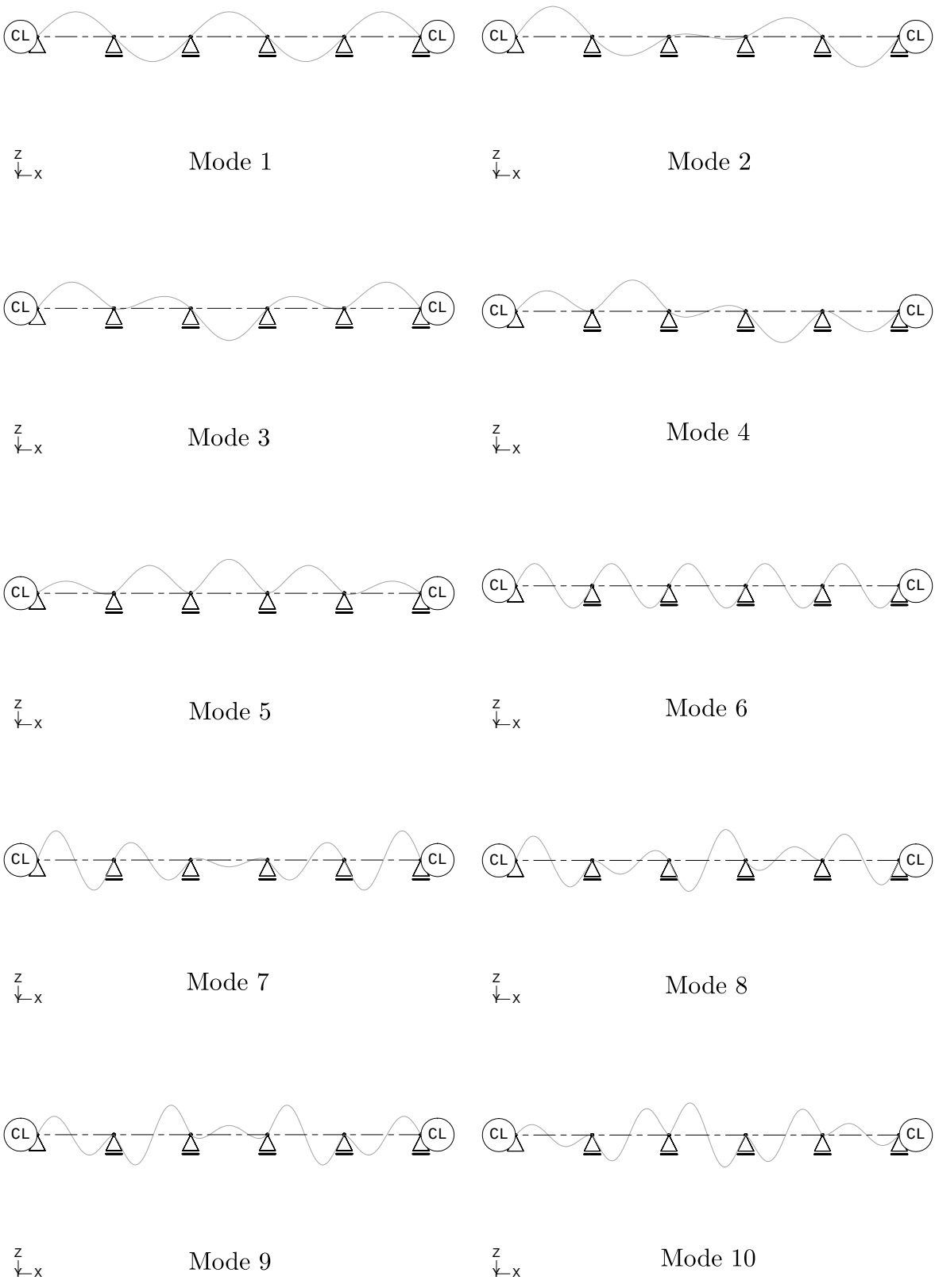

Figure B.5: Mode shapes 1 – 10 for the five span bridge.

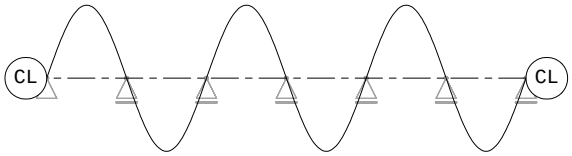

z
x

Mode 1

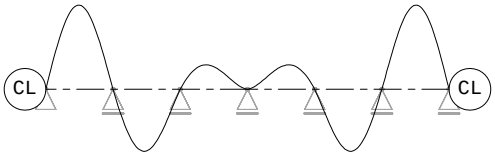

z
x

Mode 2

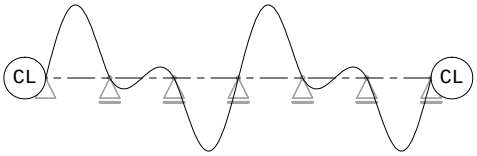

z
x

Mode 3

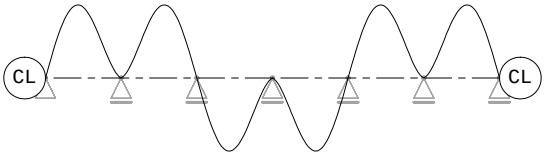

z
x

Mode 4

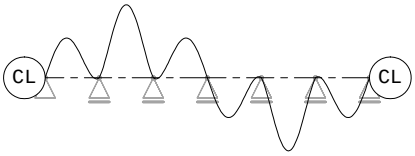

z
x

Mode 5

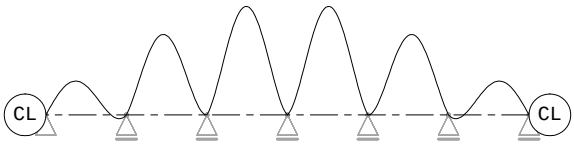

z
x

Mode 6

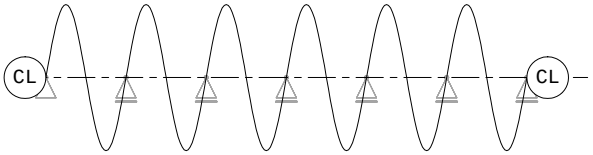

z
x

Mode 7

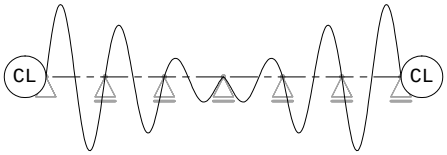

z
x

Mode 8

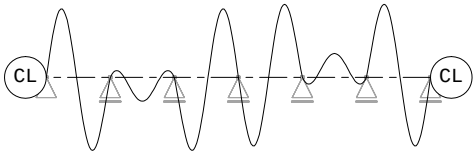

z
x

Mode 9

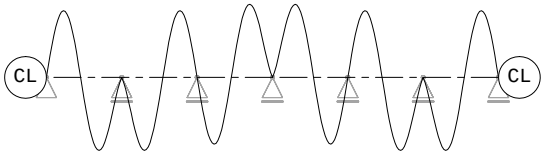

z
x

Mode 10

Figure B.6: Mode shapes 1 – 10 for the six span bridge.

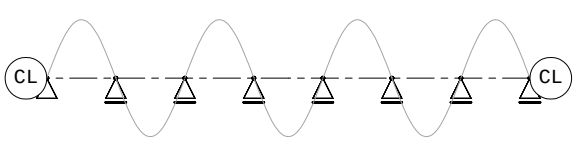

z
└x

Mode 1

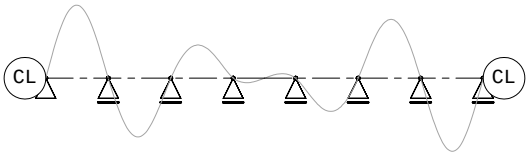

z
└x

Mode 2

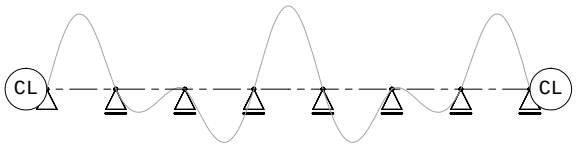

z
└x

Mode 3

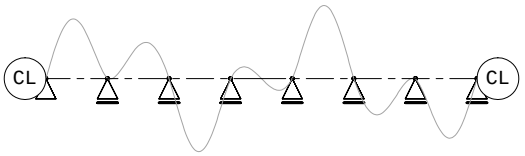

z
└x

Mode 4

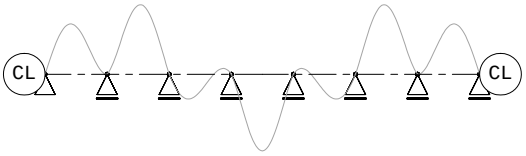

z
└x

Mode 5

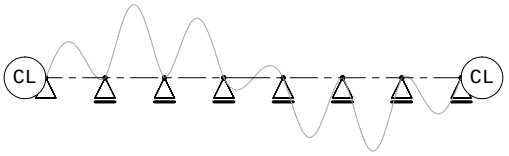

z
└x

Mode 6

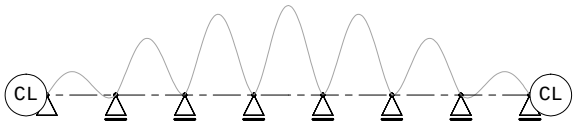

z
└x

Mode 7

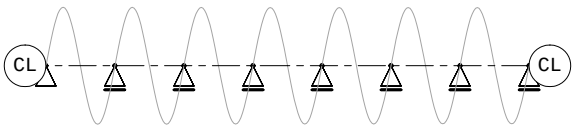

z
└x

Mode 8

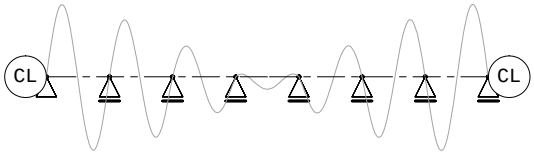

z
└x

Mode 9

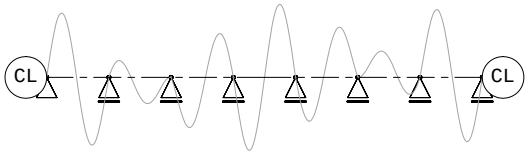

z
└x

Mode 10

Figure B.7: Mode shapes 1 – 10 for the seven span bridge.

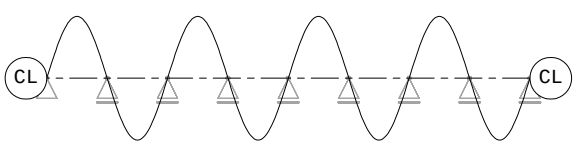

z
└x

Mode 1

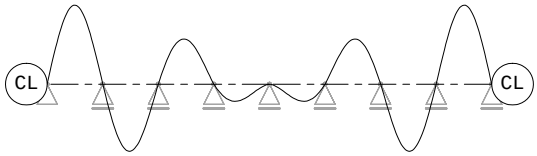

z
└x

Mode 2

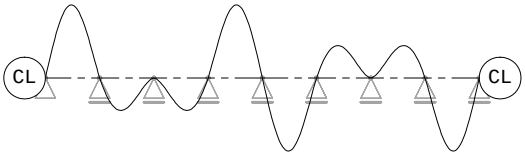

z
└x

Mode 3

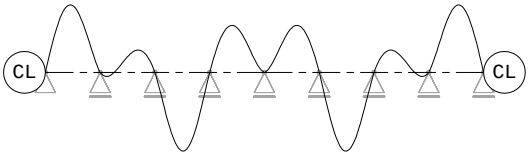

z
└x

Mode 4

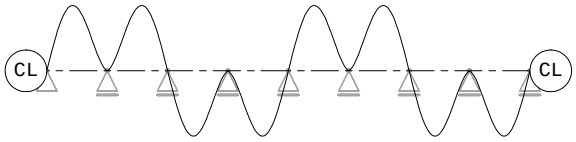

z
└x

Mode 5

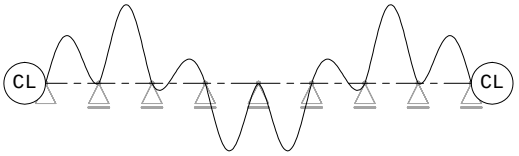

z
└x

Mode 6

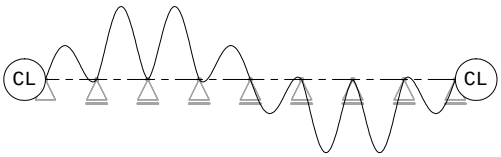

z
└x

Mode 7

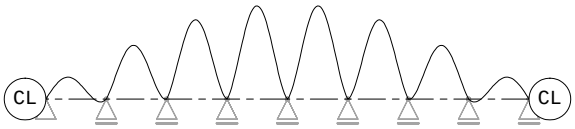

z
└x

Mode 8

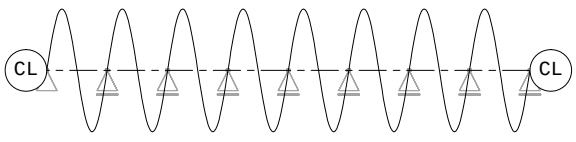

z
└x

Mode 9

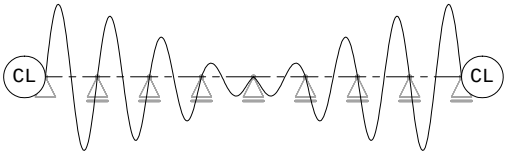

z
└x

Mode 10

Figure B.8: Mode shapes 1 – 10 for the eight span bridge.

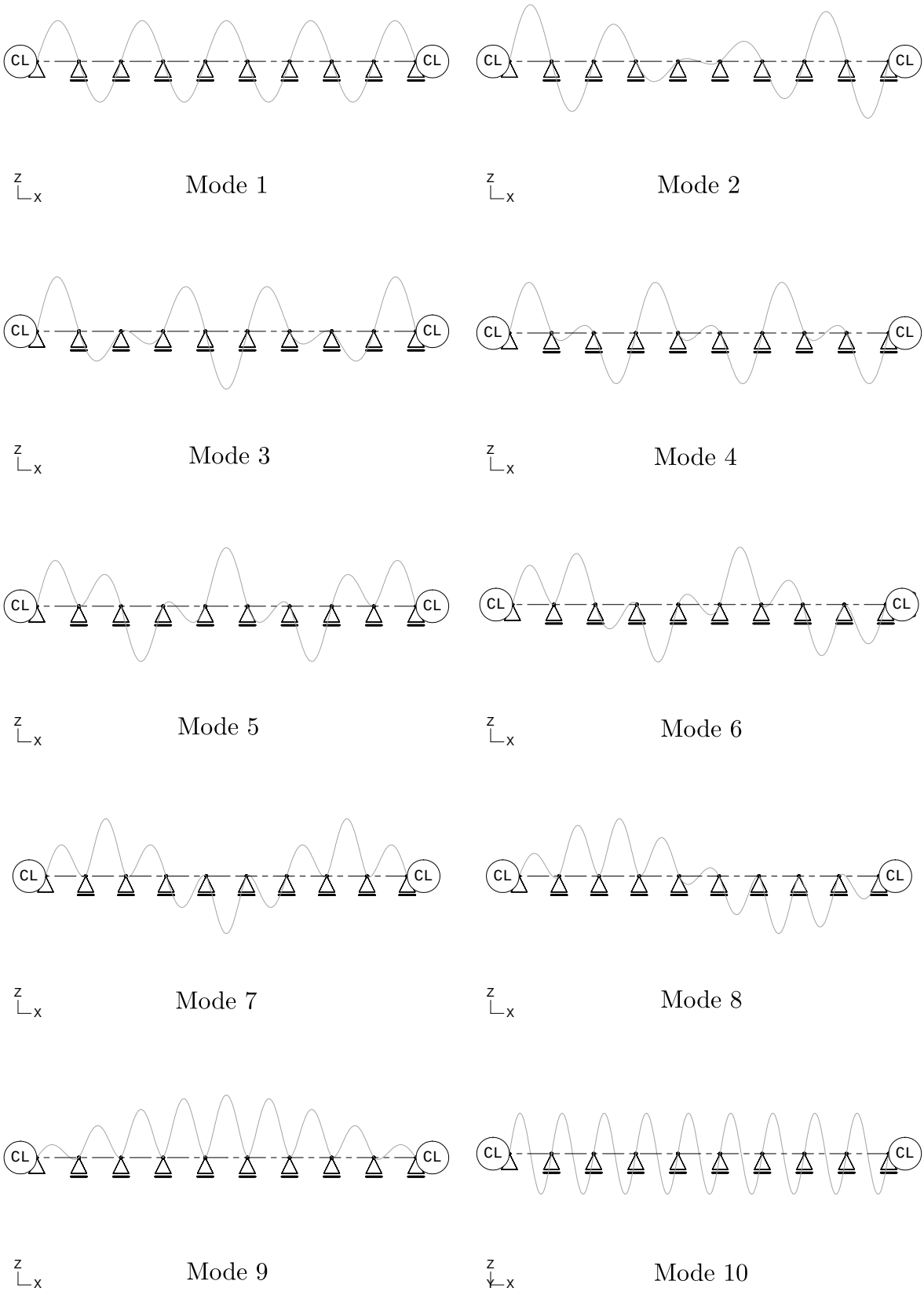

Figure B.9: Mode shapes 1 – 10 for the nine span bridge.

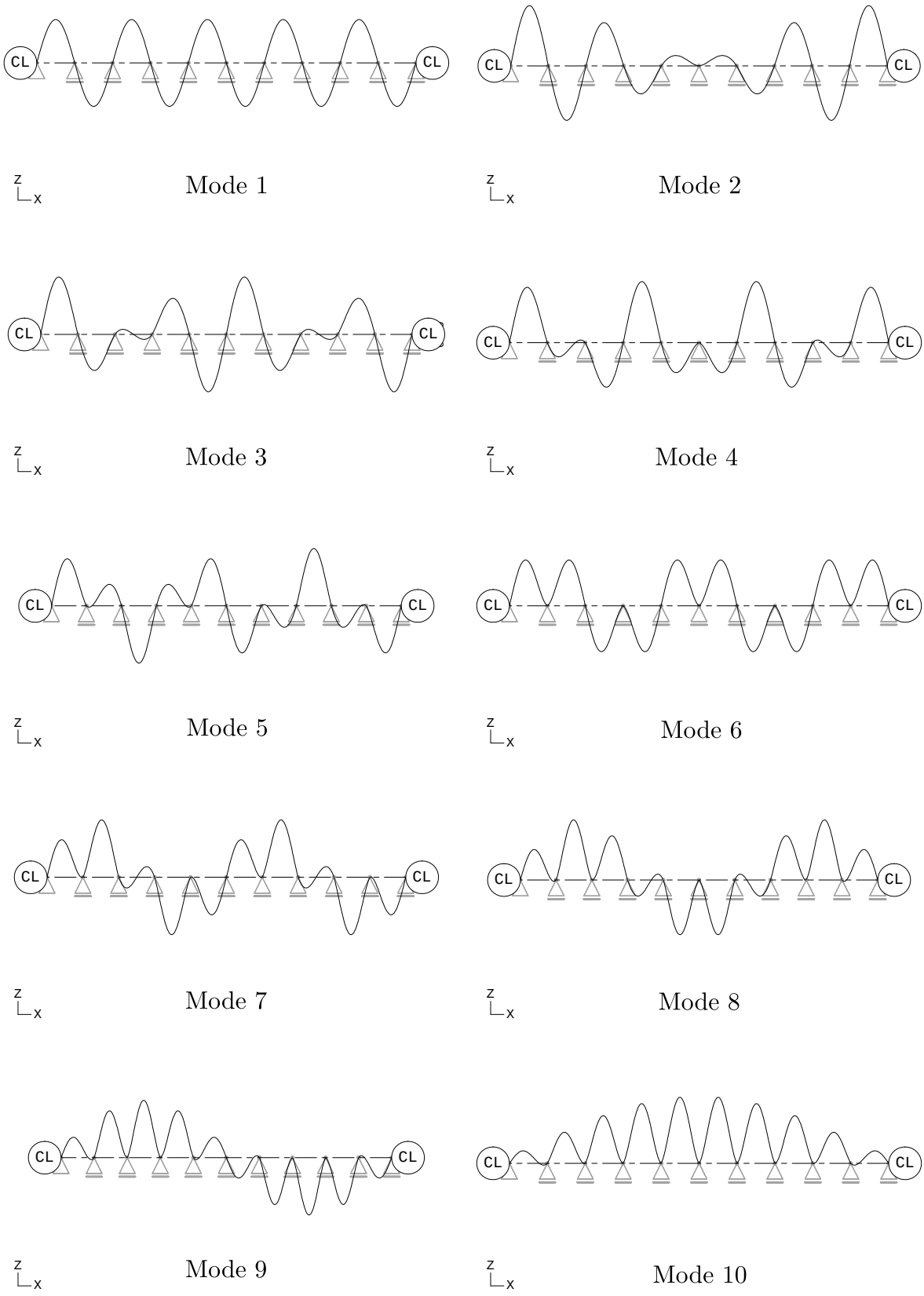

Figure B.10: Mode shapes 1 – 10 for the ten span bridge.